Organization and Regulation of Outer Kinetochore Assembly

by

Florencia Rago

M.A. Biotechnology
Boston University, 2010

B.A. Biochemistry and Molecular Biology
Boston University, 2010

Submitted to the Department of Biology in partial fulfillment
of the requirements for the degree of

Doctor of Philosophy in Biology

at the

Massachusetts Institute of Technology

June 2015

Signature of the author:_____
Department of Biology
May 22, 2015

Certified by:_____
Iain M. Cheeseman
Associate Professor of Biology
Thesis Supervisor

Certified by:_____
Amy E. Keating
Associate Professor of Biology
Chair, Committee for Graduate Students

Organization and Regulation of Outer Kinetochore Assembly

by

Florencia Rago

Submitted to the Department of Biology on May 22, 2015
in partial fulfillment of the requirements for the degree of
Doctor of Philosophy in Biology

Abstract

The kinetochore provides the connection between chromosomes and spindle microtubules. Defining the molecular architecture of the core kinetochore components is critical for understanding the mechanisms by which the kinetochore directs chromosome segregation. The KNL1/Mis12 complex/Ndc80 complex (KMN) network acts as the primary microtubule-binding interface at kinetochores, and provides a platform for recruitment of regulatory proteins. The results in this thesis demonstrate that the CENP-C and CENP-T inner kinetochore receptors form separate scaffolds for KMN network assembly. Initial biochemical results suggested a non-canonical assembly pathway mediated by a direct interaction between CENP-T and the Ndc80 complex. These results were further verified and expanded upon in cells using an ectopic targeting approach to allow careful analysis of the pathways independently of one another. The data presented here demonstrate that in addition to forming two pathways, the CENP-C and CENP-T based assemblies are each constructed uniquely, showing both distinct organization of the KMN components as well as different modes of regulation. Analysis of the CENP-C based assembly pathway has previously defined the canonical architecture of the KMN network as a stable unit that associates with CENP-C via a direct interaction mediated by the Mis12 complex, and the data herein additionally shows that assembly of this pathway is regulated at least in part by Aurora B kinase activity. In contrast, the CENP-T protein forms a direct, CDK-dependent interaction with the Ndc80 complex, and this interaction is required for downstream recruitment of KNL1 and the Mis12 complex, resulting in a novel recruitment pathway for the KMN network. Together these results allow us to generate a new and more detailed molecular model for the assembly of the core structural components of the kinetochore.

Thesis Supervisor: Iain M. Cheeseman
Title: Associate Professor of Biology

Acknowledgements

Iain, I want to thank you for letting me join your lab almost four years ago. I think you knew that this would be the right place for me to become a grown up scientist before I did, and you were right. You let me go wherever my research interests took me, and supported me when they led me on paths previously untraveled. When I started grad school I had already had one amazing mentor, setting my standards high, and you did not fail me. I don't think that there is enough space to thank you for everything you have done during my time here, so I will just leave it at thank you, thank you, thank you.

To the lab, previous and present – Julie W., Jens, Tomomi, Karen, Chelsea, David, Kara, Kuan Chung, Julie M., Tonia, and new Ian – you have all been instrumental in getting me here. To those who have left, thank you for teaching me when I knew very little and being great sounding boards and resources. Karen, without you I wouldn't have been able to accomplish what I have. You laid the groundwork for much of what I did, and for that I am so thankful. Kara, I don't think I will ever be able to thank you enough. You have been my only baymate during my time here, so you can only be the best, but you earned the title of best and more. Thank you for always offering help and advice on any scientific topic. David, thank you for all of your advice for trying to purify difficult proteins. Kuan Chung, thank you for all of your help with the Nikon, I truly appreciate all of the time you dedicated to getting the microscope to work. To the other members of the lab, I know I was not here when you came together to help me in a moment of scientific disaster, but I am so grateful that you all helped and I know that without you all there would have been no paper. The lab has been a great place to spend long nights and even longer weekends pushing through experiments.

To my parents, you are the best. Thank you for always being supportive and being willing drive me back and forth between your house and Cambridge, even if only for a few hours - I couldn't have asked for better parents. Caro, Gordo – when I left the house you guys were practically babies, and I've gotten to watch you guys grow up over the last years. You guys have become really awesome people and I am lucky that I get to call you my siblings. Please continue to defer to me for any important decisions; while I may be the shortest, I am still the oldest and therefore the wisest.

Dean, I need to thank you for letting me join your lab when I was 18 and knew nothing about being a biologist. You committed to teaching me how to be a good scientist and biochemist, and without all of your support throughout those three years at BU and even through grad school, I wouldn't have made it as far as I have.

To all of my friends, thank you for always being around to talk about non-science topics. If I hadn't gotten to step out of the grad school bubble every once in a while, this would have been a far more arduous journey. Thank you to the friends I've made at MIT, who despite being the most intelligent people I know, were still willing to sit around and talk nonsense.

I have been lucky to have particularly awesome female scientists on my committee these last few years. Tania, Sue, and recently Cathy, you have provided the best inspiration and support as successful women in science. I'd also like to thank Tom for filling the role of outside member during my defense.

Table of Contents

Chapter I: Introduction

Adapted from Rockefeller University Press:

Rago, F., and I.M. Cheeseman. 2013. Review series: The functions and consequences of force at kinetochores. *The Journal of Cell Biology*. 200:557–565. doi:10.1083/jcb.201211113.

Mitosis

Mitosis is a core cellular process that underlies reproduction, multi-cellular organism growth, and tissue repair. It is essential that duplicated chromosomes be accurately segregated to the two daughter cells to avoid outcomes like cell death or cancer, which are detrimental to the survival of the organism. This requires a complex process of chromosome attachment to the mitotic spindle, verification of proper chromosome bi-orientation, and finally, separation of the chromosome masses to opposite spindle poles to eventually end up in two daughter cells (Figure 1). The mitotic apparatus responsible for forming, maintaining and signaling the correct attachment between chromosomes and the mitotic spindle is termed the kinetochore. The kinetochore is a complex structure composed of more than 100 different proteins. Widely conserved in eukaryotes, it forms the essential connection between the centromere and microtubules.

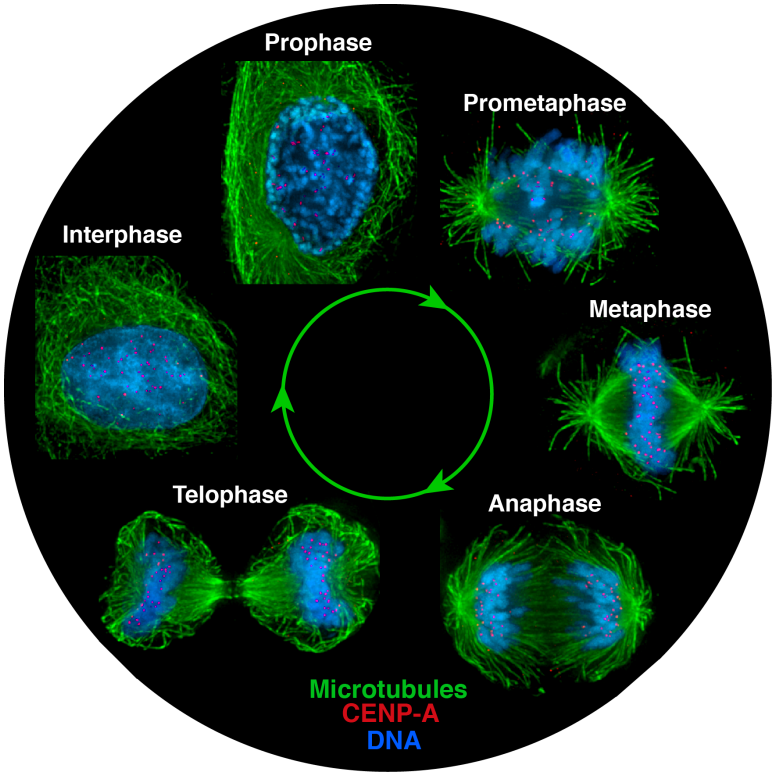

Figure 1: The Cell Cycle. As cells transition from interphase into mitosis, DNA is compacted and the nuclear envelope breaks down as cells enter prophase. Chromosomes begin to organize in prometaphase, leading to alignment at the metaphase plate. Upon chromosome alignment, degradation of cohesin marks the initial step in chromosome segregation to opposite spindle poles in anaphase. During telophase chromosomes decondense and the nuclear envelope reforms around the two daughter nuclei concurrent with the cell dividing by cytokinesis. Microtubules are shown in green, kinetochores are marked by αCENP-A in red and DNA is shown in blue (Adapted from Cheeseman and Desai, 2008).

The Inner Kinetochore

The site of attachment for microtubules on each chromosome is defined by the deposition of the non-canonical histone H3 variant, centromere protein-A (CENP-A), at the centromere (Allshire and Karpen, 2008). Ectopic deposition of CENP-A at a site distal to the endogenous centromere has been shown to lead to assembly of fully functional kinetochores (Barnhart et al., 2011), helping to define CENP-A as the sole marker of the centromere and site of kinetochore assembly. The assembly of functional kinetochores is due to the recruitment of various components of the constitutive centromere associated network (CCAN) downstream of CENP-A. Among these proteins are CENP-C and CENP-T. CENP-C directly interacts with CENP-A (Trazzi et al., 2009; Carroll et al., 2010), and in many organisms including *Caenorhabditis elegans* and *Drosophila melanogaster,* provides the only known pathway for outer kinetochore assembly (Schleiffer et al., 2012). In other organisms such as humans, *Gallus gallus* and *Saccharomyces cerevisiae,* another inner kinetochore receptor, CENP-T, provides an additional platform for outer kinetochore assembly (Gascoigne et al., 2011; Schleiffer et al., 2012), which is described in

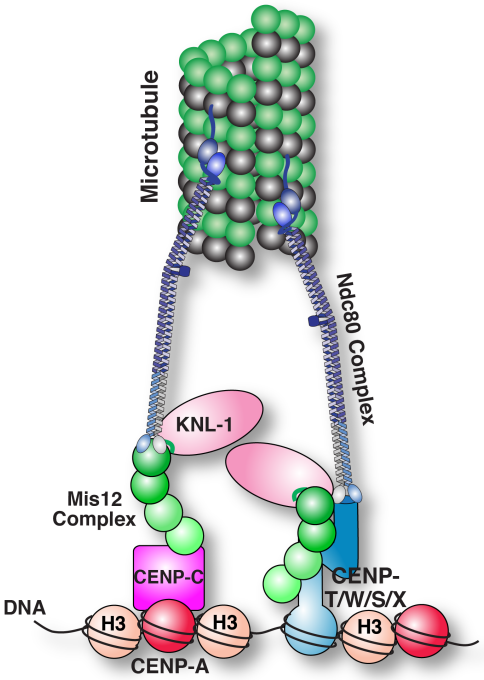

Figure 2: Model of the kinetochore architecture. The current model of the organization of the core structural components of the kinetochore is depicted. In red are CENP-A nucleosomes interspersed with the canonical histone H3 nucleosomes. In magenta is CENP-C, which directly binds to CENP-A. The three components of the KMN network (KNL1 (pink), Mis12 complex (green), Ndc80 complex (blue and gray)) are shown on their CENP-C and CENP-T (cyan) receptors.

detail here (Figure 2). While CENP-C binds directly to CENP-A providing a direct path from centromere to microtubules, CENP-T contains a histone fold domain that together with its fellow CCAN components, CENP-W/-S/-X, forms a nucleosome-like structure (Nishino et al., 2012). Thus, it has been suggested that the CENP-T-W-S-X complex provides an additional anchor point to the centromere DNA. In humans, both CENP-C and CENP-T form an inner kinetochore platform for outer kinetochore assembly, and it is the outer kinetochore that provides the direct attachment to the spindle microtubules ultimately responsible for directing chromosome segregation.

The Outer Kinetochore

The major structural components of the outer kinetochore are KNL1, the Mis12 complex, and the Ndc80 complex, which together comprise the KMN network. These three components bridge the inner kinetochore to the spindle microtubules and are responsible for forming and maintaining microtubule attachments.

The Ndc80 Complex

The Ndc80 complex is the major microtubule-binding component of the kinetochore. It is comprised of four subunits (Ndc80, Nuf2, Spc24, and Spc25) that form a dumbbell-shaped structure, with the two globular heads connected by a long coiled-coil (Ciferri et al., 2005; 2008; Wei et al., 2005). Work by many groups has characterized the microtubule binding properties of the Ndc80 complex, which are largely mediated by the Ndc80 globular domain and charged tail (Wei et al., 2007; Ciferri et al., 2008; Wang et al., 2008; Alushin et al., 2010; DeLuca et al., 2006). The Ndc80 complex has been shown to have relatively weak microtubule binding activity (Cheeseman et al., 2006),

with a preference for the straight microtubule lattice (Schmidt et al., 2012), and increased binding affinity and tip-tracking properties on a depolymerizing microtubule when clustered either by artificial tethering to a bead or mixed with another outer kinetochore component, the Ska1 complex (Powers et al., 2009; Schmidt et al., 2012). Binding to the inner kinetochore is achieved via the Spc24 and Spc25 globular head (Wei et al., 2006; Petrovic et al., 2010), positioning the long axis of the Ndc80 complex parallel to the kinetochore assembly (Figure 2).

The Mis12 Complex

Together the proteins Dsn1, Nnf1, Nsl1, and Mis12 make up the Mis12 complex. These four proteins play a major structural role at the kinetochore. It has been demonstrated that loss of the Mis12 complex at kinetochores leads to loss of kinetochore integrity and function (Kline et al., 2006; Cheeseman et al., 2004; Milks et al., 2009). Research to date has characterized the Mis12 complex as the major link between the outer kinetochore proteins and the inner kinetochore protein CENP-C. It has been shown by biochemical and cellular analyses that the Mis12 complex interacts directly with CENP-C, and that this in turn forms the base for recruitment of other components of the outer kinetochore (Screpanti et al., 2011; Petrovic et al., 2010; Przewloka et al., 2011). In addition to interacting directly with CENP-C, the Mis12 complex binds to both the Ndc80 complex via interactions with the Dsn1 and Nsl1 subunits, and to KNL1 via the Nsl1 subunit (Petrovic et al., 2010; 2014; Malvezzi et al., 2013).

KNL1

The KNL1 protein has been shown to play two important roles at the kinetochore. First, it has weak microtubule binding activity, and, in the context of the assembled KMN network, it is able to synergize with the Ndc80 complex and lead to increased microtubule-binding affinity of the entire network (Cheeseman et al., 2006). KNL1 also functions as the major platform for recruitment of the spindle checkpoint components (Reviewed by London and Biggins, 2014). Direct phosphorylation of the MELT repeats in KNL1 by Mps1 leads to downstream recruitment of the BUB (Bub3, Bub1, BubR1) and the MAD (MAD1 and MAD2) spindle assembly checkpoint proteins. These proteins are responsible for sensing microtubule attachment status and signaling a checkpoint arrest in metaphase upon detection of even a single unattached kinetochore by inhibiting the activation of the Anaphase Promoting Complex (APC/C) E3 ubiquitin ligase. A recently solved crystal structure and EM images of KNL1 truncations in complex with the Ndc80 complex and the Mis12 complex have shown that the kinetochore recruitment domain of KNL1 is located at the C-terminal end of the protein (Petrovic et al., 2014; 2010).

Together the KMN network components form the major microtubule binding and checkpoint signaling hub of the kinetochore, responsible for both making and sensing microtubule attachments. As such, defining the basis for their assembly is important for forming a clear picture of how proper chromosome segregation is achieved.

Mitotic Challenges to Kinetochore Integrity

Force plays key roles in many different cellular processes by influencing objects in a way that causes them to change their speed or direction of movement. Force can take multiple forms in a cell and have very different consequences depending on the circumstances of its action. When force pulls on an object, it creates “tension.” In contrast, a pushing force exerted upon an object is termed “compression.” To understand the contribution of force to cellular processes, it is important to determine the molecular mechanisms by which force is generated or produced at a sub-cellular structure, how these structures withstand the force, and how they detect and signal the presence of force. The process of mitotic chromosome segregation provides a particularly intriguing example of the importance of cellular force. During mitosis, force plays a critical role in directing the physical segregation of chromosomes and modulating the signals that sense and promote their proper attachment to the spindle. Because the kinetochore is the contact point between chromosomes and microtubules, the forces derived from microtubules are exerted directly on the proteins within the kinetochore. This means that the kinetochore must maintain attachment to the dynamic microtubule plus ends, as well as remain intact as chromosomes are pushed and pulled around the cell under forces that can abruptly change in direction and magnitude. A key challenge is to understand how this force is generated and accommodated, and to define the specific contributions of this force to kinetochore function.

How much force is generated at a kinetochore in cells?

The nature of the forces involved in partitioning chromosomes has been an active area of research for more than 50 years. Edwin Taylor and Bruce Nicklas were among the first to consider the forces that resist chromosome movement. Separate theoretical analyses predicted that ~0.1 pN would be required to move a chromosome at 1 μm/min when resisted only by viscous cytoplasmic drag (Taylor, 1965; Nicklas, 1965). Almost 20 years after publishing his theoretical work, Nicklas was able to test the force on a single chromosome during anaphase of meiosis I (1983). Using a microneedle to measure the stall force on chromosomes in grasshopper spermatocytes, Nicklas found that 700 pN could act on a single chromosome (1983). He estimated that the kinetochores tested in these studies were bound by approximately 15 microtubules (Nicklas, 1983), suggesting that each microtubule may be capable of generating up to ~45 pN of force, under the assumption that each microtubule was in a depolymerizing state while fully engaged by the kinetochore so that each was functioning at its max potential. In later studies, Nicklas determined that ~50 pN of force was produced on a chromosome during prometaphase (1988). This calculation was based on observations of chromosome congression and correlations with his previous work. By Nicklas' own admission, the microneedle assays to measure the force exerted on anaphase chromosomes had a high associated error, and it is unknown whether forces in the hundreds of pN would ever be produced at a kinetochore in the absence of an external perturbation. Recently, Ferraro-Gideon et al. performed experiments to measure the force produced on kinetochores in various organism (2013). They used optical tweezers to capture individual chromosomes and measure the pulling forces applied by the

spindle directly, or measured the retraction forces put on the centrosomes after laser cutting half of the spindle. In contrast to the Nicklas experiments, they found that only 0.1 to 1 pN of force were produced on meiotic and mitotic kinetochores. The cause of this large discrepancy remains unknown and it may be necessary to generate a third approach to measure the force produced by the mitotic spindle to finally know the order of magnitude of applied force under which the kinetochore functions.

As Nicklas' work suggested, it is likely that the force felt by kinetochores varies throughout the cell cycle and under different types of attachments (discussed later). In particular, the arrangement of paired sister chromatids attached to opposite spindle poles during metaphase would allow for the greatest tension to be applied to kinetochores. Recent work visualizing sister chromatid oscillations during metaphase has observed that at time points immediately prior to the switch from poleward to anti-poleward motion, the poleward moving kinetochore experiences the highest forces, at least as judged by changes in intra- and inter-kinetochore distances (Dumont et al., 2012; Wan et al., 2012). In addition, the anti-poleward moving kinetochore may experience passive forces (Maddox et al., 2003; Inoué and Salmon, 1995) that can also alter inter and intra-kinetochore stretch (Dumont et al., 2012; Wan et al., 2012). However, the magnitude of force during these directional switches and how this force is accommodated continues to be a subject of debate. As the higher order organization of kinetochores remains unknown, it is unclear how the forces from the multiple microtubule interactions at a single kinetochore are combined or what force is experienced by an individual protein within the kinetochore structure.

The Mechanisms of Force Production

With the discovery of the potentially large forces produced at kinetochores (Nicklas, 1983), a major challenge has been to define the mechanisms by which this force is generated. Many initial studies focused on the contributions of the microtubule-based motors, dynein and kinesin, that were found to localize to kinetochores (Reviewed by Inoué and Salmon, 1995). The ability of these motors to transport cargos along microtubules suggested that they might function similarly to move a chromosome within a cell. Individual kinesin and dynein motors have been shown to stall under ~5-7 pN loads (an object or another force that opposes the original force) (Visscher et al., 1999; Gennerich et al., 2007), and the combined action of multiple motors could generate the forces that Nicklas observed. However, subsequent studies have found that chromosome movement can still largely occur in the absence of these motors in fungi (Grishchuk and McIntosh, 2006; Cottingham et al., 1999). In metazoans, motors including the kinesin CENP-E and dynein contribute to chromosome segregation (Kapoor et al., 2006; Yang et al., 2007; Sharp et al., 2000), although their relative importance remains unclear. An alternative hypothesis was that the microtubules themselves generated the force to move chromosomes (Reviewed by Inoué and Salmon, 1995). Several early studies provided evidence that microtubules could direct the movement of isolated chromosomes under conditions that would not permit motor protein function (Koshland et al., 1988; Coue et al., 1991; Hunt and McIntosh, 1998). This microtubule-derived movement could be caused by forces generated either at the kinetochore by microtubule depolymerization (Grishchuk et al., 2005) or at the spindle poles due to poleward flux and microtubule disassembly at the minus end (Chen and

Zhang, 2004; LaFountain et al., 2004; 2001; Elting et al., 2014). In fact, subsequent work suggested that the stall forces measured by Nicklas were due to minus end microtubule disassembly in equilibrium with the plus end microtubule polymerization caused by the application of tension via the microneedle (LaFountain et al., 2001; 2004; Chen and Zhang, 2004). Although it is now generally accepted that dynamic microtubules generate the primary forces responsible for chromosome movement, kinetochore-localized motors do play important roles during mitosis. These motors may still generate some force, act as a "back-up" system when kinetochore capture by microtubules fails (Kapoor et al., 2006), generate tension via the production of polar ejection forces (Mazumdar and Misteli, 2005; Cane et al., 2013), function to distribute force over additional linkages, and regulate microtubule dynamics (Al-Bassam and Chang, 2011; Bader and Vaughan, 2010). In addition to forces generated either directly or indirectly by microtubules, a third model proposes that the chromosomes themselves may contribute to the segregation process due to entropic forces that act on the DNA (Jun and Wright, 2010; Finan et al., 2011). Although such forces would likely be very small, they may assist chromosome distribution, particularly in smaller cells.

In support of a primary role for microtubules in generating force at kinetochores, microtubules have been shown to generate pulling force during their depolymerization in vitro (Grishchuk et al., 2005; Powers et al., 2009; Tien et al., 2010; Akiyoshi et al., 2010) as well as pushing force during polymerization (Dogterom and Yurke, 1997). During microtubule polymerization, GTP-bound tubulin dimers are added to the growing microtubule plus end (Figure 3A; Desai and Mitchison, 1997). After these dimers are incorporated into the microtubule lattice, GTP is hydrolyzed. The resulting GDP-bound

tubulin dimers associate with each other along an individual protofilament and between neighboring protofilaments within the microtubule lattice to maintain a straight microtubule (Nogales, 2000; Nogales and Wang, 2006). However, when a microtubule switches to depolymerization, a process termed catastrophe, GDP-bound dimers exposed at the microtubule end lose these stabilizing interactions, causing the protofilaments to peel backwards. It is the dynamic plus ends of the microtubules that are embedded in the kinetochore, with the more stable minus ends anchoring the spindle in the centrosomes at either pole (Figure 3B; Cheeseman and Desai, 2008). According to measurements and calculations by Grishchuk et al., the conformational change that occurs for an individual depolymerizing protofilament can generate a power stroke of up to 5 pN, suggesting that a depolymerizing microtubule composed of 13 protofilaments could generate as much as 65 pN force (2005). In addition, polymerizing microtubules have been shown to produce up to 3-4 pN of force, suggesting that there may also be a contribution of pushing forces at the kinetochore. However, the rate of polymerization is only 0.2 μm/ min (Dogterom and Yurke, 1997), approximately 10 fold slower than the rates of chromosome motion observed in the cell (Inoué and Salmon, 1995), suggesting that depolymerization, which has been observed to occur at rates much faster than chromosome motion, is most likely the major contributor to chromosome motion. Importantly, to harness this force and ensure proper chromosome movement, it is critical to control microtubule polymerization and depolymerization at kinetochores. The formation of kinetochore-microtubule attachments as well as the resulting tension may directly modulate microtubule dynamics by slowing microtubule depolymerization and decreasing the rate of catastrophe (Akiyoshi et al., 2010; Umbreit

et al., 2012; Franck et al., 2007). In addition to modulation by kinetochore attachment, microtubule polymerization factors such as the tumor over-expressed gene (TOG) domain proteins, XMAP215 and cytoplasmid linker-associated proteins (CLASP), and depolymerases such as kinesin-13 proteins, that are present both at the kinetochore and on the spindle also play a role in controlling microtubule dynamics (Al-Bassam and Chang, 2011; Bader and Vaughan, 2010).

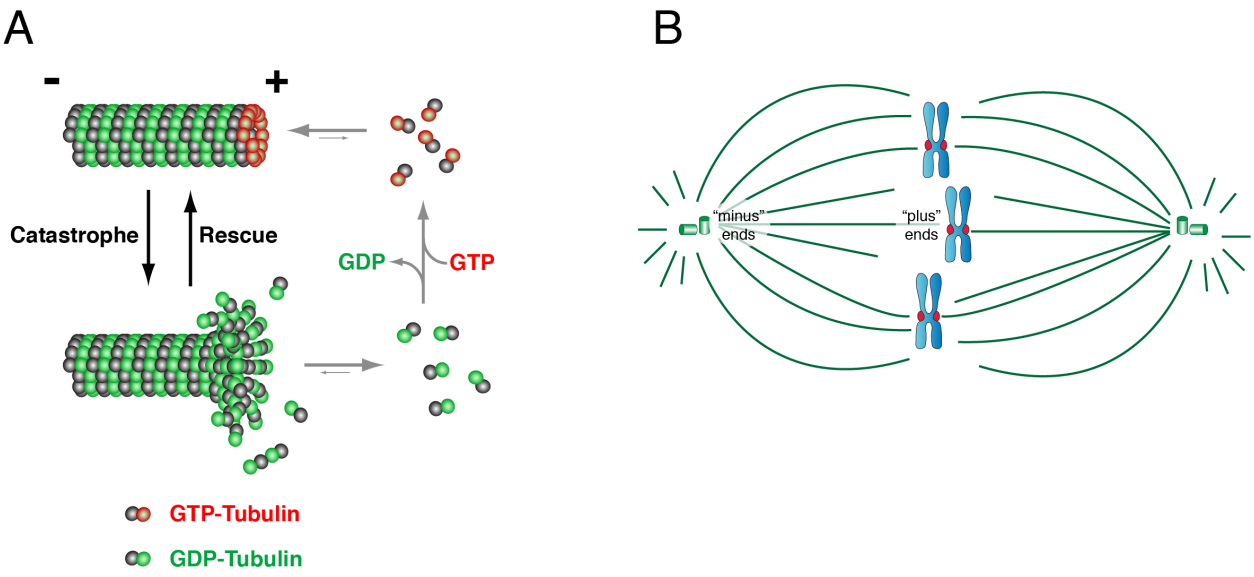

Figure 3: Dynamic microtubules form and power the mitotic spindle. A) Microtubule polymerization and depolymerization at the plus end is regulated by the nucleotide bound state of tubulin dimers. Polymerization results in a GTP-cap at the plus end of the microtubule. As the GTP is hydrolyzed, the stable cap is lost, resulting in catastrophe. As microtubule protofilaments depolymerize, the straight microtubule lattice is lost and the protofilaments curl back (Adapted from Cheeseman and Desai, 2008). B) Microtubules (green lines) emanate from the centrosomes (green cylinders) at either spindle pole, anchored by their minus ends. The plus ends extend toward the chromosomes (blue) where they can attach to kinetochores (red).

Although microtubule depolymerization has the capacity to generate force, it is important to define how kinetochores attach to and couple chromosome movement to depolymerizing microtubules. Thus far, two models that are not mutually exclusive have dominated the literature to explain how kinetochores harness the force from microtubule depolymerization. The first model, termed the “Hill Sleeve” model or “biased diffusion,”

postulates that the association of the kinetochore with a microtubule is formed by multiple weak interactions that can diffuse equally in either direction (Hill, 1985). However, due to a large free energy barrier that disfavors the loss of an interaction, this diffusion is biased toward the microtubule minus end as binding sites disappear from the plus end. The second model, termed the “forced-walk” model, proposes that the kinetochore is coupled to microtubules in such a way that, as the protofilaments peel backwards during depolymerization, the coupling protein is pushed along the microtubule (Molodtsov et al., 2005). The way in which the microtubule is connected to the kinetochore has important implications for understanding how the force produced by microtubule depolymerization manifests at the kinetochore and remains an important focus for future work.

Recent studies have focused on how kinetochores and certain kinetochore protein components harness the energy produced by microtubule depolymerization. These studies have tested key players at the kinetochore-microtubule interface, such as the Ndc80, Dam1, and Ska1 complexes (McIntosh et al., 2008; Lampert et al., 2010; Tien et al., 2010; Powers et al., 2009; Welburn et al., 2009; Schmidt et al., 2012; Volkov et al., 2013) for their abilities to track on depolymerizing microtubules, and have attempted to analyze the kinetochore as a whole using partial purifications of kinetochores from *S. cerevisiae* (Akiyoshi et al., 2010). Although individual protein complexes and isolated yeast kinetochore particles are able to track depolymerizing microtubules, studies performed using optical tweezers have found that the tested proteins and complexes are able to withstand less than 10 pN of pulling force before a rupture event is observed (Akiyoshi et al., 2010; Powers et al., 2009; Tien et al., 2010).

This is in contrast to the theoretical maximum of 65 pN that a single microtubule has been proposed to produce during depolymerization (Grishchuk et al., 2005). It is likely that in the context of a kinetochore assembled on a chromosome, the complex architecture of the kinetochore has the capacity to harness and withstand larger forces. Thus, the *in vivo* load-bearing properties of the kinetochore likely depend on a combination of the properties of both the individual protein components and the organization of the entire complex.

Signaling the Bi-orientated State of Chromosomes

During mitosis, it is critical that paired sister chromatids attach to opposite spindle poles. When this “bi-orientation” fails, this error must be detected and corrected, and a signal to delay cell cycle progression must be produced to prevent chromosome missegregation. Work performed by Bruce Nicklas and colleagues demonstrated that the external application of force to a chromosome using a microneedle could overcome the checkpoint signal generated by an unattached kinetochore (Li and Nicklas, 1995; Nicklas et al., 1995). This and other work has supported the model that the tension produced on bi-oriented sister kinetochores can alter the signaling state of the kinetochore. This tension results in two apparent physical alterations to mitotic chromosome structure: an increase in the distance between paired sister kinetochores and an increase in the distance between the inner and outer kinetochore regions of a single kinetochore. Under some conditions, this inter- and intra-kinetochore stretch can be uncoupled (Maresca and Salmon, 2009), and recent research has focused on the importance of intra-kinetochore stretch in modulating the signals that monitor

attachment state. By measuring the relative spatial positions of the different kinetochore proteins, work from several groups has found that kinetochore structure is altered when chromosomes are bi-oriented relative to conditions of reduced tension (Maresca and Salmon, 2009; Uchida et al., 2009; Wan et al., 2009; Suzuki et al., 2011; Dumont et al., 2012). Bi-orientation results in the separation of inner kinetochore components (such as CENP-A and CENP-C) from outer kinetochore components (such as Ndc80 and Mis12) as well as changes in the spatial distribution of other proteins within the kinetochore and possibly conformational changes within the proteins themselves.

Because the generation of tension is dependent upon the presence of opposing forces, changes in kinetochore structure correlate with the successful bi-oriented arrangement of chromosomes on the metaphase plate (Figure 4A; Wan et al., 2009). In contrast, when one sister kinetochore lacks an attachment to the spindle (monotelic), or if both kinetochores attach to the same pole (syntelic) (Figure 4A), it is not possible to generate similar opposing forces. However, even in these cases, some force may still be present due to the viscosity of the cytoplasm resisting chromosome movement (Taylor, 1965; Nicklas, 1965), or the action of chromokinesins that generate polar ejection forces (Mazumdar and Misteli, 2005; Cane et al., 2013). It remains unclear how force is exerted on a single kinetochore that simultaneously attaches to opposing spindle poles (merotelic) (Figure 4A), or how these incorrect attachments are resolved (Matos and Maiato, 2011; Gregan et al., 2011). Nevertheless, careful quantitative analysis of the dynamic changes in the distances between CENP-C and Hec1 or Cdc20 during sister chromatid oscillations has supported the model that changes in intra-kinetochore distance are force-dependent and play a role in signaling bi-orientation

(Dumont et al., 2012). However, it remains a possibility that these structural alterations may instead be the result of changes in the conformation, organization, or localization of proteins within the kinetochore.

Although tension plays an important role in sensing the formation of correct attachments, the first check of bi-orientation occurs at the level of microtubule attachment. The spindle checkpoint proteins work together to sense the presence of unattached kinetochores and generate a signal that propagates through the cell to prevent the metaphase to anaphase transition (Figure 4B). As described above, the checkpoint proteins are recruited to the kinetochore by MPS1 phosphorylated KNL1 in specific motifs termed the MELT repeats. These phosphorylated motifs allow recruitment of Bub3, Bub1 and BubR1. It is the presence of the BUBs at the kinetochores that leads to recruitment of MAD1, which causes the conversion of the checkpoint protein MAD2 from the open to the closed conformation. The closed conformation of MAD2 is able to bind Cdc20. In its MAD2 bound form, Cdc20 is not able to activate the APC/C, thus preventing the series of proteolysis events that result in the irreversible metaphase to anaphase transition.

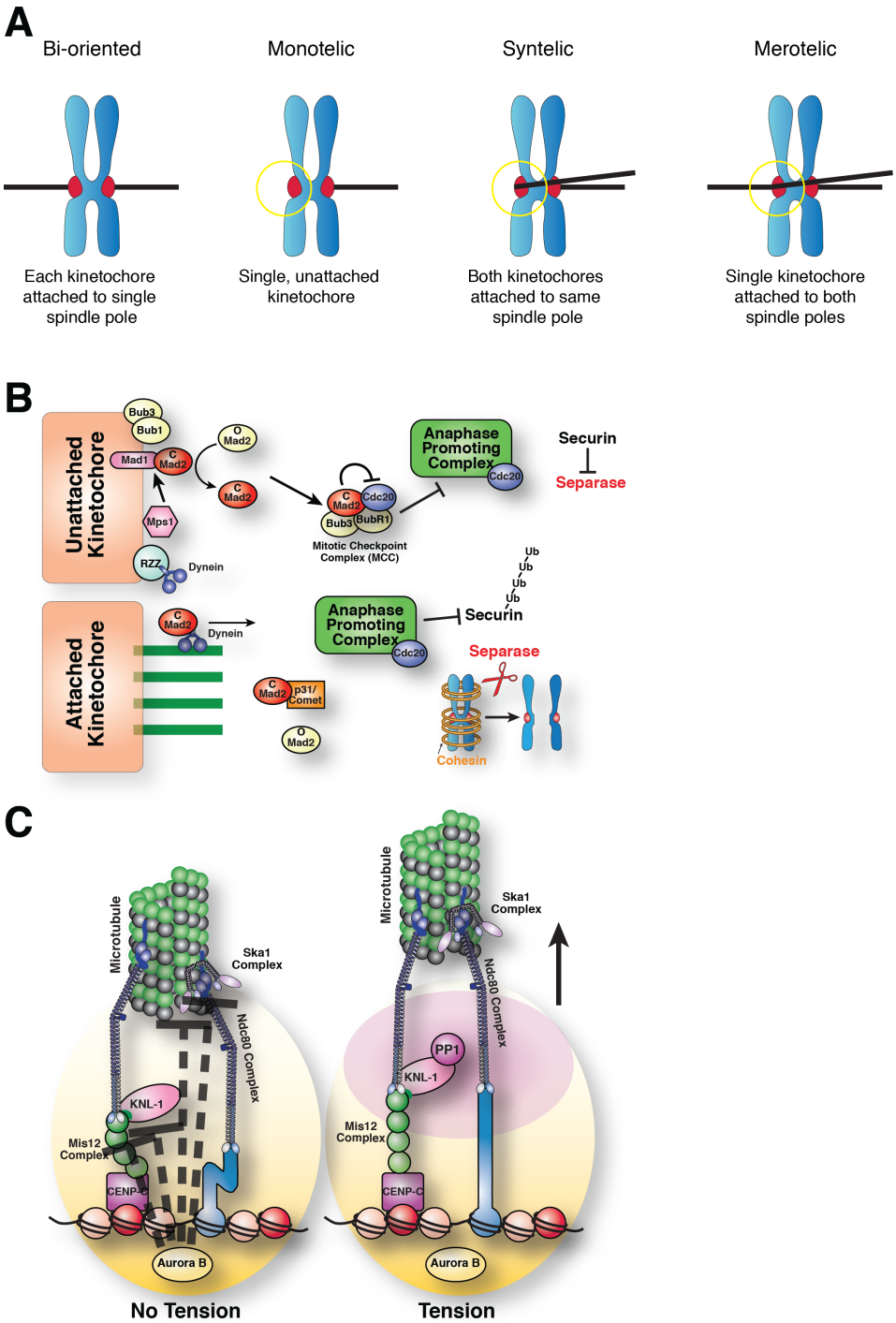

Figure 4: Assessing chromosome bi-orientation. A) Models of bi-oriented, monotelic, syntelic and merotelic attachment of chromosomes (blue, kinetochores shown in red) to the spindle (black). The misattached kinetochore is shown in a yellow circle. B) The spindle checkpoint proteins work together to sense unattached kinetochores and inhibit activation of the APC/C. Upon microtubule attachment, these proteins are stripped from the kinetochore, allowing APC/C activation and ultimately cohesin cleavage. C) Upon bi-orientation, the kinetochore is stretched relative to the no tension state, pulling the outer kinetochore proteins away from Aurora B kinase. This, combined with activity of the PP1 phosphatase results in loss of phosphorylation of many Aurora B kinase targets, thereby stabilizing microtubule attachments. (B and C reprinted with permission from Cheeseman, 2014)

Ultimately, it is important to translate the mechanical signals produced by force at kinetochores into a chemical signal that regulates the activities of kinetochore proteins. A key player in correcting errors in microtubule attachment state is the Aurora B kinase. Substrates for Aurora B show tension-sensitive phosphorylation; they are highly phosphorylated in the absence of tension and become dephosphorylated by PPI upon bi-orientation (Figure 4C; Liu et al., 2009; Welburn et al., 2010). The forces generated at kinetochores have been implicated in controlling Aurora B signaling by altering the spatial separation between the kinase and its substrates (Tanaka, 2002; Liu et al., 2009), although other models for tension-sensitive Aurora B phosphorylation have also been proposed (Sandall et al., 2006). The key substrates of Aurora B are located at the outer kinetochore, and can be more than 100 nm away from the majority of Aurora B, which is localized at the inner centromere, depending on whether the sister kinetochores are under tension (Wan et al., 2009). Therefore, structural changes caused by opposing force at kinetochores separate the kinase and its substrates. The increased separation under tension makes Aurora B less likely to phosphorylate its now distant substrates (Liu et al., 2009; Welburn et al., 2010). One effect of Aurora B phosphorylation on outer kinetochore proteins is to reduce their microtubule binding affinity (Cheeseman et al., 2006; Welburn et al., 2010; Schmidt et al., 2012). Thus, it has been proposed that the presence of tension can ultimately stabilize microtubule attachments through changes in kinetochore conformation that cause a decrease in Aurora B phosphorylation, which in turn increases the microtubule binding activities of various kinetochore components. In contrast, increased phosphorylation by Aurora B of

these outer kinetochore targets leads to decreased microtubule attachment, which activates the spindle assembly checkpoint.

In addition to altering the signaling state of kinetochores, changes in force at kinetochores may also have a direct effect on microtubule binding. One recent study suggested that outer kinetochore proteins are force sensitive and show catch-slip properties (Akiyoshi et al., 2010), resulting in less frequent detachment under increasing force. This is analogous to a “Chinese finger trap,” and would allow the attachment to become stabilized as the microtubule pulls on the kinetochore. Whether tension affects kinetochore-microtubule attachments directly or indirectly, force appears to play an essential role in establishing and signaling bi-orientation in addition to driving chromosome movement.

Theoretical Considerations for Force Resistance

Force is a vector quantity that, when applied to a bond, decreases energy barriers, increasing the likelihood of bond breakage. Although the kinetochore must function under force to perform its roles properly, this force also represents a challenge with the potential for deleterious consequences to kinetochore function. The application of tensile forces could result in protein unfolding or the breakage of protein-protein interactions (Figure 5). If a core kinetochore protein unfolded, or if protein interactions within the kinetochore were disrupted, the connectivity between centromeric DNA and the microtubules would be compromised. The typical force required to unfold a protein or break protein-protein interactions is in the range of 10-100 pN (Sułkowska and Cieplak, 2008; Weisel et al., 2003; Lin et al., 2005). Nicklas did not observe an

immediate rupture of chromosome-spindle attachments even while applying up to 700 pN on chromosomes, suggesting that the kinetochore is constructed in a way that can withstand high loads.

At kinetochores, rupture events due to force-dependent protein unfolding or the loss of protein-protein interfaces are likely avoided at least in part through the architecture and organization of the kinetochore. Previous theoretical work on the effects of force on protein structure and protein-protein interactions has highlighted organization and arrangement as key features for facilitating force resistance (Leckband, 2000; Evans, 2001). In a “series” arrangement, bonds are organized linearly such that the full force is felt by each component. However, in a “parallel” arrangement, the force is divided over multiple attachments arranged in parallel, so that the force felt by each attachment is greatly reduced. The higher order organization of the kinetochore could diffuse the microtubule-generated force over multiple attachments, significantly decreasing the force that is felt by an individual kinetochore protein molecule.

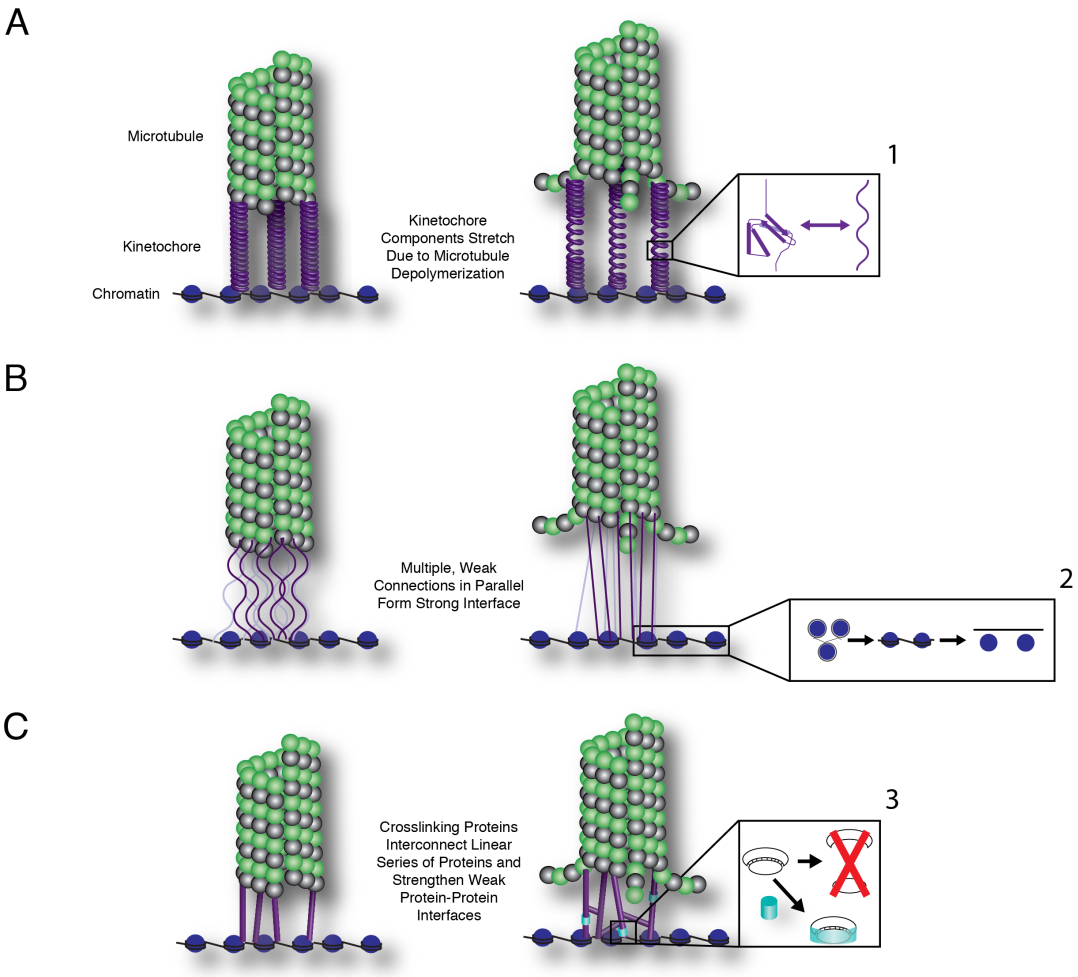

Figure 5: Models for force response at kinetochores at both the individual protein level and global scale. We propose three non-exclusive models for how kinetochores respond to the application of force: A) Kinetochore proteins with elastic properties could serve to absorb some of the force produced by depolymerizing microtubules, B) Multiple weak interfaces could form parallel attachments between the depolymerizing microtubule and chromosome such that the force produced by the microtubule would be diffused across multiple connections, and C) Additional kinetochore components could serve as dynamic crosslinkers to diffuse force and add interactions between pairs of proteins to strengthen the protein-protein interface. The kinetochore protein components themselves could have multiple responses at a molecular level including: (1) Under pulling forces, the bonds holding together the tertiary and secondary structure of a protein can break, causing the protein to unfold. If reversible, this would provide elastic properties, but if permanent, could lead to loss of functional kinetochore components. (2) The force generated by kinetochores is directed toward the limited number of protein-DNA interactions formed between the kinetochore proteins and the chromosome. Some tension may be relieved as the DNA wrapped around adjacent nucleosomes is pulled. This first results in the straightening out of the compact "beads on a string" structure, but with sufficient pulling force, the nucleosomes would be removed from the DNA. (3) Protein-protein interfaces held together by non-covalent bonds can break under pulling force, but the presence of additional proteins to strengthen interactions could prevent the loss of important interfaces.

Although the kinetochore clearly has evolved mechanisms to accommodate potentially large cellular forces, our understanding of the architecture and organization of a kinetochore remains limited. At the level of the minimal molecular path between a microtubule and centromeric DNA, the proteins involved appear to be connected linearly (Figure 2; Gascoigne et al., 2011; Gascoigne and Cheeseman, 2011; Schleiffer et al., 2012; Bock et al., 2012). However, there are multiple connections formed between the centromere and a single microtubule. For example, as many as 10-20 kinetochore-localized Ndc80 complexes have been quantified per microtubule in both fungi and vertebrate cells (Lawrimore et al., 2011; Joglekar et al., 2006; 2008; Johnston et al., 2010), supporting the parallel model. The complexities of these connections have proven a hurdle to devising methods to measure the force produced by microtubules on specific kinetochore components or the total force exerted on the kinetochore during normal mitotic processes.

In addition to defining the forces that kinetochore proteins experience, the amount of force necessary to break a bond depends upon both the loading rate (force/time) and the duration of the applied force (Merkel et al., 1999). For the kinetochore, the extended periods of force experienced during metaphase (where sister chromatids move under force in one direction for 1-2 minutes (Mitchison and Salmon, 1992)), as well as the abrupt changes in force that occur during sister chromatid oscillations, have the potential to result in a high loading rate and extended durations of applied force. As such, it will be important to account for the way that these challenges are accommodated at kinetochores. Several calculations have estimated the power output of the grasshopper and yeast spindles (Bloom, 2008; Nicklas, 1988), and

provided indirect measures for the spring constant of the kinetochore based on analysis of the chromatin spring constant during anaphase (Fisher et al., 2009). However, due to experimental limitations, it has not been possible to precisely determine the force constant and other key force parameters at kinetochores. Without knowledge of the force constant, it is not possible to calculate the loading rate experienced by a kinetochore. Thus, defining these parameters for kinetochores is an important area for future work.

Force at the Kinetochore-DNA Interface

Force also has the potential to disrupt protein-DNA interactions (Figure 5). The kinetochore is assembled on centromeric DNA, but if the kinetochore-chromatin interface were disrupted, kinetochore function would be lost. One way in which this force could be accommodated is that the force applied through the kinetochore displaces nucleosomes in pericentric regions, alleviating the mechanical stress experienced by the kinetochore itself (Bouck and Bloom, 2007; Verdaasdonk et al., 2012). Studies of the chromatin force response in *S. cerevisiae* have shown that a deformation of chromatin structure occurs in the regions immediately surrounding the centromere during mitosis (Pearson et al., 2001; Bouck and Bloom, 2007), and that there is an increased turnover of nucleosomes in these surrounding regions (Verdaasdonk et al., 2012), consistent with loss of nucleosomes from DNA under tensile stress. Directed analyses have measured the force required to displace nucleosomes from DNA. These studies have obtained values of between 4 and 20 pN to irreversibly remove a nucleosome from DNA depending upon the specific approach and source of

nucleosomes that was used (Cui and Bustamante, 2000; Yan et al., 2007; Bennink et al., 2001; Brower-Toland et al., 2002). For these studies, force was applied to the ends of the DNA rather than perpendicular to the DNA strand as would occur at kinetochores. This difference in the directionality of force may alter the amount of force necessary to remove a nucleosome from chromatin under mitotically applied forces. In addition, it has been shown that condensin and cohesin in the pericentromeric chromatin allow for remodeling of the chromatin lending elastic properties to the chromatin and may function to dissipate tension applied by the spindle microtubules on the kinetochore and centromere (Haase et al., 2012; Stephens et al., 2013; 2011).

Nucleosome displacement and chromatin stretching in pericentric regions could allow the chromosome to absorb some force. However, nucleosome-DNA interactions must be maintained at the kinetochore-centromere interface. At centromeres, there are two key connections between kinetochore proteins and the underlying DNA, one via CENP-A, and the other via CENP-T/-W/-S/-X (Gascoigne and Cheeseman, 2011; Gascoigne et al., 2011; Nishino et al., 2012). Although nucleosomes in the pericentromere could be displaced in the presence of force without severe consequences, the loss of the interaction of CENP-A or CENP-T with DNA would eliminate kinetochore function. Both the CENP-A nucleosome and the CENP-T-W-S-X complex are structurally distinct from canonical nucleosomes (Sekulic et al., 2010; Nishino et al., 2012) raising the possibility that they may have different force-resistance properties. Future work characterizing the behavior of these specialized nucleosomes and the other kinetochore components will be important to understand how intra-kinetochore and kinetochore-DNA attachments are maintained in the presence of force.

How is force accommodated at kinetochores?

Although the roles of force at kinetochores have been a focus of recent work, less is known about how kinetochores are able to accommodate the forces generated at these sites. Recent work has isolated kinetochore particles from budding yeast (Akiyoshi et al., 2009) and partially reconstituted kinetochores from *Xenopus laevis* extract on defined templates (Guse et al., 2011). Although it is not clear how accurately these assemblies represent functional kinetochores, the reconstitution of kinetochore-like structures in vitro should allow for the analysis of its force resistance properties. At present it remains unclear which proteins at kinetochores contribute to force resistance and how kinetochores are organized to achieve this. Current data suggests that there are two separate connections between centromeric DNA and microtubules. The first path involves an attachment of CENP-A to CENP-C, followed by the Mis12 complex, which contacts KNL1 and the Ndc80 complex, with Ndc80 completing the connection to the microtubule (Figure 2). The second connection is anchored to centromeric DNA by the CENP-T-W-S-X complex, which makes its own direct connection to the Ndc80 complex. The available biochemical data suggest that these two connections in their most minimal form are constructed linearly, and that there are two separate pools of Ndc80 that make connections to the microtubules from the Mis12 complex and CENP-T (Schleiffer et al., 2012; Bock et al., 2012; Nishino et al., 2013; Malvezzi et al., 2013). This suggests that some parts of the kinetochore might be held together by only a single protein-protein interface. However, it is possible that there are interactions between the CENP-C and CENP-T based pathways, either directly or via other protein components (Gascoigne et al., 2011). If the individual protein-protein interactions within each

pathway cannot withstand the force produced by the depolymerizing microtubule, then the current architectural models of the kinetochore may be incomplete.

Based on the currently available structural details for the kinetochore, several different models could explain how kinetochores withstand cellular forces (Figure 5). First, kinetochore proteins may have evolved special properties that allow them to withstand force. It is possible that a subset of kinetochore proteins have elastic properties, such as those suggested by the elongation of CENP-T (Suzuki et al., 2011; 2014), and CENP-C (Suzuki et al., 2014). Elastic properties could serve two functions within the kinetochore. They could behave in the same way as nucleosome displacement in pericentric chromatin (Verdaasdonk et al., 2012) and chromatin relaxation facilitated by higher order chromatin structures formed by cohesin and condensin (Stephens et al., 2013; 2011) to reversibly accommodate the force applied to the chromatin. In this case, the elastic components in the kinetochore would be easily able to deform under tension and then return to their resting conformation once the force was removed without causing irreversible damage to the protein. In addition, elasticity of a protein as part of a series arrangement within the kinetochore could allow it to absorb energy, thereby decreasing the force passed through the subsequent protein-protein interfaces. For an elastic protein to dampen the force applied by the spindle, the spring component would need to always be actively stretching, and not be allowed to reach equilibrium before it was allowed to relax. In this model, energy is absorbed by breaking or rearranging bonds within kinetochore proteins rather than between proteins, thereby protecting the key interfaces within the kinetochore. Without more detailed knowledge of the mechanical properties of the individual kinetochore

components, it is not possible to predict whether this can occur. Second, the connections between the microtubule and centromere are likely to be arranged in a parallel manner such that they sum to a strong interface. The multiple copies of each core kinetochore protein that are present per microtubule (Joglekar et al., 2006; 2008; Johnston et al., 2010; Lawrimore et al., 2011) support at least a partial contribution of this parallel model. Third, there may be additional kinetochore proteins that are not part of the linear connectivity between the centromere and microtubule, but that strengthen connections between kinetochore components that would otherwise be too weak. For example, the *Tetrahymena thermophila* cilia protein Bld10 has recently been proposed to structurally stabilize the basal body under the force generated during cilia beating (Bayless et al., 2012). At kinetochores, proteins could serve a similar role either by serving as dynamic crosslinkers, connecting separate linear pathways, or by reinforcing existing connections by adding contacts between proteins. It is likely that the actual force resistance properties of the kinetochore complex require a combination of all three models.

Work spanning the last 60 years has shown that the mitotic spindle can generate the force that acts on kinetochores. The work summarized here provides a preliminary foundation for understanding the consequences of force at kinetochores, but the proposed models will change as more is discovered about kinetochore structure and organization. Defining the force resistance properties of the kinetochore will provide a better understanding of how it is able to function in the presence of force, and the mechanisms by which it acts during chromosome segregation. As we look toward the future prospects of the field, the advances in the biophysical understanding of focal

adhesions (Roca-Cusachs et al., 2012) provide an excellent blueprint for generating a detailed molecular picture of a large protein complex that functions under force. For focal adhesions, researchers have defined the pathway between the extracellular matrix and the cytoskeleton, analyzed the force response of each component along this pathway, and defined how cells utilize mechanosensors to signal to the cell. Achieving a similar understanding for the kinetochore will provide key insights into the function of this central cell division structure.

The Architecture of the Kinetochore Dictates its Force Resistance Properties

When considering the force resistance properties of any large protein assembly, it is important to recognize that it is the relative organization of the various protein components that is responsible for maintaining the integrity of the macromolecular complex. Having a clear picture of this organization is particularly important for the kinetochore due to uncertainties related to the nature of the force production. At kinetochores, it is not straightforward to determine the force being applied by microtubules, as this force is not necessarily an additive property of all the microtubules present per kinetochore. As described above, each kinetochore contains many copies of each protein, which in turn form interactions with the multiple microtubules present at each chromosome. Electron microscopy has documented that multiple microtubules bind to each kinetochore, but this approach provides only a static snapshot of the kinetochore. From these data, it is not possible to ascertain how many of the microtubules are actively forming interactions with the kinetochore proteins at any given time, adding ambiguity to the kinetochore models. In addition, the microtubules are not

all necessarily fully engaged (i.e. an attachment is made to each individual protofilament by Ndc80 or another factor), so the power production by each microtubule may not be at its maximum. Finally, while the majority of microtubules at the poleward moving kinetochore are most likely depolymerizing, there may be some microtubules that are polymerizing. Since the pulling force that stabilizes such polymerization is not present in poleward movement kinetochores, polymerization events would not be favored and would only have a minor counter-acting effect on the tensile stresses produced at the kinetochore.

These considerations for the properties and behavior of entire macromolecular kinetochore structure demonstrate the complexity in trying to understand the force resistance properties of the kinetochore. In order to make strides in our understanding of the kinetochore as a molecular machine, it is important to begin by detailing the molecular architecture underlying the force resistance properties and using this to build up models for how various iterations of the basic structural unit can sum to a force resistant machine capable of making and sustaining attachment to the depolymerizing microtubules of the spindle. To do this, both the response of the individual protein components under tensile stresses as well as the properties of the protein-protein interfaces must be considered. For the kinetochore, it is not yet possible to model its force resistance properties with molecular detail because the architecture is still poorly understood. A clearer model of the various protein-protein interactions that make up the kinetochore structure will provide insight into how the various force accommodating properties proposed above may apply to the kinetochore. The organization of the various protein components will allow modeling of the various ways in which the

kinetochore may accommodate force, but in the future it will be important to also consider the microtubule binding of the larger kinetochore assembly.

Findings Presented in this Thesis

During my graduate work, I used biochemical and cellular approaches to analyze the molecular organization and regulation of the core structural components of the kinetochore. First, in a collaboration with the Fukagawa lab, I used recombinantly expressed and reconstituted protein complexes to perform in vitro binding assays and describe the direct connection between CENP-T, an inner kinetochore component, and the Ndc80 complex, the protein complex directly responsible for the kinetochore interaction with microtubules (Chapter II). During the course of these studies, I also discovered that the interaction between the Ndc80 complex and CENP-T is mutually exclusive with the interaction between the Ndc80 complex and the Mis12 complex. These biochemical studies suggested that there might be differences in construction between the previously defined CENP-C/KMN assembly and this newly defined CENP-T/KMN assembly.

To study each pathway in isolation, I separated these pathways by targeting CENP-C and CENP-T independently to an ectopic chromosomal locus in human cells. Using this approach, I was able to reveal that the organization of the KMN network components downstream of CENP-C versus CENP-T is distinct (Chapter III). CENP-C recruits the Ndc80 complex through its interactions with KNL1 and the Mis12 complex. In contrast, CENP-T directly interacts with Ndc80, which in turn promotes KNL1/Mis12 complex recruitment through a separate region on CENP-T, resulting in functional

relationships for KMN network localization that are inverted relative to the CENP-C pathway. I also investigated the regulatory mechanisms by which assembly of each pathway is controlled and found that distinct regulatory paradigms control the assembly of these pathways, with Aurora B kinase promoting KMN network recruitment to CENP-C, and cyclin-dependent kinase (CDK) regulating KMN network recruitment to CENP-T. These experiments at the ectopic foci made multiple predictions for the organization of the endogenous kinetochore, which I was able to confirm by various combinations of RNAi and drug treatments that led to disassembly of endogenous kinetochores during mitosis. This work reveals unexpected complexity for the architecture and regulation of the core components of the kinetochore-microtubule interface.

Chapter II: CENP-T and the Mis12 complex/KNL1 bind the Ndc80 complex in a mutually exclusive manner

Reprinted from EMBO Press:

Nishino, T., F. Rago, T. Hori, K. Tomii, I.M. Cheeseman, and T. Fukagawa. 2013. CENP-T provides a structural platform for outer kinetochore assembly. *EMBO J*. 32:424–436. doi:10.1038/emboj.2012.348.

Tatsuya Nishino designed and performed structural and biochemical experiments for the chicken recombinant protein complexes. Tetsuya Hori and Tatsuo Fukagawa performed cell biological experiments with DT40 cells. Kentaro Tomii analyzed CENP-T sequences in various species.

Summary

The kinetochore forms a dynamic interface with microtubules from the mitotic spindle during mitosis. The Ndc80 complex acts as the key microtubule-binding complex at kinetochores. However, it is unclear how the Ndc80 complex associates with the inner kinetochore proteins that assemble upon centromeric chromatin. Here, based on a high-resolution structural analysis, we demonstrate that the N-terminal region of vertebrate CENP-T interacts with the “RWD” domain in the Spc24/25 portion of the Ndc80 complex. Phosphorylation of CENP-T strengthens a cryptic hydrophobic interaction between CENP-T and Spc25 resulting in a phospho-regulated interaction that occurs without direct recognition of the phosphorylated residue. The Ndc80 complex interacts with both CENP-T and the Mis12 complex, but we find that these interactions are mutually exclusive, supporting a model in which two distinct pathways target the Ndc80 complex to kinetochores. Our results provide a model for how the multiple protein complexes at kinetochores associate in a phospho-regulated manner.

Introduction

The kinetochore forms a dynamic interface with microtubules from the mitotic spindle to facilitate faithful chromosome segregation during mitosis (Cheeseman and Desai, 2008; Santaguida and Musacchio, 2009). To establish a functional kinetochore, two key groups of structural proteins are required. First, a subset of inner kinetochore proteins binds to centromeric DNA to provide a platform for kinetochore assembly. Second, additional outer kinetochore proteins are recruited to centromeres to form robust interactions with spindle microtubules. The kinetochore-microtubule interface is composed of the highly conserved kinetochore complexes referred to as the KMN network, which includes KNL1, the 4 subunit Mis12 complex (Mis12, Nnf1, Nsl1, and Dsn1), and the 4 subunit Ndc80 complex (Ndc80, Nuf2, Spc24, and Spc25) (DeLuca and Musacchio, 2012). Depletion of any component of the KMN proteins results in mitotic defects and a reduction in kinetochore-microtubule attachments (Martin-Lluesma et al., 2002; DeLuca et al., 2002; McCleland et al., 2003; Hori et al., 2003; Cheeseman et al., 2004; Obuse et al., 2004; Cheeseman et al., 2006; DeLuca et al., 2006; Kline et al., 2006; Kiyomitsu et al., 2007; Cheeseman et al., 2008). The KMN network binds directly to microtubules in vitro (Cheeseman et al., 2006; McIntosh et al., 2008; Powers et al., 2009). In particular, the Ndc80 complex has structural properties including an extended rod-shaped structure and a direct interaction with the microtubule lattice that make it well suited to act as the primary kinetochore-microtubule interface (Cheeseman et al., 2006; Wei et al., 2007; Ciferri et al., 2008; Wilson-Kubalek et al., 2008; Alushin et al., 2010). However, it is still unclear how the Ndc80 complex associates with inner kinetochore proteins to target this key complex to centromeres. In contrast to the outer

kinetochore, which is required only during mitosis, inner kinetochore components localize to centromeres throughout the cell cycle. This constitutive centromere-associated network of proteins (CCAN) (Okada et al., 2006; Cheeseman and Desai, 2008; Hori et al., 2008; Amano et al., 2009; Perpelescu and Fukagawa, 2011) provides a platform for outer kinetochore assembly. For example, the CCAN component CENP-C directly associates with the Mis12 complex (Liu et al., 2006; Przewloka et al., 2011; Screpanti et al., 2011; Gascoigne et al., 2011; Kwon et al., 2007). In addition, we have previously found that the CCAN component CENP-T is required to recruit the KMN network and assemble functional kinetochores (Hori et al., 2008; Suzuki et al., 2011; Gascoigne et al., 2011). CENP-T is an extended molecule that spans the inner and outer kinetochore (Suzuki et al., 2011). The C-terminal region of CENP-T forms a complex with the histone-fold containing proteins CENP-W, CENP-S, and CENP-X to form a nucleosome-like structure that binds to centromeric DNA (Hori et al., 2008; Nishino et al., 2012). The N-terminal region of CENP-T associates with the outer kinetochore and is sufficient to direct aspects of outer kinetochore assembly, including binding to and recruitment of the Ndc80 complex in a manner that depends upon the phosphorylation of CENP-T by cyclin dependent kinase (CDK) (Gascoigne et al., 2011). Based on structural predictions, the N-terminal region of CENP-T lacks a defined structure and it is unclear how it associates with the Ndc80 complex. In addition, the basis for the phospho-regulated interaction between CENP-T and the Ndc80 complex is unknown.

To define the nature of the link between the inner and outer kinetochore, we analyzed the structural, biochemical, and functional basis for the CENP-T-Ndc80

complex interaction. We found that phosphorylated and phospho-mimetic peptides from the N-terminal region of CENP-T interact with the Spc24/Spc25 portion of the Ndc80 complex. Multiple kinetochore proteins, including Spc24/25, contain “RWD” domains that are also found in functionally diverse proteins including RING finger proteins, WD-repeat containing proteins, and DEXD-like helicases (Schmitzberger and Harrison, 2012). It has been proposed that RWD domains provide interaction platforms to mediate kinetochore assembly. However, it is unclear how other proteins associate with these domains. Our high-resolution structure of the phospho-CENP-T-Spc24/25 complex reveals that the phosphorylated residues in CENP-T are not directly involved in the interaction with Spc25, but instead form a salt bridge to allow adjacent downstream hydrophobic residues to interact with the RWD containing Spc24/25 complex. Our results provide a model for how the multiple protein complexes at kinetochores associate in a phospho-regulated manner.

Results

The N-terminal region of CENP-T is critical for outer kinetochore assembly

We have shown previously that the N-terminal region of CENP-T is essential for kinetochore assembly in both human and chicken cells (Gascoigne et al., 2011). In particular, we found that the N-terminal 100 amino acids of CENP-T are phosphorylated by cyclin dependent kinase (CDK) to regulate outer kinetochore assembly. To define which regions of CENP-T are critical for recruiting downstream proteins, we tested several deletion constructs within this region (Δ1-30, Δ1-60, Δ69-90, and Δ1-90) using a complementation assay in CENP-T-deficient chicken DT40 cells (Figure 1A). Whereas CENP-T-deficient cells expressing either Δ1-30 or Δ1-60 grew similarly to control cells, CENP-T Δ1-90 and Δ69-90 could not rescue CENP-T depletion (Figure 1A and B). This suggests that a ~20 aa sequence near the N-terminal region of CENP-T that includes the CDK phosphorylation sites T72 and S88 is critical for CENP-T function. Indeed, we found that Ndc80 localization to kinetochores was reduced in cells expressing only CENP-T Δ69-90 or ∆1-90 (Figure 1C; data not shown). Interestingly, an in frame fusion between Spc25 and CENP-T Δ1-90 recruited Ndc80 to kinetochores (Figure 1D) and partially rescued the loss of viability resulting from the depletion of endogenous CENP-T (Figure 1E). This suggests that a primary function for the CENP-T N-terminal region is to interact with the Ndc80 complex and direct outer kinetochore assembly.

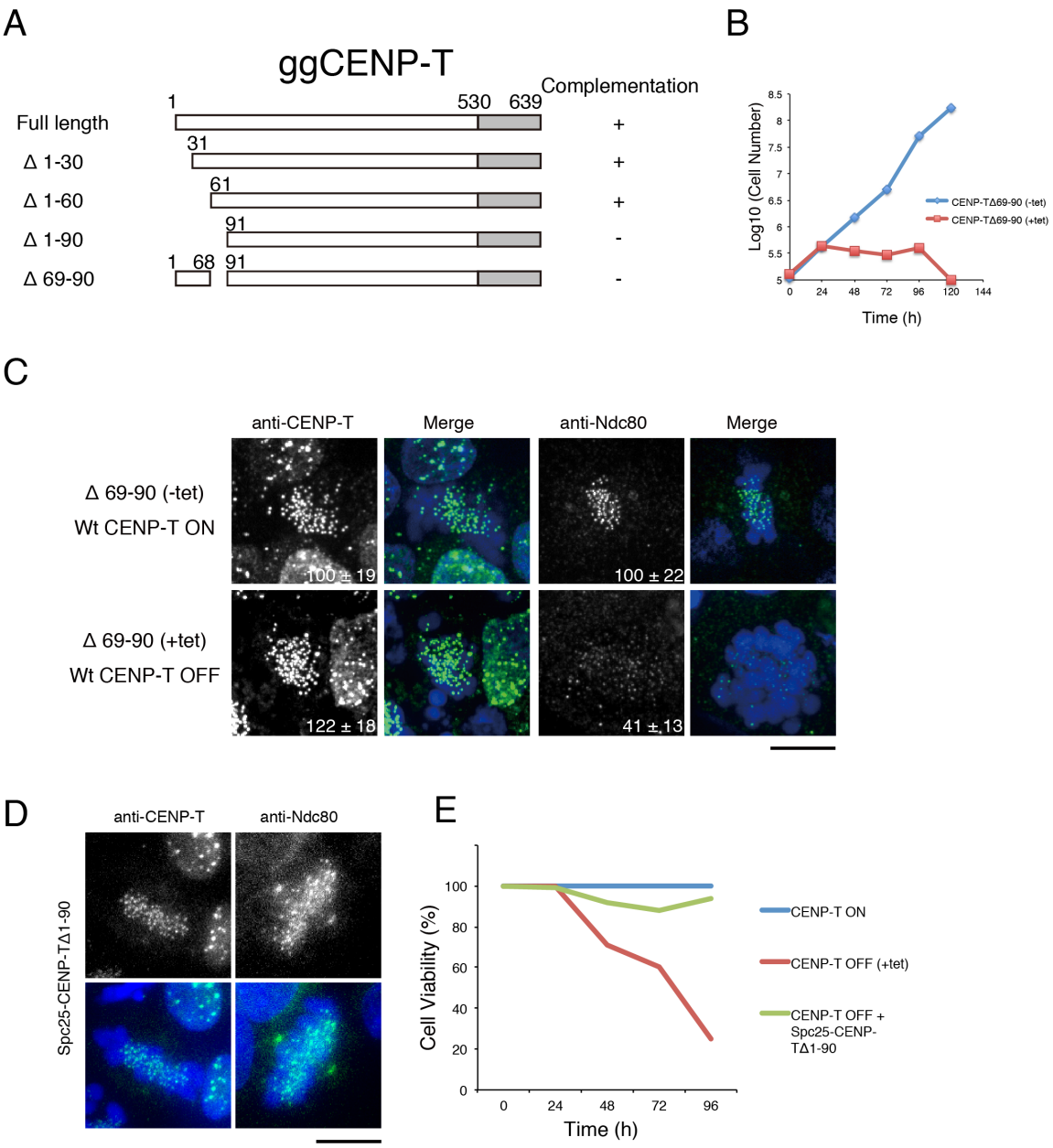

Figure 1: The CENP-T N-terminal region is required for kinetochore localization of the Ndc80 complex. A) Diagram showing the chicken CENP-T sequence and the tested deletion mutants in the CENP-T N-terminal region. "+" or "-" indicates whether the given deletion mutant can complement growth when endogenous CENP-T is depleted. B) Graph showing the growth curve of cells expressing CENP-TΔ69-90 in the presence (red rectangle) or absence (blue diamond) of tetracycline to repress the expression of wild-type CENP-T. C) Immunofluorescence analysis of cells expressing CENP-TΔ69-90 after 72 h in the presence (lower panel) or absence (upper panel) of tetracycline to repress the expression of wild-type CENP-T. Cells were probed for either CENP-T or Ndc80 and the kinetochore signal intensities of each protein were measured relative to an adjacent background signal. Bar, 10 μm. D) Immunofluorescence analysis of cells in which expression of CENP-T is replaced with a Spc25-Δ1-90-CENP-T fusion protein. Ndc80 localizes to kinetochores in these cells, unlike the CENP-T Δ69-90 mutant alone in (C). E) Cell viability analysis for CENP-T conditional knockout cells in the presence (CENP-T OFF) or absence (CENP-T ON) of tetracycline, or expressing a Spc25-Δ1-90 CENP-T fusion protein in the presence of tetracycline (CENP-T OFF + Spc25-Δ1-90 CENP-T).

The CENP-T N-terminal region displays phospho-dependent binding to the Spc24/25 complex

We next sought to define the specific interactions between the N-terminal region of CENP-T and outer kinetochore components. We have shown previously that recombinant human CENP-T-W complex binds directly to the engineered Ndc80^{Bonsai} complex (Gascoigne et al., 2011). The Ndc80 complex has two globular regions separated by an extended coiled-coil with the Ndc80/Nuf2 portion binding to microtubules (Cheeseman et al., 2006; Wei et al., 2007; Ciferri et al., 2008; Wilson-Kubalek et al., 2008; Alushin et al., 2010) and the Spc24/25 portion facing the inner kinetochore (DeLuca et al., 2006; Wei et al., 2006). To determine whether the CENP-T N-terminal region can interact directly with the Spc24/25 portion of the Ndc80 complex, we analyzed the binding between the globular regions of the chicken Spc24/25 sub-complex (125-195 aa of chicken Spc24 and 132-234 aa of chicken Spc25) and chicken CENP-T fragments in vitro. For these experiments, we used both unmodified and phospho-mimetic CENP-T (T72D and S88D) as a Maltose Binding Protein (MBP) fusion. Based on the shift in migration for the Spc24/25 sub-complex as assessed by size exclusion chromatography, the phospho-mimetic CENP-T N-terminal region (using either amino acids 2-98 or 63-98) binds efficiently to Spc24/25 (Figure 2A and 3A). In contrast, either fragment of unphosphorylated wild-type CENP-T or phospho-deficient CENP-T (T72A and S88A) did not bind as strongly to the Spc24/25 complex (Figure 2B and 3C). In addition, although CENP-T fragments containing the extreme N-terminal region of CENP-T (chicken aa 2-50 or human aa 2-32) also have CDK phosphorylation

sites, these fragments did not show detectable interactions with the Spc24/25 complex (Figure 3D).

As we found that both short (63-98) and long (2-98) peptides of CENP-T bound to the Spc24/25 complex (Figure 2A and 3A), we next determined KD's for this binding using composition gradient multi-angle light scattering (CG-MALS) and isothermal titration calorimetry (ITC) (Figure 2C-H). Based on ITC measurements, the KD for binding of the wild-type chicken CENP-T peptide to the chicken Spc24/25 complex was 6.67 μM (Figure 2F). Due to this weaker interaction, it was not possible to define a precise KD for this interaction by CG-MALS. In contrast, phospho-mimetic and synthetic phosphorylated CENP-T peptides bound to more strongly to the Spc24/25 complex and formed a 1:1 stoichiometric complex. The doubly phospho-mimetic CENP-T (T72D and S88D) peptide bound to Spc24/25 with a KD of 381 nM as measured by CG-MALS and 481 nM as measured by ITC (Figure 2C and 2D). Singly modified CENP-T (T72D) bound to the Spc24/25 complex with a KD of 610 nM based on ITC (Figure 2E). Similarly, singly or doubly synthetic phosphorylated CENP-T peptides (either a T72p/S88p double phospho-peptide or a T72p single phospho-peptide) bound to the Spc24/25 complex with KD's of 518 nM or 1.29 μM, respectively, based on ITC measurements (Figure 2G and H). As doubly phosphorylated or phospho-mimetic CENP-T showed increased binding to Spc24/25 relative to singly phosphorylated CENP-T, we used the T72D and S88D double mutant for all subsequent assays.

We have previously shown that unphosphorylated human CENP-T-W binds to the engineered human Ndc80^{Bonsai} complex (Gascoigne et al., 2011). Unlike chicken CENP-T, the unphosphorylated human CENP-T N-terminal fragment (amino acids 76-

106) fused with MBP bound to the human Spc24/25 (137-197 aa of human Spc24 and 129-224 aa of human Spc25) complex with a KD of 645 nM based on ITC (Figure 3E, G) and to the Ndc80^{Bonsai} complex based on gel filtration (Figure 4A). We also confirmed that the unphosphorylated human CENP-T N-terminal region (1-375 aa) without the MBP fusion bound to the Ndc80^{Bonsai} complex by gel filtration (Figure 4B). However, phospho-mimetic human CENP-T showed increased binding to the Ndc80^{Bonsai} complex based on gel filtration (Figure 4A and 4B) and bound to the human Spc24$^{131-197}$/Spc25$^{129-224}$ complex with a KD of 150 nM by ITC (Figure 3 F, H). Based on the combination of these biochemical data, we conclude that the phosphorylated human or chicken CENP-T N-terminal region directly associates with the Spc24/25 portion of the Ndc80 complex.

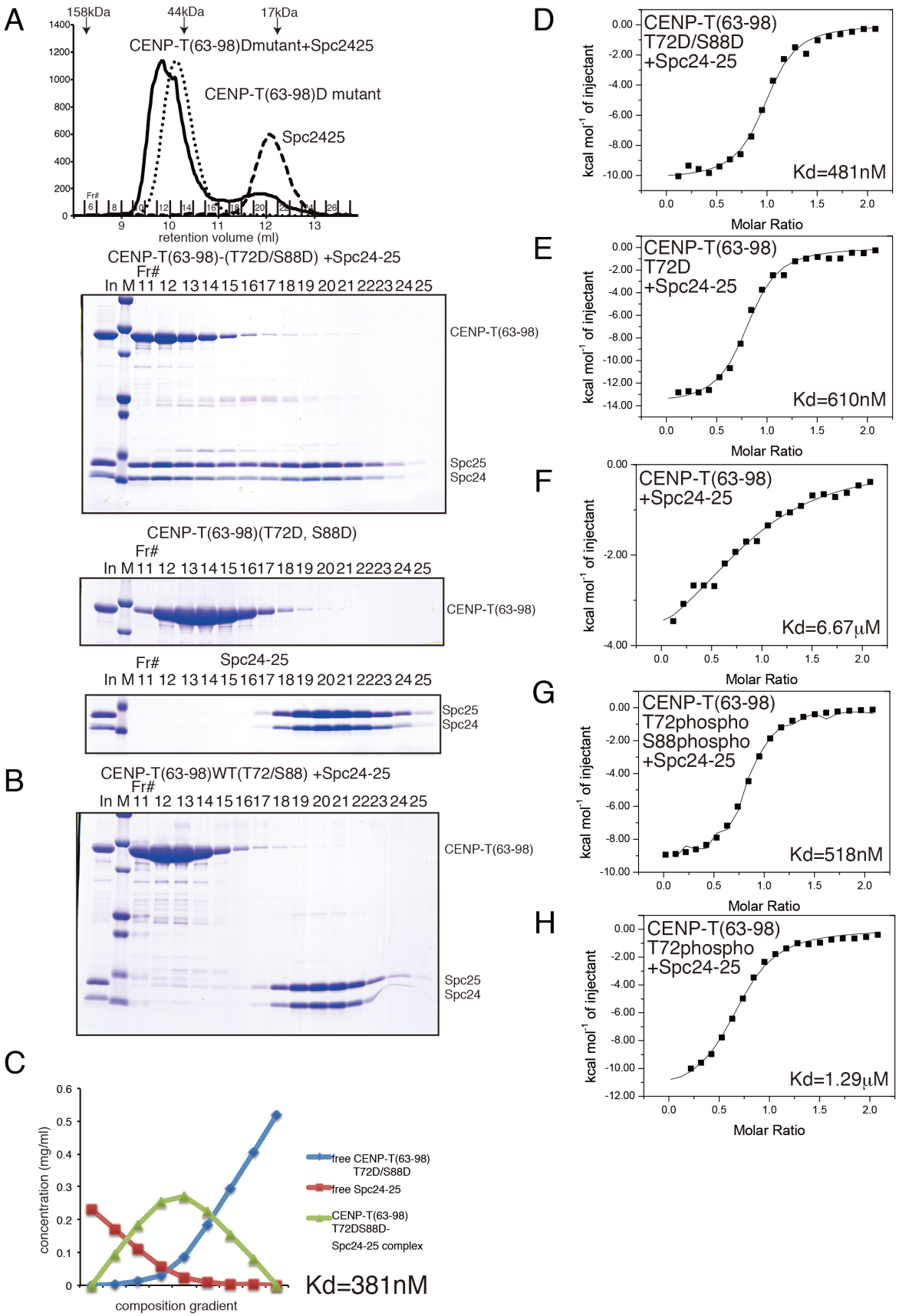
A
158kDa
44kDa
17kDa
CENP-T(63-98)Dmutant+Spc2425
CENP-T(63-98)D mutant
Spc2425
retention volume (ml)
CENP-T(63-98)-(T72D/S88D) +Spc24-25
Fr#
In M 11 12 13 14 15 16 17 18 19 20 21 22 23 24 25
CENP-T(63-98)
Spc25
Spc24
CENP-T(63-98)(T72D, S88D)
Spc24-25
B
CENP-T(63-98)WT(T72/S88) +Spc24-25
C
concentration (mg/ml)
composition gradient
free CENP-T(63-98) T72D/S88D
free Spc24-25
CENP-T(63-98) T72DS88D-Spc24-25 complex
Kd=381nM
D
CENP-T(63-98) T72D/S88D +Spc24-25
Kd=481nM
E
CENP-T(63-98) T72D +Spc24-25
Kd=610nM
F
CENP-T(63-98) +Spc24-25
Kd=6.67μM
G
CENP-T(63-98) T72phospho S88phospho +Spc24-25
Kd=518nM
H
CENP-T(63-98) T72phospho +Spc24-25
Kd=1.29μM
kcal mol-1 of injectant
Molar Ratio

Figure 2: Phospho-mimetic CENP-T binds directly to the Spc24/25 portion of the Ndc80 complex. A) Top, traces (OD214) from the gel filtration column showing the co-migration of chicken Spc24$^{125-195}$/Spc25$^{132-234}$ with phospho-mimetic chicken CENP-T (63-98; T72D and S88D). The phospho-mimetic CENP-T fused with MBP and the globular domains of the Spc24/25 complex were tested individually or mixed and incubated for 15 min at room temperature prior to separation by gel filtration using a Superdex 75 column. Bottom, peak fractions were analyzed by SDS-PAGE and stained with Coomassie. B) Non-phosphomimetic CENP-T$^{63-98}$ does not strongly interact with Spc24/25. Wild-type MBP-CENP-T$^{63-98}$ and the Spc24$^{125-195}$/Spc25$^{132-234}$ complex were analyzed as in (A). C) The phospho-mimetic chicken CENP-T N-terminal region binds to Spc24/25 with high affinity. Composition gradient multi-angle light scattering (CG-MALS) analysis of phospho-mimetic MBP-CENP-T$^{63-98}$ together with the globular domain of the Spc24$^{125-195}$/Spc25$^{132-234}$ complex. Nine different composition gradients were analyzed by multi-angle light scattering to measure the molar mass. Composition of various forms of proteins was calculated by fitting the CG-MALS data and the concentration distribution graph is shown. The two components interacted with 1:1 stoichiometry with a KD of 381nM. D) ITC binding curve for the interaction of phospho-mimetic chicken CENP-T peptide$^{63-98}$ (T72D and S88D) with the Spc24$^{125-195}$/Spc25$^{132-234}$ complex. The measured KD is 481 nM. E) ITC binding curve for the interaction of singly phospho-mimetic chicken CENP-T peptide$^{63-98}$ (T72D) with the Spc24$^{125-195}$/Spc25$^{132-234}$ complex. The measured KD is 610 nM. F) ITC binding curve for the interaction of wild-type chicken CENP-T peptide$^{63-98}$ with the Spc24$^{125-195}$/Spc25$^{132-234}$ complex. The measured KD is 6.67 µM. G) ITC binding curve for the interaction of a synthetic phosphorylated chicken CENP-T peptide$^{63-98}$ (T72p and S88p) with the Spc24$^{125-195}$/Spc25$^{132-234}$ complex. The measured KD is 518 nM. H) ITC binding curve for the interaction of a synthetic phosphorylated chicken CENP-T peptide$^{63-98}$ (T72p) with the Spc24$^{125-195}$/Spc25$^{132-234}$ complex. The measured KD is 1.29 µM.

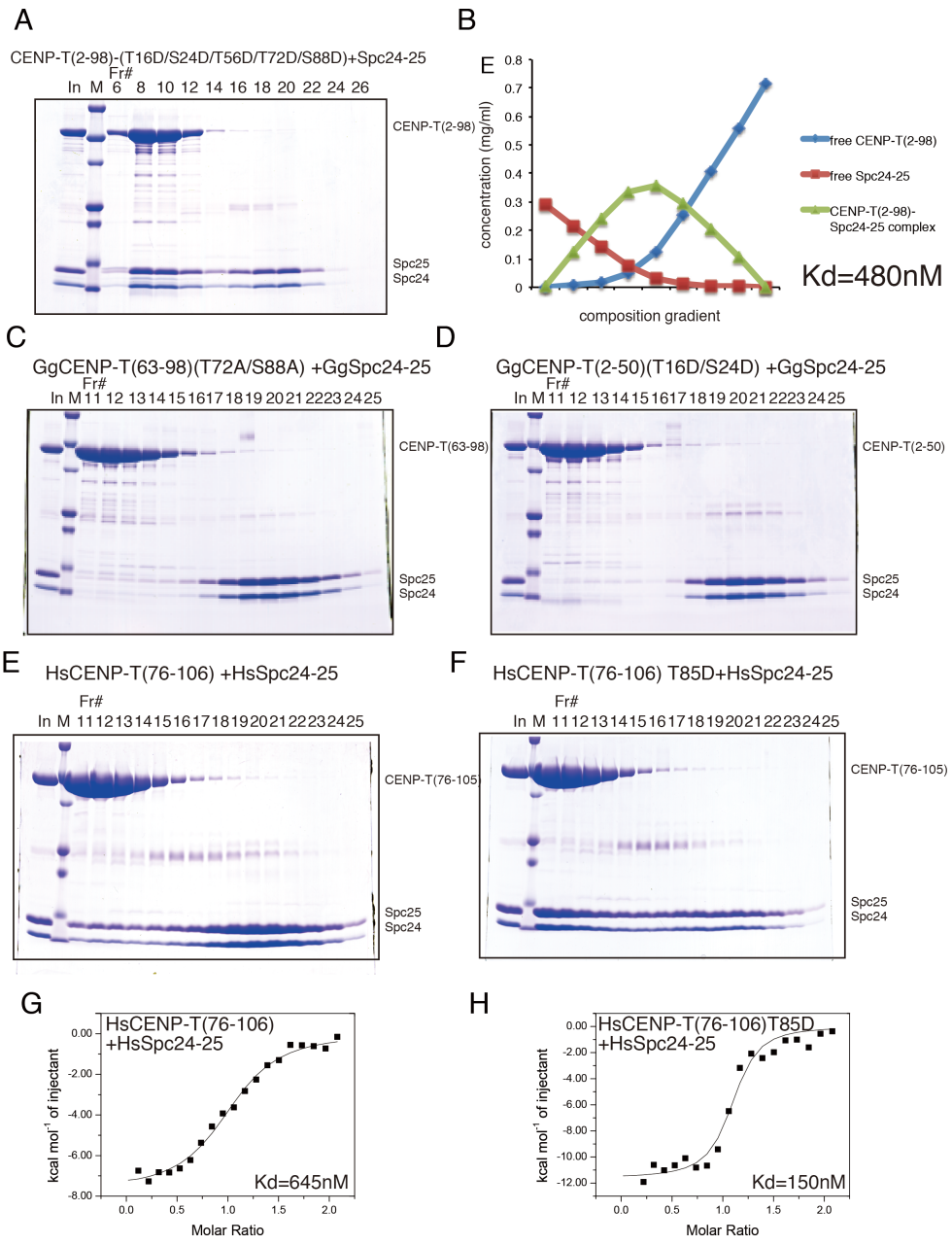

Figure 3: Phospho-mimetic CENP-T, but not phospho-deficient CENP-T, directly binds to the Spc24/25 portion of the Ndc80 complex. A) Stoichiometric amount of CENP-T (2-98 aa) D mutant (T16D, S24D, T56D, T72D, and S88D) fused with MBP (MBP-CENP-T^{2-98}) and globular domain of the Spc24/25 complex were mixed and incubated for 15 min at room temperature. The mixture was separated by gel filtration using a Superdex 75. Peak fractions were analyzed by SDS-PAGE. B) CG-MALS analysis of phospho-mimetic chicken MBP-CENP-T^{2-98} together with the globular domain of the chicken $Spc24^{125-195}$/$Spc25^{132-234}$ complex. Two components interacted with 1:1 stoichiometry and the Kd was 480nM. C) Gel filtration experiment as in (A) of MBP-CENP-T^{63-98} T72A and S88A with the chicken $Spc24^{125-195}$/$Spc25^{132-234}$ complex. D) Coomassie-stained gels of fractions from a gel filtration assessing the co-migration of stoichiometric amounts of chicken MBP-CENP-T^{2-50} T16D and S24D with the globular domains of the chicken Spc24/25 complex (as in (A)). E) Coomassie-stained gels of fractions from a gel filtration assessing the co-migration of stoichiometric amounts of unphosphorylated human MBP-CENP-T^{76-106} with the globular domain of the human $Spc24^{131-197}$/$Spc25^{129-224}$ complex. F) Coomassie-stained gels of fractions from a gel filtration assessing the co-migration of stoichiometric amounts of MBP-hsCENP-T^{76-106} (T85D) with the globular domain of the human $Spc24^{131-197}$/$Spc25^{129-224}$ complex. G) ITC binding curve for the interaction of unphosphorylated MBP-hsCENP-T^{76-106} with the globular domain of the human $Spc24^{131-197}$/$Spc25^{129-224}$ complex. Kd is 645 nM. H) ITC binding curve for the interaction of MBP-hsCENP-T^{76-106} (T85D) with the globular domain of the human $Spc24^{131-197}$/$Spc25^{129-224}$ complex. Kd is 150 nM.

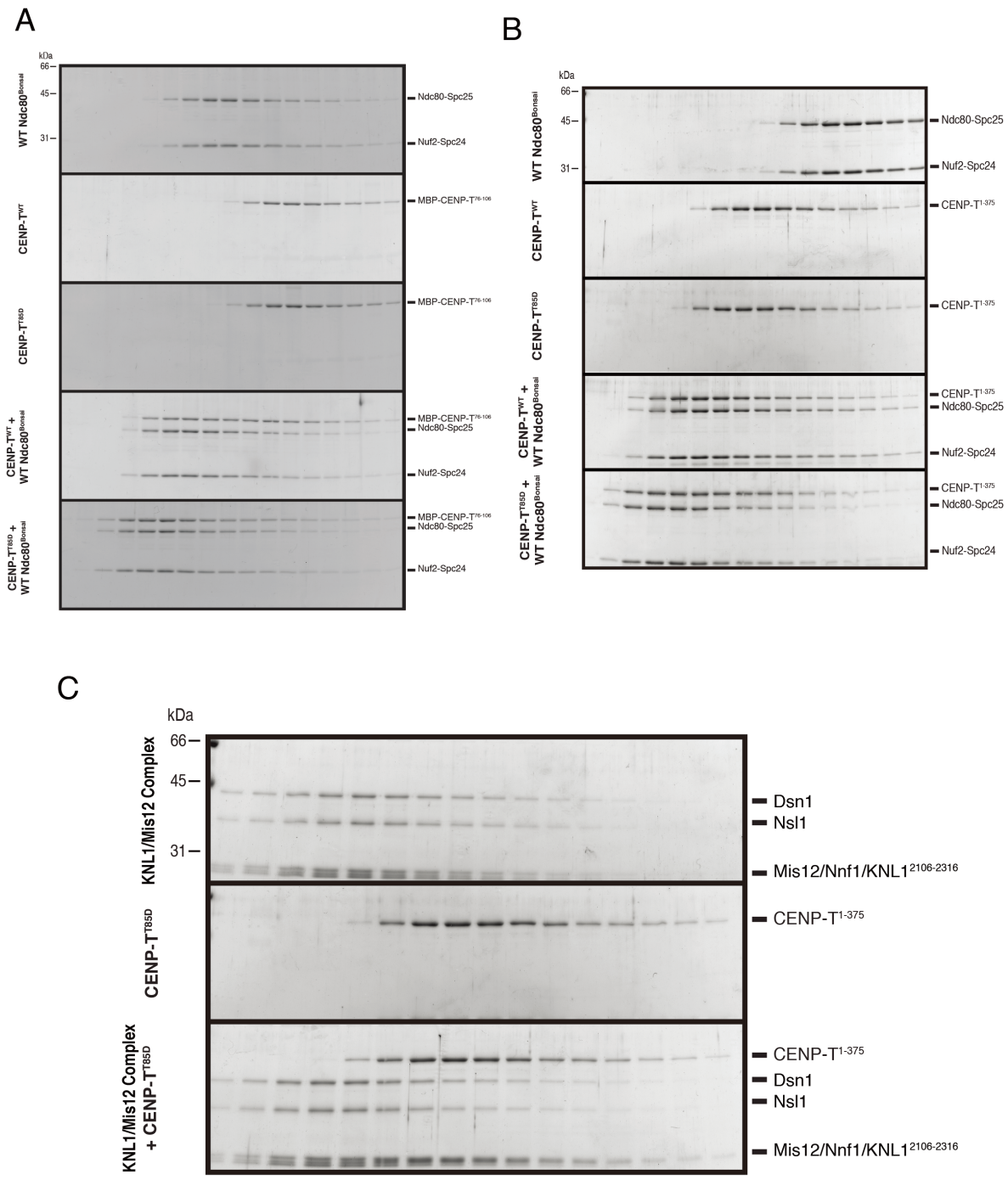

Figure 4: The human CENP-T N-terminal region binds to the Ndc80^{Bonsai} complex, but not to the Mis12 complex. The indicated protein constructs were separated by size exclusion chromatography on an Superose 6 column and the coomassie-stained gels of the corresponding fractions from various runs are shown. A) The MBP-fused unphosphorylated or phosphomimetic (T85D) human CENP-T$^{76-106}$ and the Ndc80^{Bonsai} complex were mixed or run individually as indicated. B) The human unphosphorylated CENP-T N-terminal region (1-375 aa) or the human phosphomimetic CENP-T N-terminal region (T85D) and the Ndc80^{Bonsai} complex were mixed or run individually as indicated. C) The human phospho-mimetic CENP-T N-terminal region (1-375 aa, T85D) and the Mis12 complex were mixed or run individually as indicated.

The CENP-T N-terminal region binds to the Spc24/25 complex through hydrophobic and electrostatic interactions

The Spc24/25 complex contains two "RWD" domains, which are found in multiple proteins and are thought to provide a platform for protein-protein interactions (Schmitzberger and Harrison, 2012). To define the mechanisms by which the phosphorylated CENP-T N-terminal region binds to the RWD-containing Spc24/25, we conducted a high-resolution structural analysis of phospho-mimetic chicken CENP-T (63-98 aa) together with the globular regions of recombinant Spc24 and Spc25 (125-195 aa of chicken Spc24 and 132-234 aa of chicken Spc25) (Figure 5A). We also determined the structure of the Spc24/25 complex alone. Following crystallization of these protein complexes, we determined their structures by molecular replacement methods with a model based on the engineered human $Ndc80^{Bonsai}$ complex (Figure 5B-E and Table 1; Ciferri et al., 2008). The chicken Spc24/25 complex was refined to 1.0 Å resolution with refinement statistics of Rwork = 0.193 (Rfree = 0.207) and the CENP-T-Spc24/25 complex was refined to 1.9 Å resolution with refinement statistics of Rwork = 0.167 (Rfree = 0.216). We superimposed each structural model and confirmed that the structures of the Spc24/25 sub-complex from each model were identical (Figure 5B and C). The CENP-T peptide (63-98 aa) contains two α-helices (Figure 5B-E and 6) with the second helical region closely associated with a β sheet from Spc25 (Figure 5 and 7A). An extended coil follows the CENP-T helices and there are additional hydrophobic and electrostatic interactions with the β sheets from Spc25 (Figure 5 and 7A). In addition to this interaction between CENP-T and Spc25, we also found a second potential contact

site for CENP-T with the Spc24 portion of the Spc24/25 complex. This interaction involves the first helix of the CENP-T peptide including the L68 residue (Figure 7A).

	Spc24-Spc25 globular domain	**CENP-T(63-98)T72DS88D Spc24-Spc25 globular domain**
Data collection		
Space group	P212121	$P3_1$
Unit-cell parameters (Å)	a=47.21, b=58.08Å, c=58.41Å, α=β=γ=90°	a=b=61.32Å, c=111.28Å, α=β=90°, γ=120°
Wavelength (Å)	1	1
Resolution (Å)	1.03	1.9
Completeness (%)*	99.2 (100)	99.9 (99.9)
f'/f"		
R_{mrgd-F} (%)*	4.3 (30.5)	6.0 (53.6)
I/σ(I))*	49.0 (5.25)	30.4 (3.55)
Number of reflections	79657	36934
Refinement statistics		
Resolution range (Å)	41.2–1.03	30.41–1.90
R_{work}/R_{free} (%)*	19.3 (25.2)/20.7(24.4)	16.7(22.1)/21.6(23.4)
Number of atoms (Mean B value)		
Protein	1366 (9.9)	3175 (26.1)
Water	251 (37.0)	357 (45.7)
r.m.s. deviations		
Bond length (Å)	0.006	0.022
Bond angle (°)	1.092	1.92
Ramachandran plot (%)	98.7/1.3/0.0	98.7/1.3/0.0

* number in parenthesis are values from highest resolution shell

Table 1: X-ray diffraction data and model refinement statistics for the Sps24/25 complex and CENP-T$^{63-98}$T72DS88D-Spc24/25 complex.

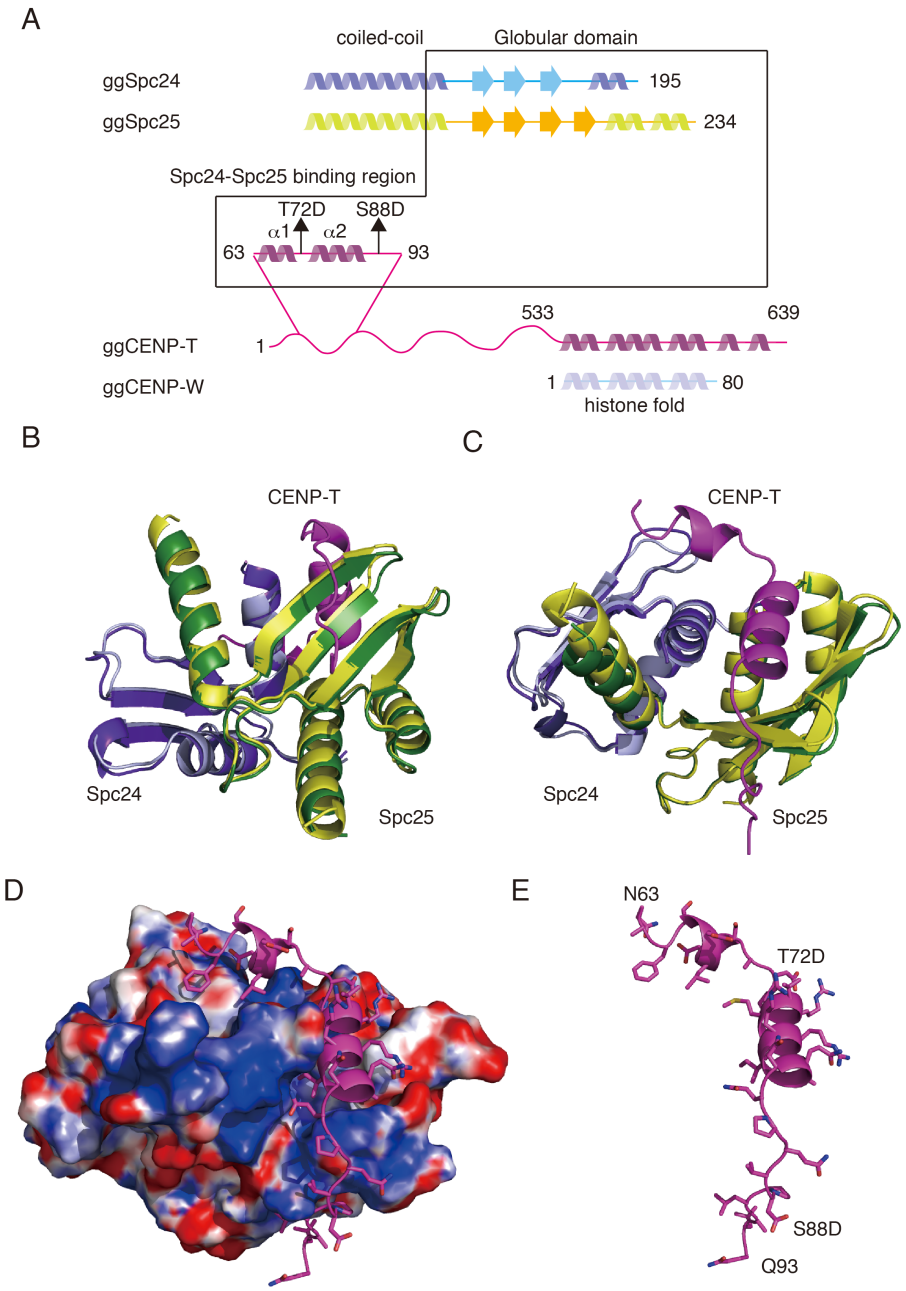

Figure 5: Crystal structure of the phospho-mimetic CENP-T-Spc24/25 complex. A) Schematic diagram of Spc24, Spc25, CENP-T and CENP-W showing the presence of alpha helices and beta sheets. The expression constructs used for the structural analyses are indicated by the box. B) Structural model showing the side view of the Spc24/25 complex superimposed with the CENP-T-Spc24/25 complex. For the Spc24/25 complex, Spc24 is colored in light cyan and Spc25 is in light green. For the CENP-T-Spc24/25 complex, CENP-T is colored in magenta, Spc24 is cyan, and Spc25 is green. C) Structural model showing the top view of the superimposed structures of the Spc24/25 complex and the CENP-T-Spc24/25 complex as in (B). D) Structural model showing the surface charge of the Spc24/25 complex interacting with phospho-mimetic CENP-T peptide. Electrostatic surface charges of the Spc24/25 complex were calculated by APBS and are contoured from -8.0 (red) to 8.0 (blue). The complex is viewed from the same angle as in (C). Side chains of CENP-T are shown as stick models. E) Structural model showing the phospho-mimetic CENP-T peptide from the CENP-T-Spc24/25 complex structure in (D) on its own.

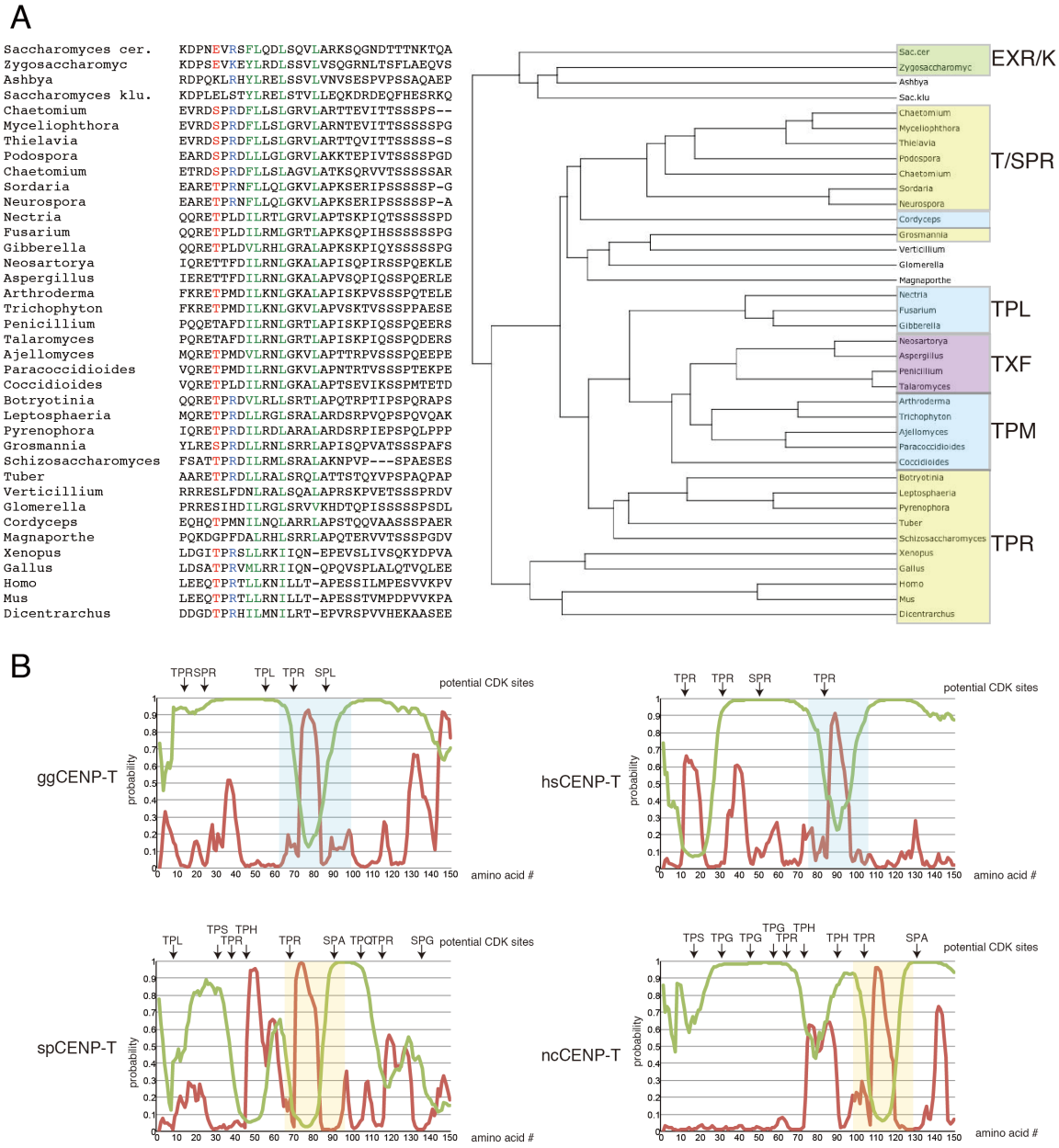

Figure 6: Sequence comparison of CENP-T N-terminus in various species. A) Sequence alignment of CENP-T from various species. The conserved T-P-R motif is highlighted. The motif is diverged in some species. Phylogenetic tree is also shown. B) Prediction of the unstructured region of CENP-T from chicken, human, *S. pombe*, and *N. crassa* by the DISOPRED2 prediction tool. Disordered-probability is shown as green. Prediction of α-helical regions is shown in red. Potential CDK sites are also shown. The blue shading indicates the Spc24/25 complex binding region. The shaded yellow region in *S. pombe*, and *N. crassa* is predicted as the Spc24/25 binding region based on sequence comparison and helix probabilities.

As the Spc24/25 complex shows increased binding to the phospho-mimetic CENP-T peptide relative to unphosphorylated CENP-T (Figure 2), we examined how the phospho-mimetic residues are involved in the interaction with the Spc24/25 complex. We found that this interaction is not electrostatic and that instead a hydrophobic interface from CENP-T contributes to this interaction to bind to Spc25 directly (Figure 7A). Therefore, T72D and S88D in CENP-T are not direct contact sites for the CENP-T-Spc25 interaction. Thus, we hypothesized that the T72D residue forms a salt bridge with R74 to allow the subsequent hydrophobic residues to orient towards the hydrophobic residues in Spc25 (Figure 7B). To test this, we generated R74 mutants (R74E or R74A) in phospho-mimetic CENP-T (T72D and S88D) to prevent the phospho-mimetic residue from forming a salt bridge between the 72 and 74 residues. As shown in Figure 7C, these CENP-T mutant peptides failed to interact with Spc24/25. To test the role of the hydrophobic residues in mediating interactions between CENP-T and Spc24, we generated an L68R mutation in the context of the phospho-mimetic CENP-T peptide. The L68R mutant disrupted the CENP-T-Spc24/25 interaction even when the salt bridge between 72 and 74 was formed (Figure 7D). Based on our structural and mutational analysis, we conclude that phosphorylation of T72 facilitates formation of a salt bridge with R74 to allow the downstream hydrophobic residues in CENP-T to interact with the Spc24/25 complex. This interaction region of CENP-T, which contains T-P-R residues (72-74) and downstream hydrophobic residues, is well conserved in various eukaryotic species including *S. pombe* (Figure 6 and 7A).

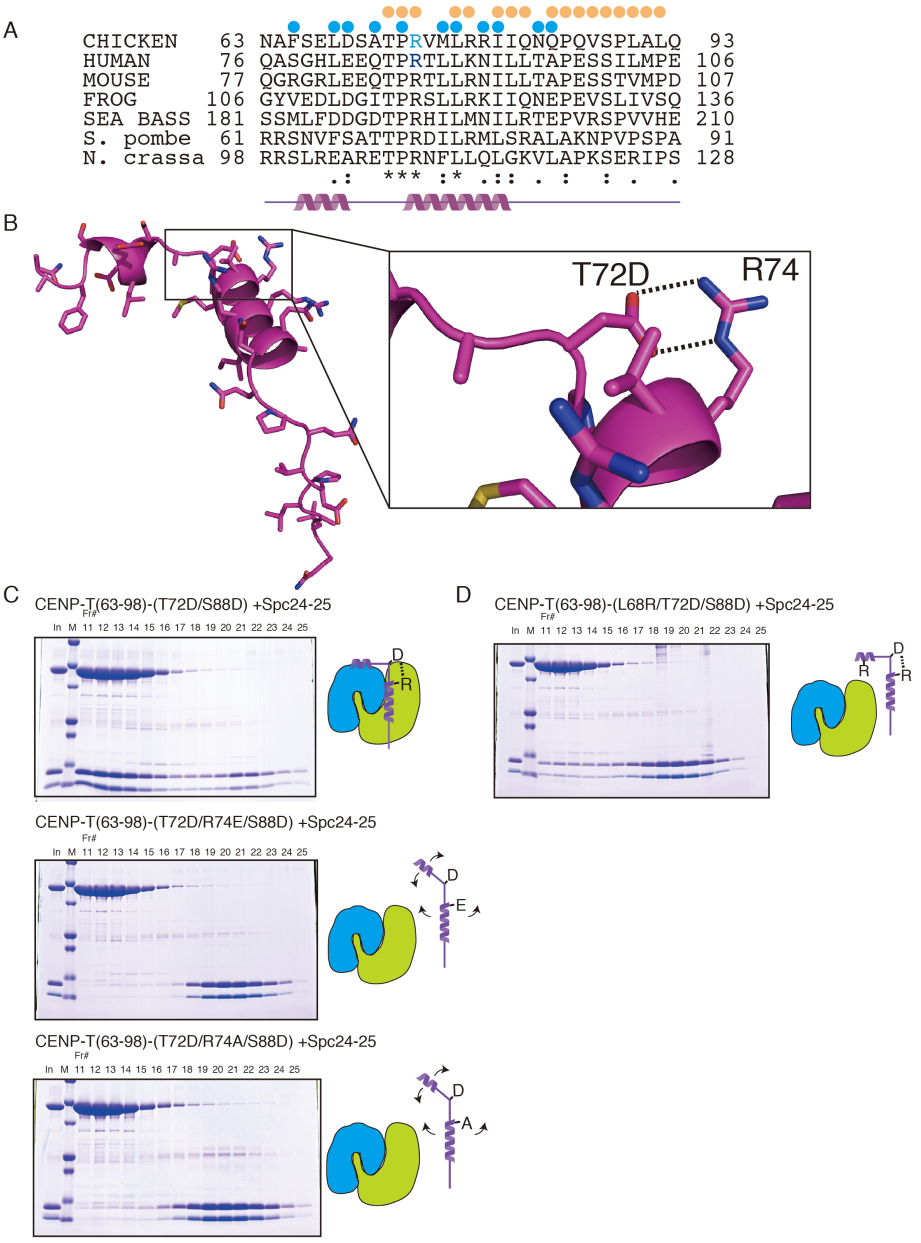

Figure 7: A conserved salt bridge is essential for the interaction of CENP-T with the Spc24/25 complex. A) Sequence alignment of CENP-T from chicken, human, mouse, frog, sea bass, fission yeast, and filamentous fungi. Residues involved in the interaction of CENP-T with Spc24 and Spc25 are denoted by blue and orange dots, respectively. B) Structural model showing a close-up view of the phospho-mimetic CENP-T peptide. The salt bridge between T72D and R74 is highlighted. C) Mutation of CENP-T R74 (R74E or R74A) disrupts complex formation even in the presence of phospho-mimetic T72D and S88D residues. Stoichiometric amounts of MBP-CENP-T$^{63-98}$ mutant (T72D/R74E/S88D or T72D/R74A/S88D) and the Spc24$^{125-195}$/Spc25$^{132-234}$ complex were mixed and analyzed by gel filtration as in Figure 2A. Upper panel: phospho-mimetic CENP-T (T72D/S88D) and the Spc24/25 complex interaction as in Figure 2A. Middle panel: CENP-T mutant (T72D/R74E/S88D) with the Spc24$^{125-195}$/Spc25$^{132-234}$ complex. Lower panel: CENP-T mutant (T72D/R74A/S88D) with the Spc24$^{125-195}$/Spc25$^{132-234}$ complex. Schematic diagrams of CENP-T and the Spc24/25 complex are shown to the right (Blue: Spc24, Green: Spc25). D) CENP-T mutation at L68 disrupts complex formation with Spc24/25. Gel filtration analysis of the MBP-CENP-T$^{63-98}$ mutant (L68R7/T72D/S88D) with the Spc24$^{125-195}$/Spc25$^{132-234}$ complex as in (C).

The binding of CENP-T and the Mis12 complex to the Spc24/25 complex is mutually exclusive

Based on our structural analysis of the CENP-T-Spc24/25 complex, we also predicted critical hydrophobic residues in the Spc24/25 complex (I156 and L161 in chicken Spc25 and I149 and L154 in human Spc25) that would be required for the CENP-T-Spc25 interaction. These residues are conserved between human and chicken Spc25 (Figure 8A). To test the role of these residues for the CENP-T-Spc24/25 interaction, we generated mutant Spc24/25 complexes containing chicken Spc25 (I156R) or Spc25 (L161R). These mutations did not affect complex formation with Spc24, but they failed to interact with the phospho-mimetic CENP-T peptide (Figure 9A and B). Similarly, phospho-mimetic human CENP-T showed reduced interactions with $Ndc80^{Bonsai}$ complex containing an Spc25 mutant (I149A L154A) by gel filtration (Figure 9C). We also confirmed the reduced interactions of the Spc25 mutant with CENP-T using human Spc24/25 complex (57-197 aa of human Spc24 and 70-224 aa of human Spc25) based on gel filtration and ITC measurements (Figure 10A and B). This suggests that these hydrophobic residues in Spc25 are directly involved in the interaction with vertebrate CENP-T.

Above we demonstrated that CENP-T interacts directly with the Spc24/25 sub-complex. However, the Ndc80 complex also associates with the Mis12 complex and KNL1 (Cheeseman et al., 2004; 2006; Obuse et al., 2004; Petrovic et al., 2010; DeLuca and Musacchio, 2012; Maskell et al., 2010), and it was unclear whether the Ndc80 complex can simultaneously interact with both CENP-T and Mis12/KNL1, or whether these represent mutually exclusive assembly pathways. The human $Ndc80^{Bonsai}$

complex mutated for Spc25 (I149A L154A) displayed reduced binding to phospho-mimetic CENP-T (Figure 9C), but we found that the mutant Ndc80^{Bonsai} or the Spc24$^{57-197}$/Spc25$^{70-224}$ complex still bound to the Mis12 complex based on gel filtration (Figure 9D and 10C). However, the binding affinity of the mutant Spc24$^{57-197}$/Spc25$^{70-224}$ complex for the Mis12 complex was reduced (KD = 291 nM) compared with the wild-type Spc24$^{57-197}$/Spc25$^{70-224}$ complex (KD = 18.9 nM) based on ITC measurements (Figure 10D), suggesting that the binding sites of Spc24/25 for the Mis12 complex and CENP-T partially overlap.

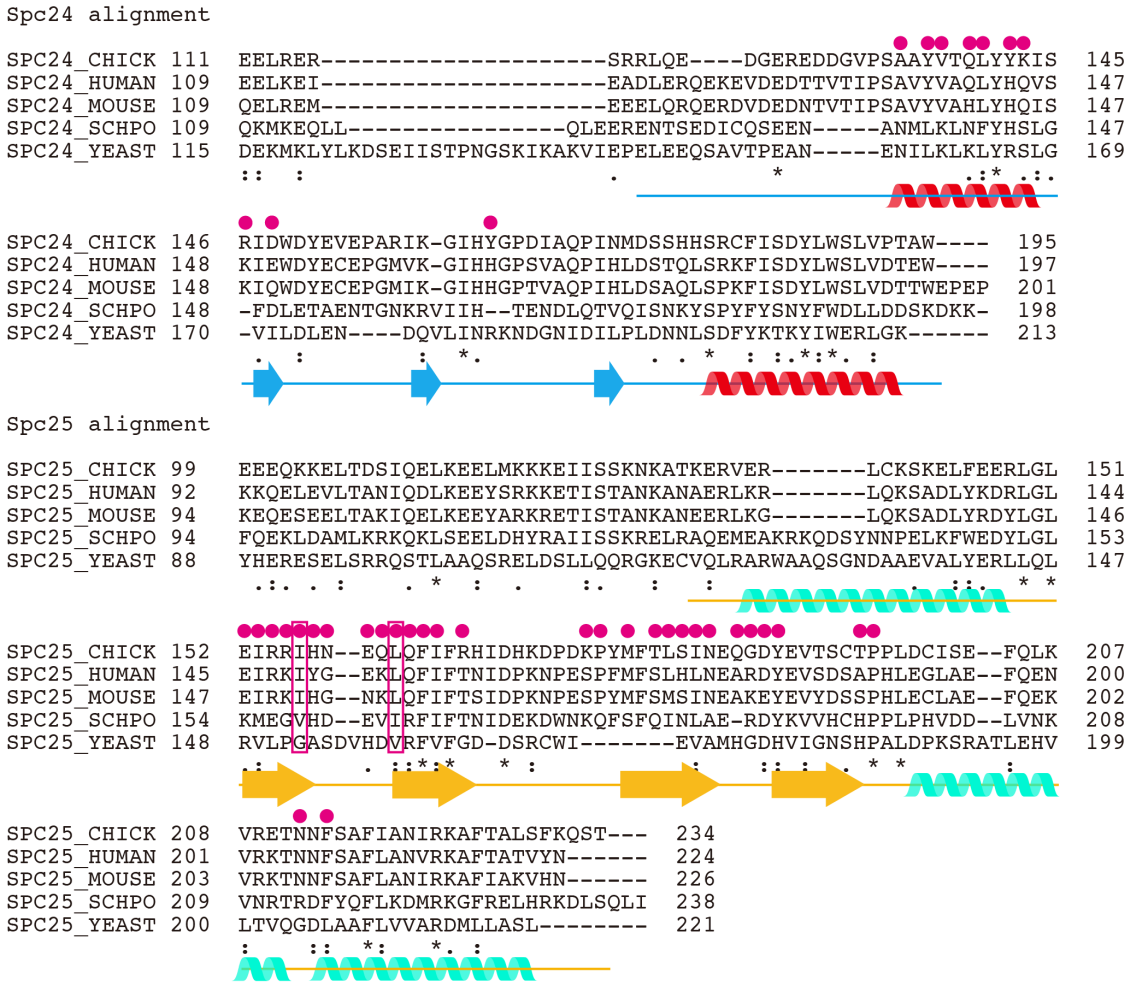

Figure 8: Binding region of Spc24 and 25 to CENP-T in various species. Sequence alignment of Spc24 and Spc25 from chicken, human, mouse, fission yeast, and budding yeast. Residues involved in interactions with CENP-T are denoted by magenta. Secondary structures are also indicated.

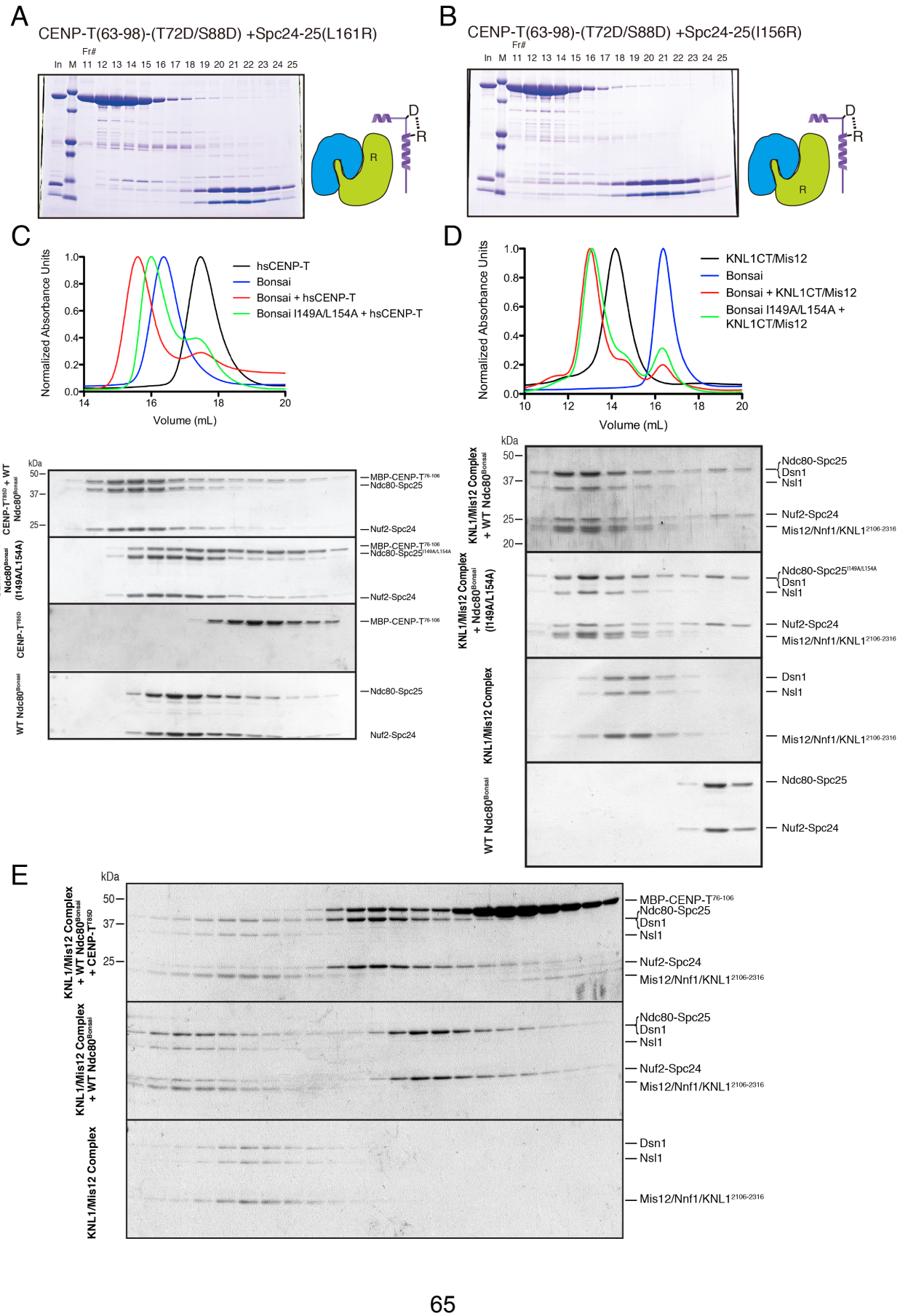
A
CENP-T(63-98)-(T72D/S88D) +Spc24-25(L161R)
Fr#
In M 11 12 13 14 15 16 17 18 19 20 21 22 23 24 25
D
R
B
CENP-T(63-98)-(T72D/S88D) +Spc24-25(I156R)
Fr#
In M 11 12 13 14 15 16 17 18 19 20 21 22 23 24 25
D
R
C
Normalized Absorbance Units
1.0
0.8
0.6
0.4
0.2
0.0
14 16 18 20
Volume (mL)
hsCENP-T
Bonsai
Bonsai + hsCENP-T
Bonsai I149A/L154A + hsCENP-T
D
Normalized Absorbance Units
1.0
0.8
0.6
0.4
0.2
0.0
10 12 14 16 18 20
Volume (mL)
KNL1CT/Mis12
Bonsai
Bonsai + KNL1CT/Mis12
Bonsai I149A/L154A +
KNL1CT/Mis12
CENP-T^T85D + WT Ndc80^Bonsai
CENP-T^T85D + Ndc80^Bonsai (I149A/L154A)
CENP-T^T85D
WT Ndc80^Bonsai
kDa
50
37
25
MBP-CENP-T^76-106
Ndc80-Spc25
Nuf2-Spc24
MBP-CENP-T^76-106
Ndc80-Spc25^I149A/L154A
Nuf2-Spc24
MBP-CENP-T^76-106
Ndc80-Spc25
Nuf2-Spc24
KNL1/Mis12 Complex + WT Ndc80^Bonsai
KNL1/Mis12 Complex + Ndc80^Bonsai (I149A/L154A)
KNL1/Mis12 Complex
WT Ndc80^Bonsai
kDa
50
37
25
20
Ndc80-Spc25
Dsn1
Nsl1
Nuf2-Spc24
Mis12/Nnf1/KNL1^2106-2316
Ndc80-Spc25^I149A/L154A
Dsn1
Nsl1
Nuf2-Spc24
Mis12/Nnf1/KNL1^2106-2316
Dsn1
Nsl1
Mis12/Nnf1/KNL1^2106-2316
Ndc80-Spc25
Nuf2-Spc24
E
KNL1/Mis12 Complex + WT Ndc80^Bonsai + CENP-T^T85D
KNL1/Mis12 Complex + WT Ndc80^Bonsai
KNL1/Mis12 Complex
kDa
50
37
25
MBP-CENP-T^76-106
Ndc80-Spc25
Dsn1
Nsl1
Nuf2-Spc24
Mis12/Nnf1/KNL1^2106-2316
Ndc80-Spc25
Dsn1
Nsl1
Nuf2-Spc24
Mis12/Nnf1/KNL1^2106-2316
Dsn1
Nsl1
Mis12/Nnf1/KNL1^2106-2316

Figure 9: Binding of CENP-T and the Mis12 complex to the Ndc80 complex is mutually exclusive. A) L161R mutations in Spc25 disrupt the interaction with CENP-T. Phospho-mimetic chicken MBP-CENP-T^{63-98} (T72D/S88D) and the mutant $Spc24^{125-195}$/$Spc25^{132-234}$ (L161R) complex were separated by gel filtration using a Superdex 75, analyzed by SDS-PAGE, and stained with Coomassie. B) I156R mutations in Spc25 disrupt the interaction with CENP-T. Phospho-mimetic MBP-CENP-T^{63-98} (T72D/S88D) and the mutant $Spc24^{125-195}$/$Spc25^{132-234}$ (I156R) complex were analyzed by gel filtration as in (A). C) I149A L154A double mutants in human Spc25 disrupt binding to human CENP-T. Human phospho-mimetic CENP-T (MBP-hsCENP-T^{76-106}T85D) and the wild-type $Ndc80^{Bonsai}$ complex or the $Ndc80^{Bonsai}$ I149A L154A mutant complex were mixed and analyzed by gel filtration. Protein mixtures were incubated on ice for 30 minutes before conducting the chromatography using a Superose 6 column. Fractions were collected, analyzed by SDS-PAGE, and stained with Coomassie. Elution profiles from the size exclusion chromatography for the experiment are shown (top). Elution of proteins was monitored at A280 nm. D) The $Ndc80^{Bonsai}$ complex or the $Ndc80^{Bonsai}$ I149A L154A mutant complex and the human Mis12-$KNL1^{2106–2316}$ complex were mixed and analyzed by gel filtration chromatography using a Superose 6 column as in (C). Elution profiles from the size exclusion chromatography are shown (top). E) CENP-T and the Mis12/KNL1CT complex show mutually exclusive binding to the $Ndc80^{Bonsai}$ complex. Human phospho-mimetic MBP-CENP-T^{76-106} (T85D), wild-type $Ndc80^{Bonsai}$ complex, and the human Mis12-$KNL1^{2106–2316}$ complex were mixed in the indicated combinations and analyzed by gel filtration. A large complex containing all components was not detected, although both CENP-T and KNL1/Mis12 bound individually to the Ndc80 complex based on altered migration.

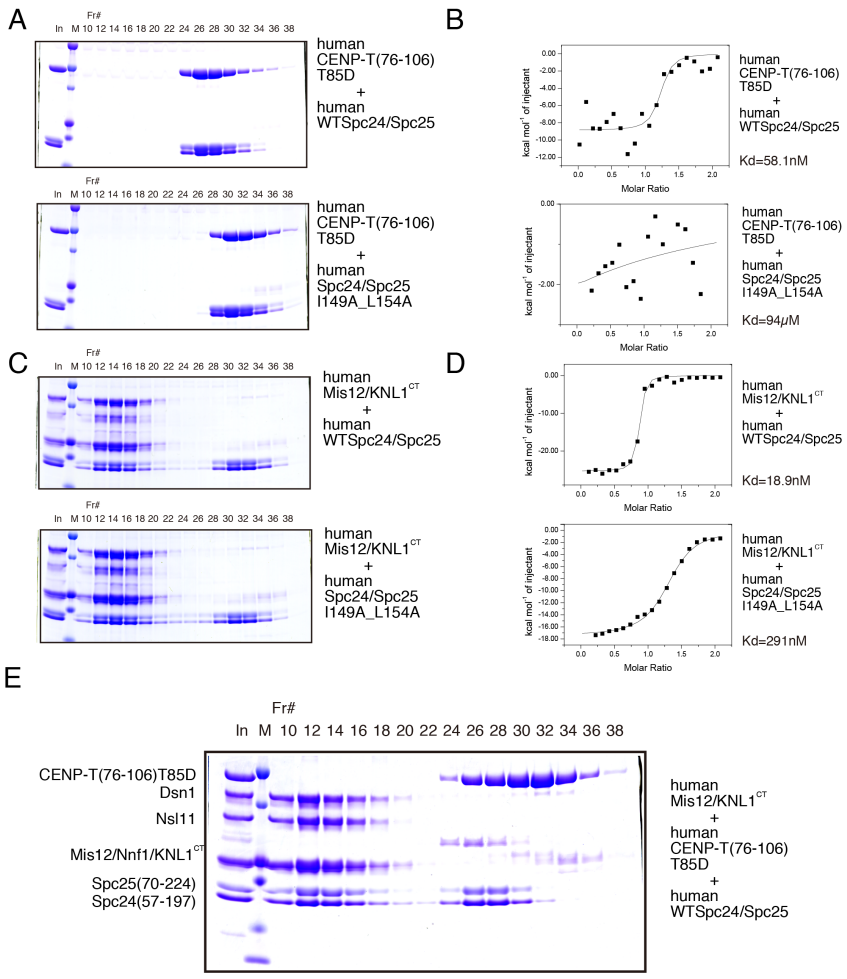

Figure 10: Binding of CENP-T and the Mis12 complex to Spc24/25 is mutually exclusive. A) I149A_L154A double mutants in human Spc25 disrupt binding to human CENP-T. Human phospho-mimetic CENP-T (MBP-hsCENP-T$^{76\text{-}106}$T85D) and the wild-type Spc24$^{57\text{-}197}$/Spc25$^{70\text{-}224}$ complex or the Spc24$^{57\text{-}197}$/Spc25$^{70\text{-}224}$ complex (I149A L154A for Spc25) mutant complex were mixed and analyzed by gel filtration using a Superdex 200 column. Fractions were collected, analyzed by SDS-PAGE, and stained with Coomassie. B) ITC binding curve for the interaction of the human wild-type Spc24$^{57\text{-}197}$/Spc25$^{70\text{-}224}$ complex or the Spc24$^{57\text{-}197}$/Spc25$^{70\text{-}224}$ complex (I149A L154A for Spc25) mutant complex with human phospho-mimetic CENP-T (MBP-hsCENP-T$^{76\text{-}106}$T85D). The measured KD's for interaction of the wild-type Spc24$^{57\text{-}197}$/Spc25$^{70\text{-}224}$ complex and the mutant Spc24/25 complex with human CENP-T are 58.1 nM and 94 μM, respectively. C) The wild-type the Spc24$^{57\text{-}197}$/Spc25$^{70\text{-}224}$ complex or the Spc24$^{57\text{-}197}$/Spc25$^{70\text{-}224}$ complex (I149A L154A for Spc25) mutant complex and the human Mis12-KNL1$^{2106\text{–}2316}$ complex were mixed and analyzed by gel filtration chromatography using a Superdex 200 column. Fractions were collected, analyzed by SDS-PAGE, and stained with Coomassie. D) ITC binding curve for the interaction of the human Spc24$^{57\text{-}197}$/Spc25$^{70\text{-}224}$ complex (wild-type or I149A L154A double mutants) with the Mis12/KNL1CT complex. The measured KD's for interaction of the wild-typeSpc24$^{57\text{-}197}$/Spc25$^{70\text{-}224}$ complex and the mutant Spc24/25 complex with human Mis12/KNL1CT complex are 18.9 nM and 291 nM, respectively. E) CENP-T and the Mis12/KNL1CT complex show mutually exclusive binding to the Spc24/25 complex. Human phospho-mimetic CENP-T, the human wild-type Spc24$^{57\text{-}197}$/Spc25$^{70\text{-}224}$ complex, and the human Mis12-KNL1$^{2106\text{–}2316}$ complex were mixed and analyzed by gel filtration. Fractions were collected, analyzed by SDS-PAGE, and stained with Coomassie. A large complex containing all components was not detected, although both CENP-T and KNL1/Mis12 bound individually to the Spc24/25 complex based on altered migration.

Next, we tested whether the Ndc80^{Bonsai} complex could interact simultaneously with CENP-T and KNL1/Mis12 complex (Figure 9E). In separate experiments, we detected co-migration of the KNL1 and the Mis12 complex with the Ndc80^{Bonsai} complex and CENP-T with the Ndc80^{Bonsai} complex by gel filtration. However, co-migration of all proteins was not detected (Figure 9E; note lack of CENP-T in the largest fractions). Similar results were obtained with the Spc24$^{57-197}$/Spc25$^{70-224}$ complex (Figure 10E). We have previously shown that the Mis12 complex bound weakly to CENP-T in pull-down assays (Gascoigne et al., 2011). In that case, we detected small amounts of Mis12 by Western blot analysis. As we did not detect co-migration of the Mis12 complex with CENP-T (Figure 9E and 4C), this suggests that the Mis12 complex does not associate strongly with CENP-T. Based on these biochemical analyses, we conclude that the binding of the CENP-T N-terminal region and the Mis12 complex to the Spc24/25 is mutually exclusive likely due to competition for this interaction surface, as well as possibly steric exclusion.

The Ndc80 complex is recruited into kinetochores by two parallel pathways

We next sought to test the significance of the hydrophobic interaction of CENP-T with the Spc24/25 complex in cells. To do this, we generated a stable DT40 cell line expressing GFP-Spc25 (I156R) mutant and analyzed the localization of this fusion protein. Wild-type Spc25 co-localized with CENP-T. In contrast, the localization of Spc25 (I156R) at kinetochores was reduced to ~60% of wild-type Spc25 (Figure 11A). To assess the functional consequences of the Spc25 mutant, we generated a conditional knock-out for Spc25 in DT40 cells (Figure 12). Although DT40 cells in which expression of wild-type Spc25 was replaced with the Spc25 (I156R) mutant were viable,

the growth rate of these cells was slightly reduced (Figure 11B). Based on these data, we conclude that the hydrophobic interaction of CENP-T with the Spc24/25 complex is required for the robust localization of the Spc24/25 complex to kinetochores.

We have previously shown that Ndc80 localization is greatly reduced in both CENP-T- and Mis12-deficient cells (Kline et al., 2006; Kwon et al., 2007; Gascoigne et al., 2011; Nishino et al., 2012). For these previous analyses, we conditionally repressed gene expression by addition of tetracycline such that protein levels were gradually reduced over several cell cycles. To evaluate the acute effects of CENP-T or Mis12 complex depletion on the localization of downstream factors, we used an auxin-based degron system (Nishimura et al., 2009) in which proteins are rapidly targeted for degradation. Using this system, we found that degradation of either CENP-T or the Mis12 complex subunit Dsn1 reduced the levels of Ndc80 at kinetochores by 43% or 32%, respectively (Figure 12). As Ndc80 localization was not abolished in either case, these data support a model in which there are two parallel pathways for targeting the Ndc80 complex to kinetochores. However, we note that CENP-T depletion also causes a reduction in Mis12 complex and KNL1 localization (Gascoigne et al., 2011). Therefore, we cannot exclude additional contacts with other regions of CENP-T that create an interrelationship between the Mis12 and CENP-T pathways.

Above, we found that the Spc25 (I156R) mutant failed to interact with CENP-T, but was still able to localize to kinetochores in DT40 cells (Figure 11A) suggesting that the Mis12 pathway for recruiting the Ndc80 complex is still active when the CENP-T-Spc25 interaction is compromised. Indeed, we found that Spc25 (I156R) localization to kinetochores was most completely abolished in Dsn1-degron cells, whereas weak

Spc25 (I156R) signals were still visible in CENP-T-degron cells (Figure 11C). This result supports a model in which the Ndc80 complex is recruited by two-parallel-pathways during mitosis and is consistent with biochemical analysis showing mutually exclusive interactions between CENP-T, the Ndc80 complex, and the Mis12 complex (Figure 9 and 10).

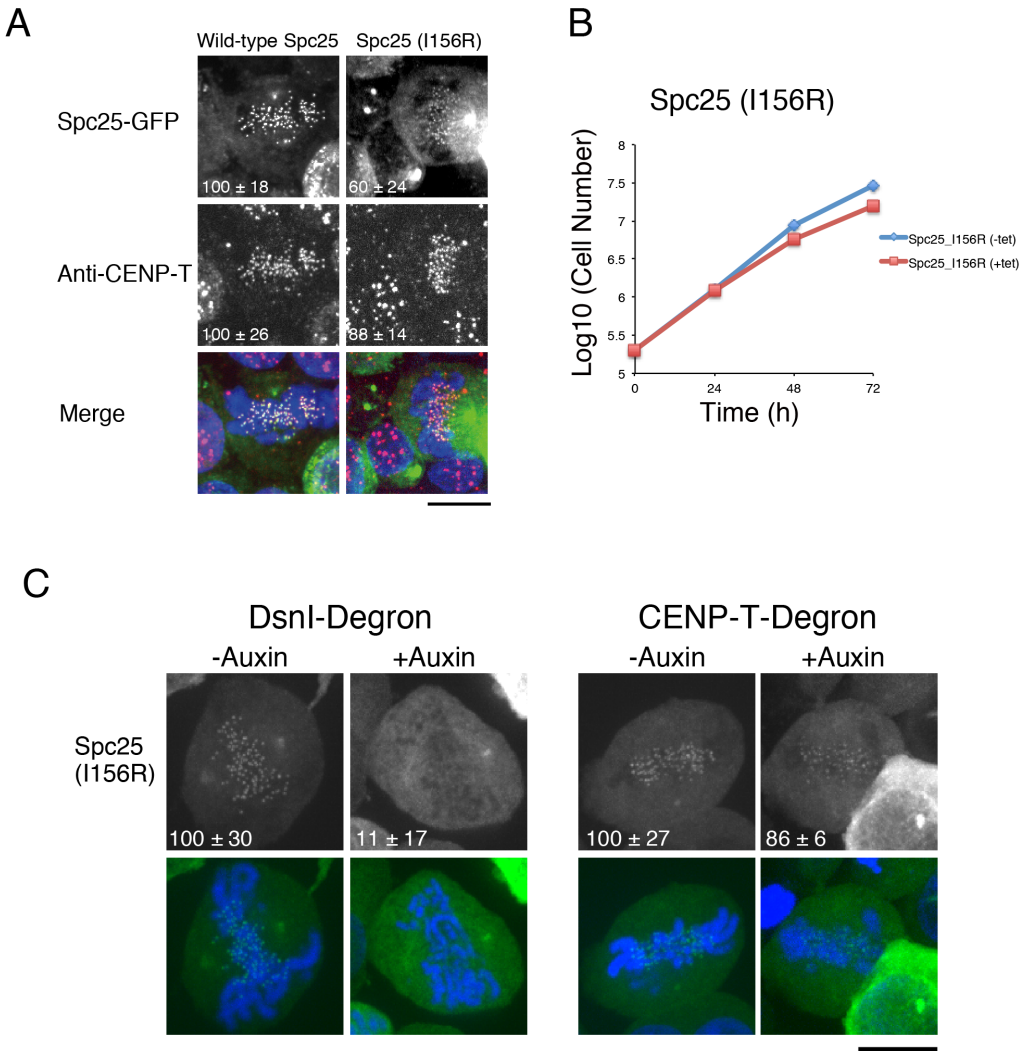

Figure 11: The Ndc80 complex is targeted to kinetochores by two parallel pathways. A) Kinetochore localization of Spc25 I156R mutants was reduced to ~60% in DT40 cells. Immunofluorescence images showing the co-localization of chicken wild type or I156R mutant Spc25-GFP with CENP-T. Signal intensities of each protein were measured relative to an adjacent background signal. Bar, 10 μm. B) Graph showing growth curves of DT40 cells in which expression of Spc25 is replaced with Spc25 I156R mutant. The doubling time of these cells was 14.2 h compared to 13.1 h for control cells. Tetracycline was added at time 0 to repress transcription of wild-type Spc25. C) Spc25 mutants defective for CENP-T interactions require the Mis12 complex to localize to kinetochores. Images showing localization of Spc25 (I156R) in Dsn1- or CENP-T-degron cells. Dsn1 or CENP-T was degraded within 1 h after the addition of auxin (see Figure 12).

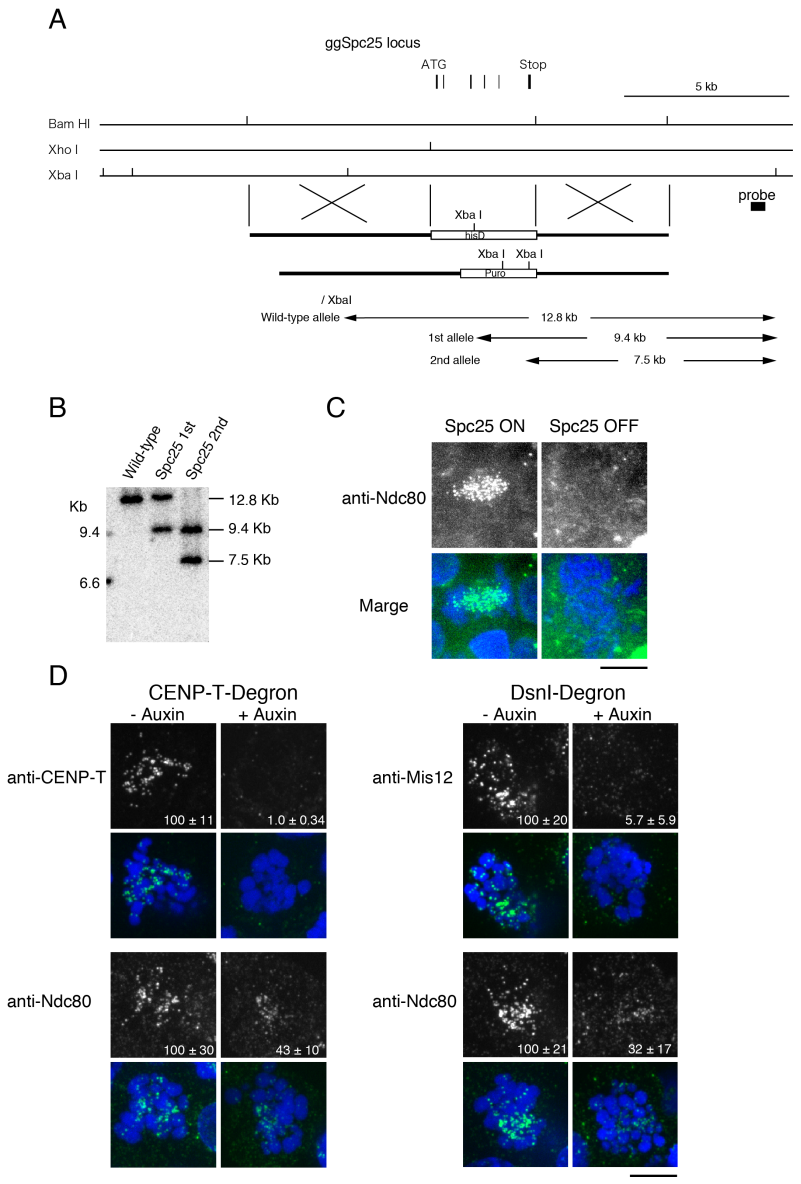

Figure 12: Creation of Spc25-conditinal knock-out, Dsn1-degron, and CENP-T-degron cells. A) Restriction maps of the chicken Spc25 locus, the gene disruption constructs, and the targeted locus. Black boxes indicate the positions of exons, and the targeted constructs that are expected to disrupt the entire region of the gene. XbaI and XhoI restriction sites are shown. The position of the probe used for Southern hybridization is indicated. Novel 9.4 kb or 7.5 kb fragments digested with XbaI will hybridize to the probe if the targeted integrations of the constructs occur. B) Restriction analysis of the targeted integration of the Spc25 disruption constructs. Genomic DNA from wild type DT40 cells, a clone after the first round targeting (+/-, 1st) and a clone after the second round targeting (-/- Spc25 cDNA+) were digested with XbaI and analyzed by Southern hybridization with the probe indicated in (A). Expression of Spc25 cDNA is repressed by addition of tet in the clone after the second round targeting. C) Ndc80 localization is eliminated Spc25-conditinal knock-out cells. Immunofluorescence images of cells 24 h after the addition of tet to Spc25 OFF cells. Bar, 10 μm. D) Immunofluorescence analysis of Ndc80 in Dsn1- or CENP-T-degron cells. Endogenous Dsn1 or CENP-T was replaced with auxin-degron tagged Dsn1 or CENP-T, respectively. Cells were synchronized at mitosis and Dsn1 and CENP-T were degraded by addition of auxin (IAA). Degron tagged proteins were undetected in 1 h after addition of IAA. Ndc80 signals are reduced ~43% and ~32% in CENP-T- and DsnI-degron cells, respectively. Ndc80 signal intensities were measured relative to an adjacent background signal. Bar, 10 μm.

Discussion

A major function for the kinetochore is to generate robust contacts with spindle microtubules to facilitate faithful chromosome segregation. The Ndc80 complex is a key kinetochore microtubule-binding component (Figure 13; Alushin et al., 2010). However, it was unclear how the Ndc80 complex is targeted to centromeric regions. Here, we demonstrated that the CENP-T N-terminal region binds directly to the Spc24/25 portion of the Ndc80 complex when CENP-T is phosphorylated to target the Ndc80 complex to kinetochores during mitosis. This interaction appears to be evolutionarily conserved as the budding yeast CENP-T homologue Cnn1 binds to Spc24/25 (Schleiffer et al., 2012) and the crystal structure of the Cnn1-Spc24/25 complex is similar to that of the chicken CENP-T-Spc24/25 complex (Malvezzi et al., 2013), although with some intriguing differences in orientation and phospho-regulation.

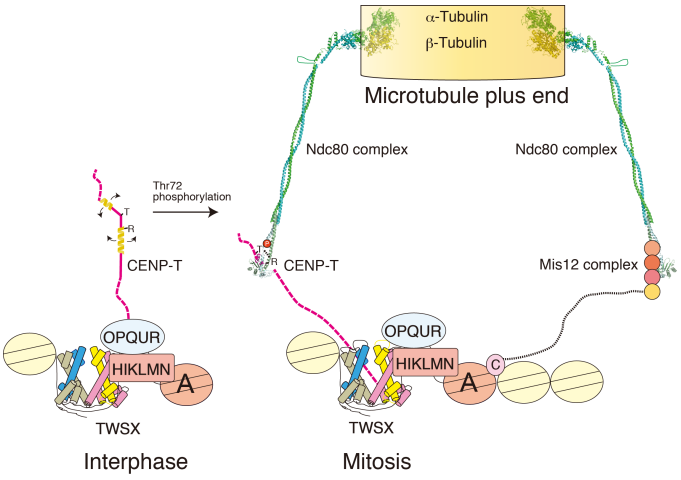

Figure 13: Parallel pathways for outer kinetochore assembly. Model for the molecular architecture of the kinetochore based on the structural, biochemical, and cell biological work presented in this paper. The CENP-T N-terminal region is unphosphorylated during interphase and phosphorylated by CDK during mitosis. The phosphorylated residue (T72 in chicken CENP-T) forms a salt bridge with R residues to allow adjacent downstream hydrophobic residues to interact with Spc24/25. The CENP-T pathway serves an important role to recruit the Ndc80 complex to kinetochores. In addition, a second parallel pathway for Ndc80 complex localization is mediated by the Mis12 complex.

The phosphorylated CENP-T N-terminal region binds to the Ndc80 complex using unique structural features

Our structural studies indicate that phosphorylation of several residues in the CENP-T N-terminal region is required for its interaction with the Ndc80 complex, but that these sites are not directly involved in the interaction with Spc24/25. Instead, the phospho-mimetic T72D CENP-T residue forms a salt bridge with R74 to allow the downstream hydrophobic residues to interact with Spc24/25. This is in contrast with a canonical phospho-peptide-protein interaction such as phospho-S/T binding for 14-3-3 family proteins (Yaffe and Smerdon, 2001; Yaffe and Elia, 2001). Negatively charged phospho-peptides bind to a positively charged pocket in 14-3-3 proteins with the phosphorylated residues directly involved in the interaction. This interaction mode has provided a major model for phospho-dependent protein interactions (Yaffe and Elia, 2001). The binding of phosphorylated CENP-T with the Spc24/25 complex represents a distinct model for generating phospho-dependent protein interactions. The binding mode of phosphorylated CENP-T is similar to that of RNA polymerase II recognition by 3'-RNA processing factors in which phosphorylation of RNA polymerase II is not directly involved in recognition of 3'-RNA processing factors, but stabilizes the β-turn with an additional hydrogen bond (Meinhart and Cramer, 2004).

In addition to the phospho-dependent interaction of CENP-T with Spc25, we also found a second hydrophobic-interaction surface between CENP-T and Spc24 that involves the L68 residue of CENP-T. CENP-T L68R mutants failed to interact with the Spc24/25 complex even in the phospho-mimetic form (Figure 7). This indicates that CENP-T has multiple hydrophobic-interaction sites for the Spc24/25 complex. Although

CENP-T phosphorylation strongly enhances binding to the Spc24/25 complex, the hydrophobic interactions form the basis for the CENP-T-Spc24/25 association.

Structure predictions suggest that the CENP-T N-terminal region is largely unstructured (Figure 6; Suzuki et al., 2011). In recent years, many proteins have been discovered that are unstructured alone, but form defined structures upon binding their biological targets (Dyson and Wright, 2005). For example, the N-terminal histone tails are unstructured alone, but when modifications such as methylation occur in this region, the modified tail is able to bind to target proteins such as HP1 resulting in the formation of a discrete structure. Moses et al. proposed that CDK target sites are frequently clustered in such unstructured regions (2007). Indeed, we have found that CDK target sites are clustered in the unstructured region of CENP-T (Figure 6). Once the CENP-T N-terminal region is phosphorylated, CENP-T binds to the Spc24/25 complex and forms a defined three-dimensional structure. The T-P-R residues (72-74) that are required for CENP-T phosphorylation and the downstream hydrophobic residues are well conserved. However, the T72 residue is absent in some fungi including *S. cerevisiae* Cnn1/CENP-T (Figure 6; Bock et al., 2012; Schleiffer et al., 2012). Instead, the phosphorylated threonine residue is replaced with a glutamate in budding yeast. Pearlman et al. demonstrated that some phosphorylation sites in proteins such as DNA-topoII, enolase, and C-Raf are changed to negatively charged amino acids (D/E) during evolution, thus mimicking the presence of a constitutively phosphorylated residue (2011). Although budding yeast Cnn1/CENP-T does not appear to use a similar binding mode (Malvezzi et al., 2013), the glutamate residue may form an unidentified salt-bridge with positively-charged residues to generate a non-regulated interaction between

CENP-T/Cnn1 and the Ndc80 complex. The T-P-R sequence and the downstream hydrophobic residues found in CENP-T efficiently enhance the hydrophobic interaction between CENP-T and Spc24/25, providing a unique way to facilitate protein-protein interactions.

RWD domains serve as interaction modules at kinetochores

The globular region of the Spc24/25 complex contains an “RWD” domain found in RING finger proteins, WD-repeat containing proteins, and DEXD-like helicases, which is composed of two similar folded α + β sandwiches (Schmitzberger and Harrison, 2012). Recently, the structure of the yeast Ctf19-Mcm21 complex, which corresponds to the vertebrate CENP-P-O complex, was determined and found to also contain an RWD domain (Schmitzberger and Harrison, 2012). An RWD domain is also found in the kinetochore protein Csm1 (Corbett et al., 2010). As at least five different kinetochore proteins contain this RWD domain, Schmitzberger and Harrison proposed that the RWD domain is an important interaction module to assemble the kinetochore (2012). However, it was unclear how other kinetochore proteins interact with this domain. The structure of the CENP-T-Spc24/25 complex provides evidence that the RWD domain serves as an interaction module for kinetochore assembly. RWD domains are also found in Gcn2, ubiquitin ligase, and FANCL (Schmitzberger and Harrison, 2012). Based on the work described here for the CENP-T-Spc24/25 interaction, hydrophobic residues in RWD domains make important contributions to protein-protein interactions, and phosphorylation of RWD binding partners may facilitate additional hydrophobic interactions.

CENP-T is a structural hub for formation of functional kinetochores

Previous biochemical studies revealed that the Ndc80 complex associates with the Mis12 complex, which in turn interacts with the inner kinetochore protein CENP-C (Cheeseman et al., 2004; Obuse et al., 2004; Przewloka et al., 2011; Screpanti et al., 2011; Gascoigne et al., 2011). Petrovic et al. demonstrated that the Nsl1 subunit of the Mis12 complex binds to tightly to Spc24/25 (2010). We previously found that, although the localization of the Ndc80 complex to kinetochores is reduced in Mis12- or CENP-C-deficient cells (Kline et al., 2006; Kwon et al., 2007; Gascoigne et al., 2011), Ndc80 localization was also reduced in CENP-H- or CENP-T-deficient cells (Okada et al., 2006; Hori et al., 2008; Gascoigne et al., 2011). As CENP-C and CENP-T localization is independent (Hori et al., 2008; Gascoigne et al., 2011) and we demonstrated that the binding of CENP-T and the Mis12 complex to Spc24/25 was mutually exclusive in this study, we propose that there are two parallel pathways for outer kinetochore assembly. Such parallel pathways have also been proposed from the study of the yeast CENP-T homologue Cnn1 (Malvezzi et al., 2013). It is important to define how these pathways are organized to recruit the Ndc80 complex to kinetochores. It is possible that the Ndc80 complex shows temporally regulated binding such that it interacts with the Mis12 complex and CENP-T at distinct times in mitosis. However, CENP-T is phosphorylated throughout mitosis (Gascoigne et al., 2011) and the interaction of the Mis12 complex with the Ndc80 complex also occurs during mitosis. Therefore, in vertebrates it is likely that these two pathways act simultaneously. *C. elegans* and *D. melanogaster* lack visible CENP-T homologues and the analyses that have been done indicate that compromising the Mis12 pathway results in a kinetochore null phenotype. Therefore, it

may be sufficient to have a single Ndc80 recruitment pathway to assemble the chromosome-segregation machinery. The two pathways that are present in vertebrates and fungi may act redundantly to strengthen the connection between the inner and outer kinetochore, or may recruit functionally distinct populations of the Ndc80 complex.

Materials and methods

Protein preparation and size-exclusion chromatography

Chicken and human Spc24 and Spc25 globular domains were cloned into pRSFduet co-expression vector. 6xhis-TEV-Spc25 (chicken 132-234 aa, human 70-224 aa, and human 129-224 aa) and StrepII-TEV-Spc24 (chicken 125-195 aa, human 57-197 aa, and human 131-197 aa) were expressed in BL21 (DE3) Star-pRARE2LysS by the addition of 0.2 mM IPTG for 16 h at 16°C. The Spc24/25 complex was purified using Ni-Sepharose, TEV cleavage and a Superdex 200 column. Chicken CENP-Ts (2-98 aa, 63-98 aa, or 2-50 aa) and human CENP-Ts (76-106 aa or 2-32 aa) were cloned into pMal-TEV-CENPT-6xHis vector to prepare MBP-fused proteins. MBP-CENP-Ts were expressed in same condition as the Spc24/25 complex. MBP-CENP-Ts were purified by Ni-Sepharose and Superdex200 column. For crystallography, the CENP-T-Spc24/25 complex was co-expressed in BL21(DE3)Star-pRARE2Lys by co-transforming pRSFduet-Spc24-Spc25 and pMal-6xHis-TEV-CENPT vectors. The CENP-T-Spc24/25 complex was purified by Ni-Sepharose, Superdex 200 column, TEV cleavage and Superdex 200 column. For expression of the human 6xHis-Mis12-KNL1$^{2106–2316}$ complex, 6xHis-Mis12 complex (Kline et al., 2006) was co-expressed with untagged KNL1$^{2106–2316}$ and purified as described previously. Also see Petrovic et al. (2010). CENP-T-6xHis (aa 1-375) wild-type and T85D (created by site-directed mutagenesis using QuikChange (Agilent Technologies)) constructs were expressed under the same conditions as the 6xHis-Mis12. The Ndc80^{Bonsai} complex was expressed as described previously (Ciferri et al., 2008). The Ndc80^{Bonsai} I149A_L154A mutant was generated by site-directed mutagenesis using QuikChange (Agilent Technologies). Proteins were

purified using Glutathione agarose (Sigma) or Ni-NTA agarose (QIAGEN) according to the manufacturer's guidelines and then exchanged into 50 mM Tris (pH 7.6), 200 mM NaCl, 1 mM DTT, followed by size-exclusion chromatography.

Analytical size-exclusion chromatography experiments were performed on a calibrated Superose6 10/300 column in the presence of 50 mM Tris (pH 7.6), 200 mM NaCl, 1 mM DTT at a flow rate of 0.3 ml/min. Elution of proteins was monitored at A280 nm. To detect complex formation, proteins were mixed together in a volume of 500 µl at final concentrations of 4 µM each for pairwise mixing experiments and 1 µM, 5 µM, and 25 µM in competition experiments for KNL1CT/Mis12, Ndc80^{Bonsai}, and hsCENP-T-MBP, respectively. Protein mixtures were incubated on ice for 30 minutes before conducting the chromatography. Fractions were collected and analyzed by SDS-PAGE and Coomassie staining.

Crystallization and structural determination of the Spc24/25 complex and CENP-T-Spc24/25 complex

The chicken Spc24/25 complex was crystallized by mixing equal amounts of the protein solution (10mg/ml) and MORPHEUS crystallization screening kit F1 solution (Molecular Dimensions; Gorrec, 2009), which contained a mixture of 0.12 M Monosaccharides, 0.1 M MES-Imidazole pH 6.5, and 30% PEG20K/P550MME. Crystals were harvested in crystallization solution and were flash frozen under nitrogen stream. X-ray diffraction data were collected at BL44XU in the SPring8 synchrotron facility. Diffraction data was processed by HKL2000 package. Structure was determined by molecular replacement using Phenix package (Adams et al., 2010). The Spc24/25 coordinate from the human Ndc80^{Bonsai} complex (PDB ID=2VE7) was used as a search model. Model was refined

using iterative modeling and refinement. The final model contains Spc24 (136 -195 aa), Spc25 (131-233 aa) and 251 water molecules. The chicken CENP-T-Spc24/25 complex was crystallized by mixing equal amount of protein solution (10 mg/ml) and PACT premier F10 solution (Molecular Dimensions; Newman et al., 2005) which contained a mixture of 0.02 M Na/K phosphate, 0.1 M Bis Tris propane pH 6.5 and 20% PEG 3350. Crystals were harvested in crystallization solution and were cryoprotected by the addition of 20% glycerol in final concentration. X-ray diffraction data were collected at BL38B1 in the SPring8 synchrotron facility. Diffraction data was processed by HKL2000 package. Structure was determined by molecular replacement using Phenix package. The chicken Spc24/25 complex was used as a search model and refined iteratively. The final model contains CENP-T (63-93 aa), Spc24 (134-195 aa), Spc25 (134-232 aa) and 357 water molecules. Figures were prepared using PyMOL package (DeLano Scientific LLC).

Cell Culture

DT40 cells were cultured as described previously (Okada et al., 2006). Spc25-deficient cells were created using standard methods.

Immunofluorescence and light microscopy

Chicken DT40 cells were cultured and transfected as described previously (Okada et al., 2006). Immunofluorescent staining of DT40 cells was performed as described previously using anti-CENP-T, anti-Mis12, or anti-Ndc80 antibodies (Okada et al., 2006; Kline et al., 2006; Hori et al., 2008). Immunofluorescence images were collected with a cooled EM CCD camera (QuantEM, Roper Scientific) mounted on an Olympus IX71

inverted microscope with a 100X objective together with a filter wheel and a DSU confocal unit. 15-25 Z-sections were acquired at 0.3 μm steps. Fluorescence intensity measurements were conducted using MetaMorph software (Molecular Devices). Kinetochore fluorescence intensities were determined by measuring the integrated fluorescence intensity within a 6 × 6 pixel square positioned over a single kinetochore and subtracting the background intensity of a 6 × 6 pixel square positioned in a region of cytoplasm lacking kinetochores. Maximal projected images were used for these measurements.

Isothermal Titration Calorimetry (ITC)

For interaction between CENP-T fusion protein, CENP-T peptides, and the Spc24/25 complex, proteins were dialyzed in 10mM HEPES pH 7.4, 500 mM NaCl and 1 mM DTT. CENP-T was diluted to 100 μM and titrated into 10 μM of Spc24/25. For interaction between human CENP-T, the Mis12 complex and the Spc24/25 complex, proteins were dialyzed in 10mM HEPES pH 7.4, 150 mM NaCl and 1 mM TCEP. The Spc24/25 complex was diluted to 100 μM and titrated into 10 μM of the Mis12 complex. CENP-T was diluted to 100μM and titrated into 10 μM of the Spc24/25 complex. Interaction between CENP-T, the Mis12 complex and the Spc24/25 complex were measured by AutoiTC200 (GE Healthcare) and data were analyzed with Origin 7 software (MicroCal).

Composition Gradient-Multi Angle Light Scattering (CG-MALS)

CG-MALS between MBP-CENP-T and the Spc24/25 complex were measured by CalypsoII system (Wyatt Technology Corp.) 10 μM of each solution were mixed in ten

different composition gradients and their static light scattering was measured by DAWN-HELIOS system. Optilab differential refractometer and UV absorption detector were used to measure the protein concentration. Data was analyzed by CalypsoII system software.

Accession Numbers

The Protein Data Bank (PDB) IDs of the chicken the Spc24/25 complex and the CENP-T-Spc24/25 complex are 3VZ9 and 3VZA, respectively.

Chapter III: Distinct organization and regulation of the outer kinetochore KMN network downstream of CENP-C and CENP-T

Reprinted with permission from Cell Press:

Rago, F., K.E. Gascoigne, and I.M. Cheeseman. 2015. Distinct Organization and Regulation of the Outer Kinetochore KMN Network Downstream of CENP-C and CENP-T. *Curr. Biol.* 25:671–677. doi:10.1016/j.cub.2015.01.059.

Karen Gascoigne performed the initial characterization of the localization of the Dsn1 Aurora B mutant in HeLa cells throughout the cell cycle.

Summary

The kinetochore provides a vital connection between chromosomes and spindle microtubules (Cheeseman and Desai, 2008; Rago and Cheeseman, 2013). Defining the molecular architecture of the core kinetochore components is critical for understanding the mechanisms by which the kinetochore directs chromosome segregation. The KNL1/Mis12 complex/Ndc80 complex (KMN) network acts as the primary microtubule binding interface at kinetochores (Cheeseman et al., 2006), and provides a platform to recruit regulatory proteins (London and Biggins, 2014). Recent work found that the inner kinetochore components CENP-C and CENP-T act in parallel to recruit the KMN network to kinetochores (Nishino et al., 2013; Gascoigne et al., 2011; Malvezzi et al., 2013; Schleiffer et al., 2012). However, due to the presence of these dual pathways, it has not been possible to distinguish differences in the nature of kinetochore assembly downstream of CENP-C or CENP-T. Here, we separated these pathways by targeting CENP-C and CENP-T independently to an ectopic chromosomal locus in human cells. Our work reveals that the organization of the KMN network components downstream of CENP-C and CENP-T is distinct. CENP-C recruits the Ndc80 complex through its interactions with KNL1 and the Mis12 complex. In contrast, CENP-T directly interacts with Ndc80, which in turn promotes KNL1/Mis12 complex recruitment through a separate region on CENP-T, resulting in functional relationships for KMN network localization that are inverted relative to the CENP-C pathway. We also find that distinct regulatory paradigms control the assembly of these pathways, with Aurora B kinase promoting KMN network recruitment to CENP-C, and cyclin-dependent kinase (CDK) regulating KMN network recruitment to CENP-T. This work reveals unexpected

complexity for the architecture and regulation of the core components of the kinetochore-microtubule interface.

Results

Distinct regions of CENP-T recruit KMN network components

Previous work has analyzed kinetochore assembly primarily at endogenous kinetochores, which contain both CENP-C- and CENP-T-based assembly pathways (Nishino et al., 2013; Gascoigne et al., 2011; Malvezzi et al., 2013; Schleiffer et al., 2012). To circumvent the challenge posed by the presence of these dual pathways at endogenous kinetochores, we targeted CENP-C or CENP-T separately to an ectopic chromosomal locus in human cells. For these experiments, we utilized our established assay in which a lac repressor (LacI) fusion protein targets CENP-C or CENP-T to an integrated lac operon (*lacO*) array in U2OS cells in the absence of the reciprocal protein (Gascoigne et al., 2011). We found that the N-terminal 100 amino acids of CENP-C were necessary and sufficient to recruit all KMN network components (KNL1, Mis12 complex, Ndc80 complex) to the *lacO* array (Figure 1A, 1B, 2A), consistent with prior work (Przewloka et al., 2011; Screpanti et al., 2011; Milks et al., 2009; Gascoigne et al., 2011). However, despite previous reports that the N-terminal 21 amino acids of CENP-C were sufficient to interact with the Mis12 complex in vitro (Screpanti et al., 2011), we found that CENP-C 1-21 was unable to recruit the KMN network to LacI foci in cells (Figure 1B, 2A). Direct interactions between the CENP-C N-terminus (residues 1-234) and the entire KMN network can also be reconstituted in vitro (Figure 3A).

We next analyzed the requirements for KMN network recruitment downstream of CENP-T. Previous work found that all three KMN network components are recruited to GFP-CENP-T-LacI foci via the N-terminal 375 amino acids of CENP-T (Gascoigne et al., 2011). Although CENP-T binds to the Ndc80 complex directly (Nishino et al., 2013),

biochemical experiments cannot recreate robust interactions between CENP-T and the KNL1/Mis12 complex, even with Ndc80 present (Figure 3B; Nishino et al., 2013; Schleiffer et al., 2012). In addition, the Mis12 complex and N terminus of CENP-T (aa 76-106) bind to the Ndc80 complex in a mutually exclusive manner, precluding assembly of the KMN network in the canonically defined manner (Schleiffer et al., 2012; Nishino et al., 2013; Malvezzi et al., 2013; Ciferri et al., 2005; 2008; Wei et al., 2005; 2006; 2007; Cheeseman et al., 2006; DeLuca et al., 2006; Wilson-Kubalek et al., 2008). We found that the first 106 amino acids of CENP-T were sufficient to recruit the Ndc80 complex to the *lacO* array (Figure 1C, 1D), consistent with previous data (Nishino et al., 2013; Malvezzi et al., 2013). However, neither the Mis12 complex nor KNL1 were recruited by this CENP-T fragment. A reciprocal truncation (CENP-T residues 107-375) was unable to recruit any KMN network components (Figure 1C, 1D). A series of additional CENP-T truncations (Figure 1D, 2B) allowed us to refine the minimal functional region required for the recruitment of the complete KMN network to residues 1-230. This analysis suggests that a conserved domain in the vicinity of amino acids 200-230 in CENP-T (Figure 2C) is important for KNL1/Mis12 complex recruitment. Therefore, although the KMN network is biochemically stable on its own (Cheeseman et al., 2006; Petrovic et al., 2014; 2010), the recruitment of KMN network components to CENP-T foci is separable.

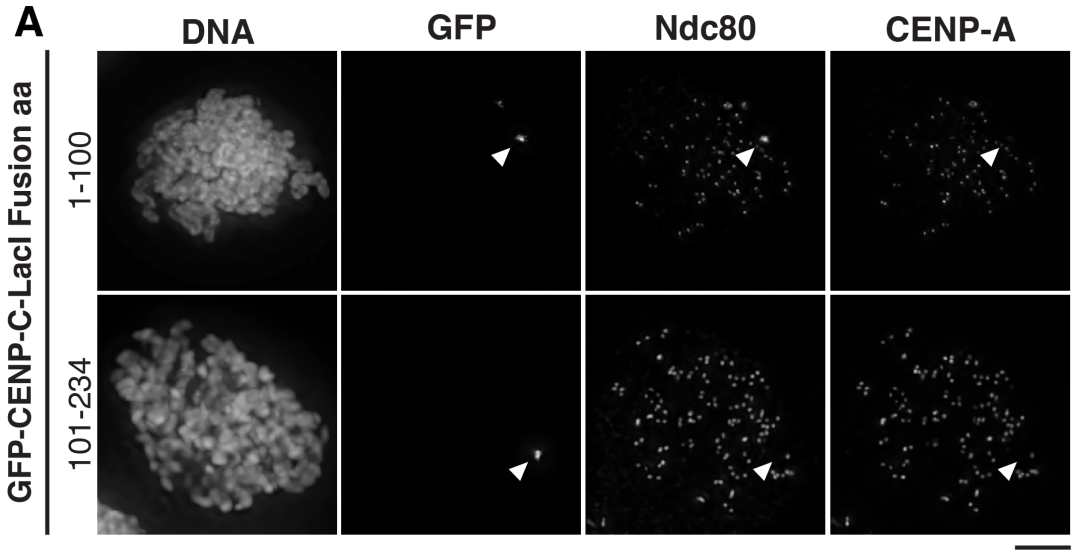

B

GFP-LacI Fusion	Colocalization with GFP?		
CENP-C aa	Ndc80	Mis12	KNL1
1-234	+	+	+
1-21	-	-	-
1-100	+	+	+
101-234	-	-	-

D

GFP-LacI Fusion	Colocalization with GFP?		
CENP-T aa	Ndc80	Mis12	KNL1
1-375	+	+	+
1-106	+	-	-
107-375	-	-	-
1-150	+	-	-
1-200	+	-	-
1-250	+	+	+
1-230	+	+	+

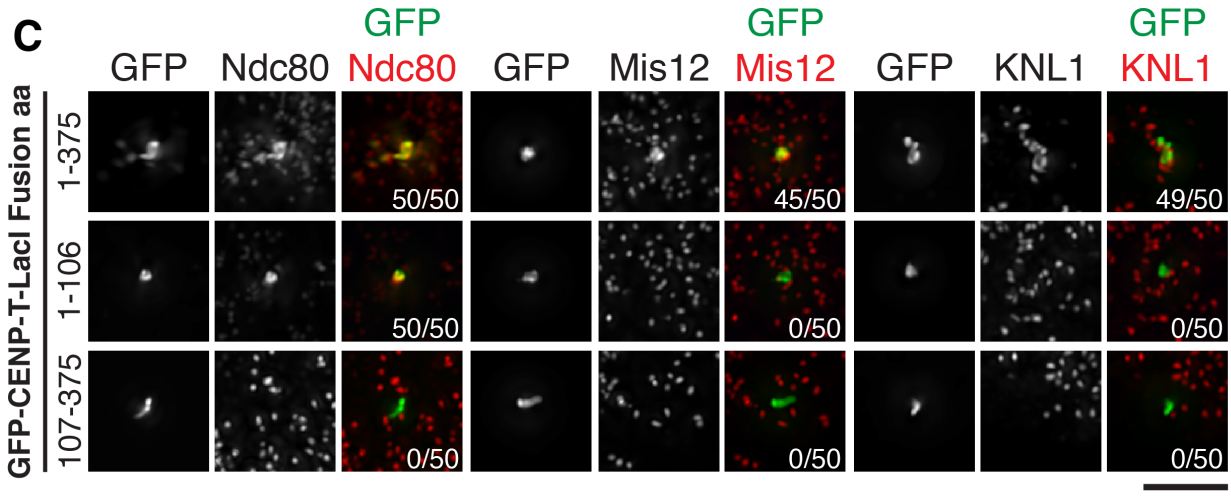

Figure 1: KMN network components display separable recruitment to CENP-T. A) Immunofluorescence images showing positive (GFP-CENP-C (1-100)-LacI) or negative (GFP-CENP-C (101-234)-LacI) co-localization with anti-Ndc80 in nocodazole-treated cells. Chosen cells lacked overlap between the GFP focus and endogenous kinetochores marked by anti-CENP-A. Images were scaled independently to show the full range of data. Arrowheads indicate position of the GFP focus. B) Summary of immunofluorescence experiments assessing co-localization of KMN components with the indicated CENP-C-LacI fusions. >90% of cells display indicated behavior (N = 50 cells/condition). C) Representative immunofluorescence images showing localization of GFP-CENP-T-LacI foci and KMN components in nocodazole-arrested mitotic cells. Images were scaled independently to show full range of data. Numbers in lower right indicate number of mitotic cells showing co-localization. D) Summary of co-localization of KMN components with CENP-T-LacI fusions. >90% of cells observed display indicated behavior (N = 50 cells/condition). Scale bars, 5 μm.

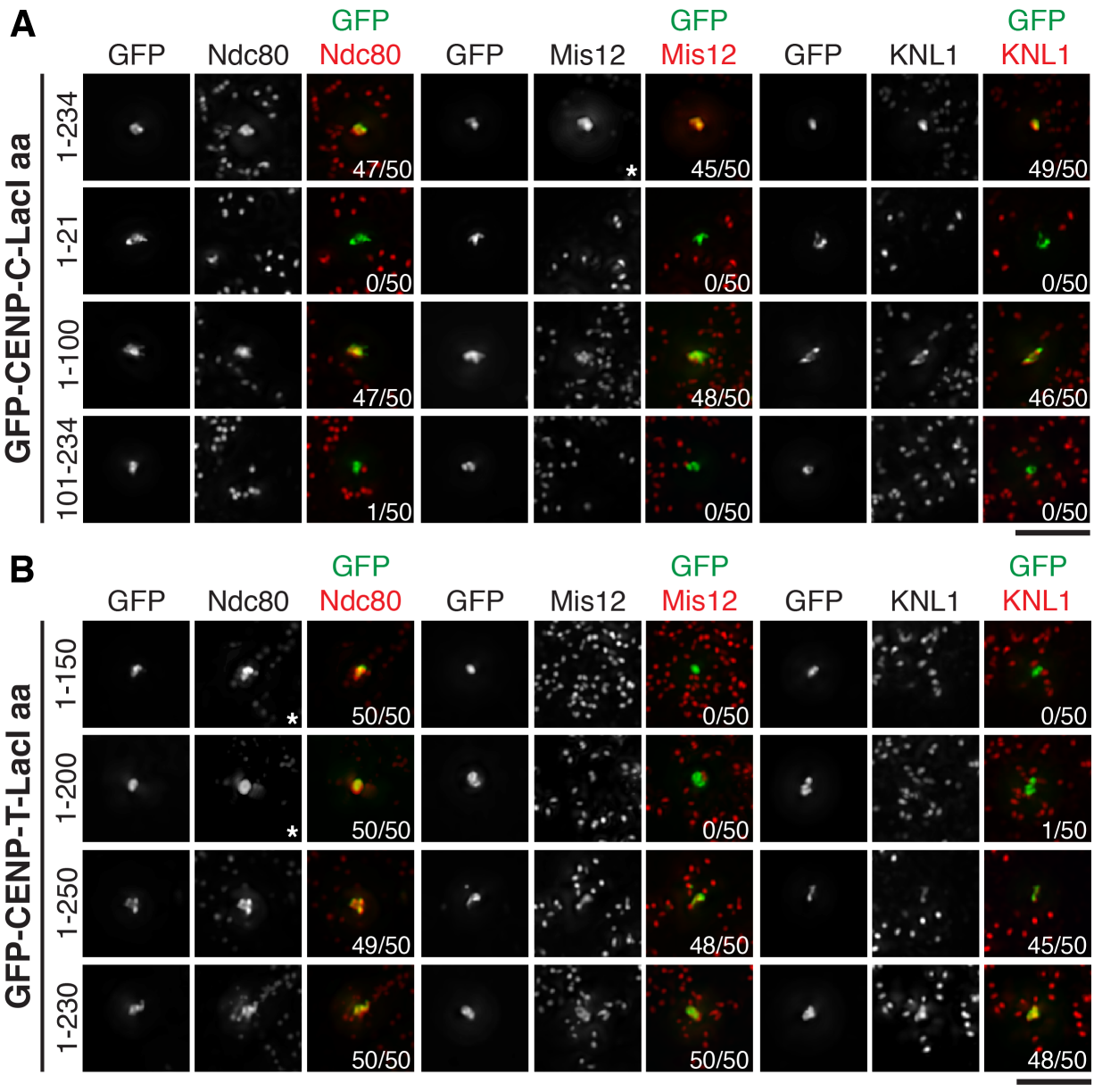

C

```
Homo sapiens 200 qsvqrpglarrpparravdvgaflrdlrdtsla----------------ppnivledtqpfsqpmvg 250
Mus musculus 203 etverpglarrrpirqlvnagallqdlednslasalpgdshrtpvaalpmdvgledtqpfsqslaa 268
Macaca mulatta 200 qsvqrpglarrpparravdvgaflrdlrdtsla----------------ppnivledtqpfsqptvg 250
Pongo abelii 200 qsvqrpglarrpparravdvgaflrdlrdtsla----------------ppnivledtqpfsqptvg 250
Rattus norvegicus 201 qtvdrpglarrrpvrrpvnigaflqnlenksltsalpgdshrtpvaalptdvvfedtqpfsqplag 266
Ailuropoda melanoleuca 201 qsvqrpglarrpptrravdvgaflqdlrdtslalas------------padtvledtqpfsqplvg 254
Equus caballus 201 qsvqrpglarrpptrravdvgaflqdlrdtslalap-------------pdtvledtqpfsqplvg 253
                   ::*:******* * *: *: **:*::*.:.**:                :  :********  ..
```

Figure 2: CENP-C recruitment of KMN network proteins occurs at the N-terminus and CENP-T recruits Ndc80 and KNL1/Mis12 via two separate domains. A) Representative immunofluorescence images showing the GFP-CENP-C-LacI foci stained for each of the corresponding KMN network components in mitotic cells arrested using nocodazole. Images of Ndc80 localization for CENP-C aa 1-100 and 101-234 were replicated from Figure 1A. All images were scaled independently to show the full range of the data. Images marked with * were scaled in gamma. Numbers in lower right corner indicate number of mitotic cells out of 50 that showed co-localization between the GFP focus and the indicated test protein. B) Representative immunofluorescence images showing localization of the GFP-CENP-T-LacI foci as well each of the corresponding KMN network components in mitotic cells arrested using nocodazole. All images were scaled independently to show the full range of the data. Images marked with * were scaled in gamma. Numbers in lower right corner indicate number of mitotic cells out of 50 that showed co-localization between the GFP focus and indicated test protein. C) Alignment of CENP-T from the indicated species was performed using Clustal Omega (McWilliam et al., 2013). Scale bars, 5 μm.

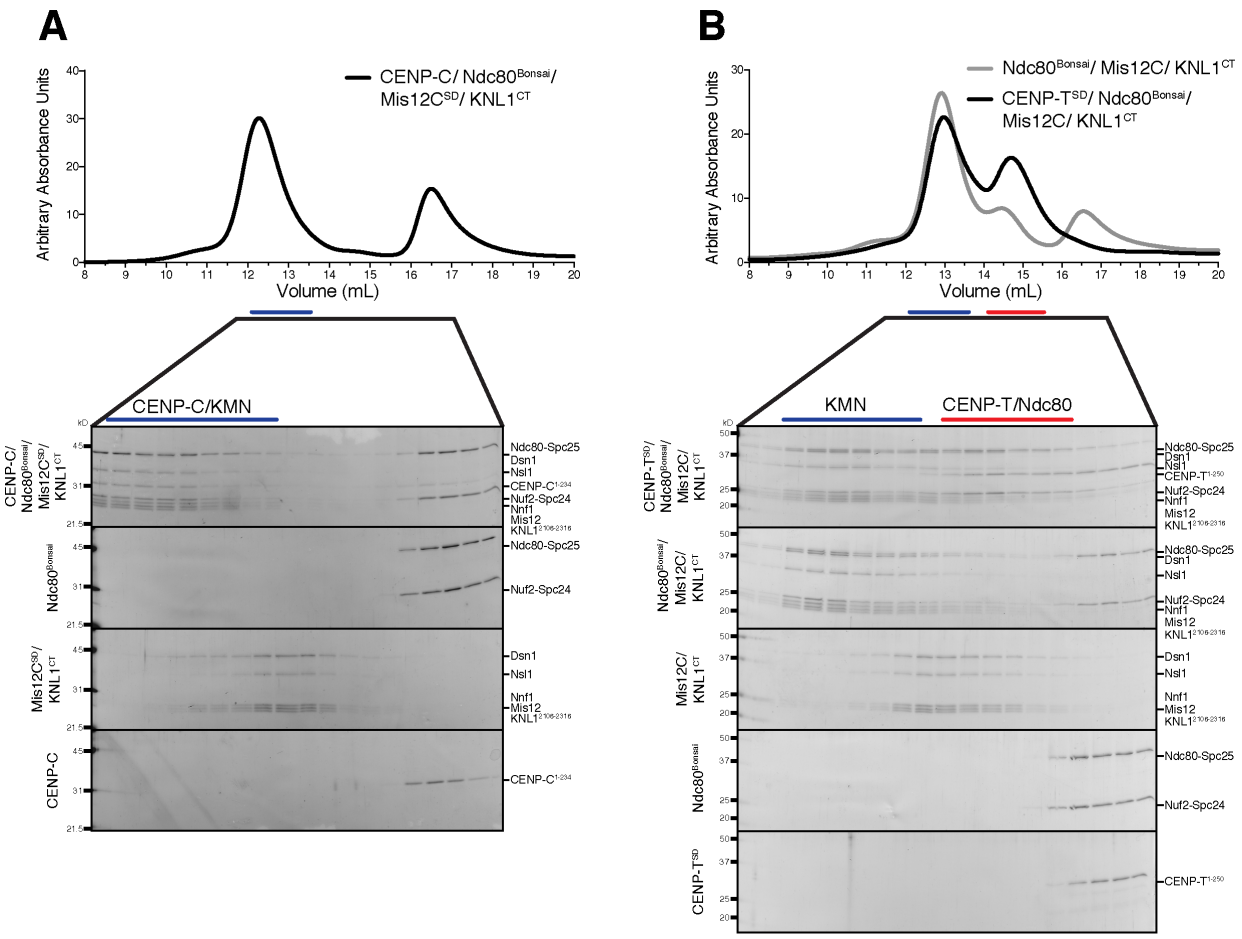

Figure 3: Binding of KMN network components to CENP-C and CENP-T in vitro. A) Top: Size exclusion chromatography elution profile of CENP-C$^{1-234}$, Ndc80^{Bonsai}, Mis12C^{SD}, KNL1$^{2106-2316}$ purified from bacteria. Bottom: SDS-PAGE of equivalent fractions for the indicated proteins, in combination and separately. B) Top: Size exclusion chromatography elution profile of recombinant purified CENP-T^{SD}(1-250), Ndc80^{Bonsai}, Mis12C, KNL1$^{2106-2316}$ (black) and Ndc80^{Bonsai}, Mis12C, KNL1$^{2106-2316}$ (gray) purified from bacteria. Bottom: SDS-PAGE of equivalent fractions for the indicated proteins, in combination and separately.

KMN network components display inverted functional relationships downstream of CENP-C and CENP-T

We next sought to dissect the dependency relationships between KMN network components at CENP-C and CENP-T foci. Prior work analyzing the kinetochore assembly hierarchy downstream of CENP-C (Kline et al., 2006; Screpanti et al., 2011; Milks et al., 2009; Przewloka et al., 2011) suggested that the Mis12 complex and KNL1 act upstream to recruit the Ndc80 complex (Cheeseman et al., 2004; 2006; Kline et al., 2006; Liu et al., 2006). To define the relationships between KMN components, we performed RNAi depletions and quantified KMN network recruitment to CENP-T-LacI or CENP-C-LacI foci. Consistent with previous models for KMN network organization, we found that KNL1 and the Mis12 complex are interdependent at both CENP-C and CENP-T foci (Petrovic et al., 2014; Cheeseman et al., 2006). In addition, we found that depletion of KNL1 or the Mis12 complex subunit Dsn1 led to the loss of the Ndc80 complex at CENP-C-LacI foci (Figure 4A). In contrast, depletion of the Ndc80 complex subunit Nuf2 did not strongly disrupt the recruitment of KNL1 or Mis12 to CENP-C-LacI foci (Figure 4A). Partial loss of KNL1/Mis12 complex localization following Nuf2 depletion has been described previously (Cheeseman et al., 2004) and is consistent with a stabilizing role for the Ndc80 complex in KMN network assembly. These dependency relationships agree with previous analyses of the CENP-C pathway, with Ndc80 complex recruitment occurring downstream of KNL1 and Mis12 (Figure 4C).

In contrast, we found distinct relationships for the KMN network components downstream of CENP-T. KNL1 or Dsn1 depletion resulted in a modest reduction in Ndc80 complex localization (Figure 4B), suggesting that these proteins are not required

for Ndc80 complex recruitment, but may stabilize Ndc80 bound to the CENP-T receptor. Strikingly, depletion of Nuf2 eliminated KNL1 and Mis12 recruitment to CENP-T-LacI foci (Figure 4B). These data suggest that the Ndc80 complex acts upstream of KNL1 and the Mis12 complex for the CENP-T-based kinetochore assembly pathway (Figure 4D), such that these functional relationships are inverted relative to the CENP-C-based pathway.

To test whether this organization also exists at endogenous kinetochores, we next conducted RNAi experiments in HeLa cells. Co-depletion of CENP-C and CENP-T significantly reduced KMN network localization relative to the individual depletions (Figure 4C; Gascoigne et al., 2011), consistent with the presence of dual pathways. As we found that the Ndc80 complex was required upstream of KNL1 and the Mis12 complex at CENP-T foci (Figure 4B), we predicted that depletion of either Ndc80 or CENP-T should cause a similar failure of KNL1/Mis12 complex recruitment. Indeed, co-depletion of CENP-C and the Ndc80 complex subunit Nuf2 resulted in a severe reduction of Mis12 localization to levels equivalent to those observed when both the CENP-T and CENP-C pathways were disrupted directly (Figure 4E). These data support a model in which KMN network recruitment downstream of CENP-T is promoted by the Ndc80 complex.

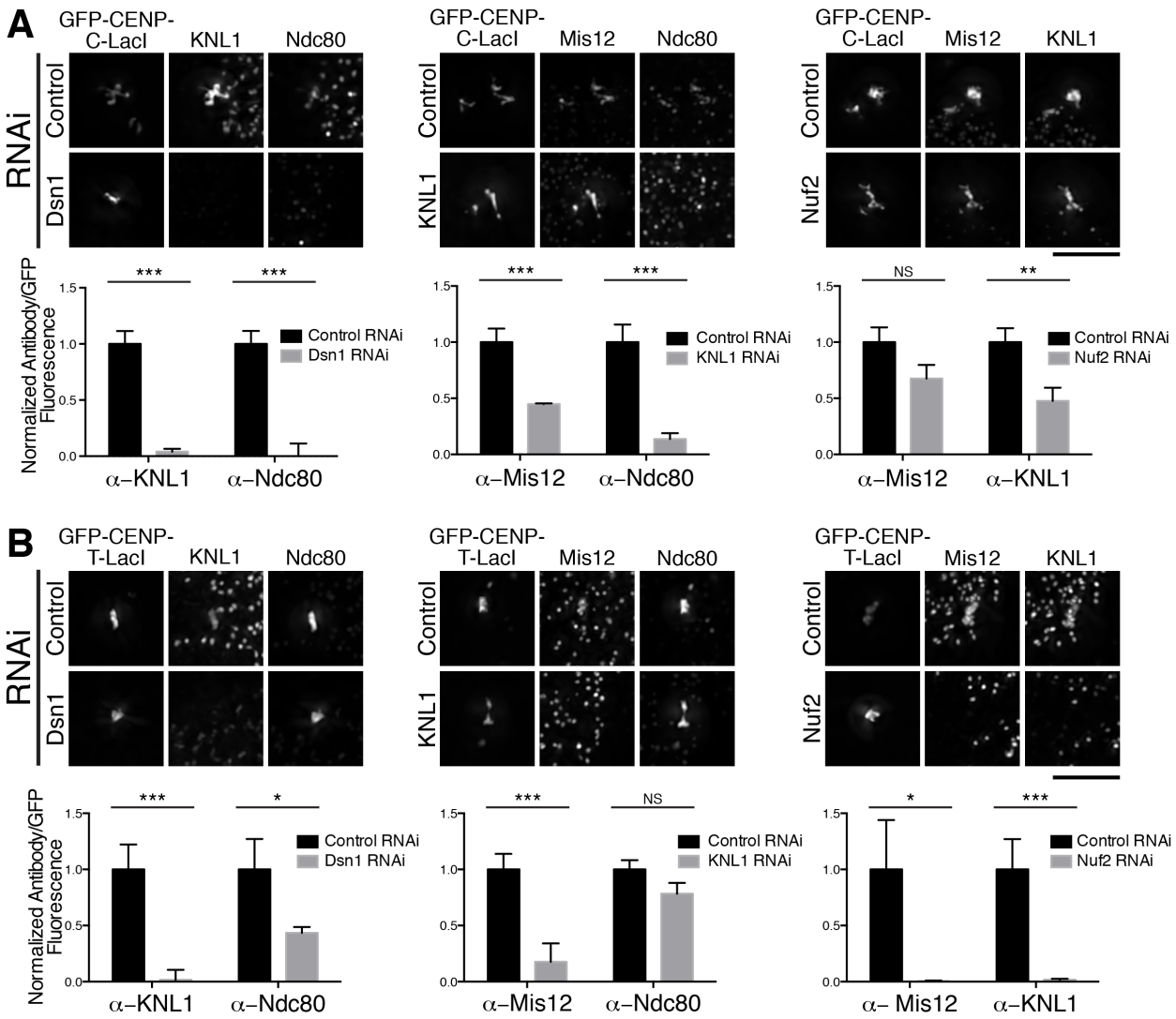
A
GFP-CENP-C-LacI
KNL1
Ndc80
Mis12
Nuf2
RNAi
Control
Dsn1
KNL1
Normalized Antibody/GFP Fluorescence
Control RNAi
Dsn1 RNAi
KNL1 RNAi
Nuf2 RNAi
α–KNL1
α–Ndc80
α–Mis12
***
**
*
NS
B
GFP-CENP-T-LacI
α– Mis12

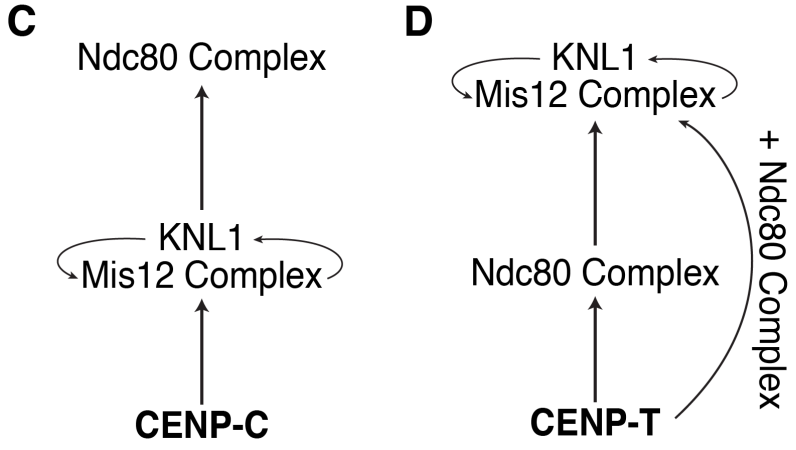
C
Ndc80 Complex
KNL1
Mis12 Complex
CENP-C
D
KNL1
Mis12 Complex
Ndc80 Complex
CENP-T
+ Ndc80 Complex

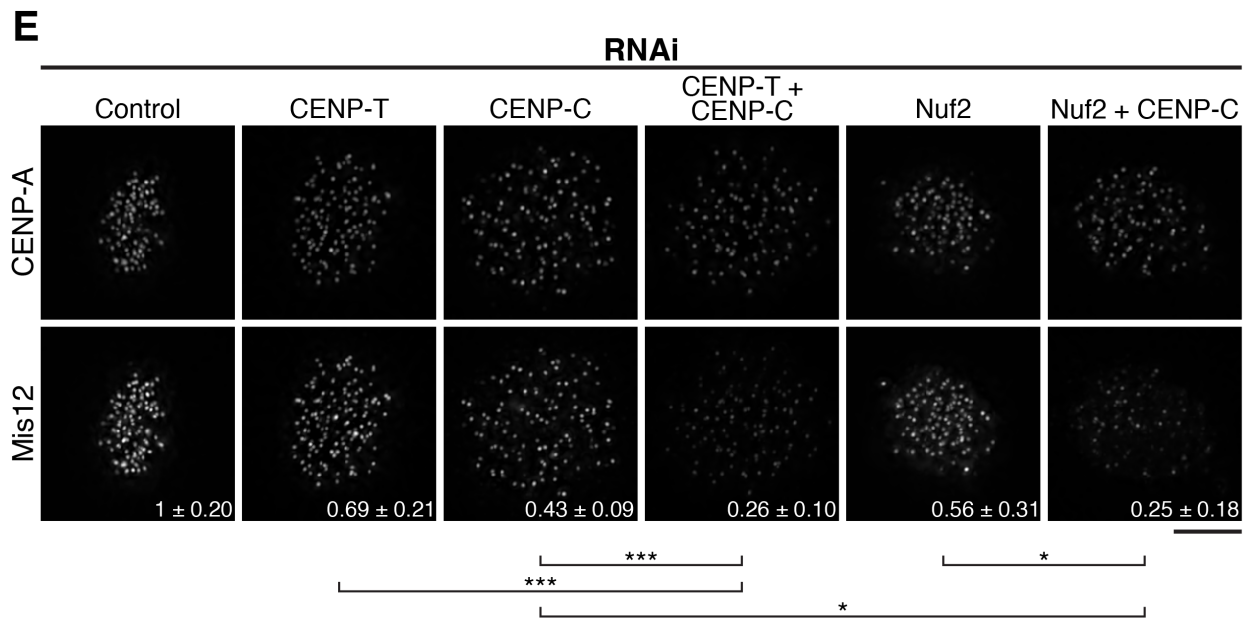

Figure 4: The KMN network displays distinct dependency relationships for recruitment downstream of CENP-C and CENP-T. A and B) Top: Representative immunofluorescence images of GFP-CENP-C (1-100)-LacI (A) and GFP-CENP-T (1-250)-LacI (B) foci following depletion of KMN components. Bottom: Quantification of antibody/GFP intensity ratio at the focus, normalized to control RNAi (+/- SEM). N = 20. C) Schematic of interdependency of KMN components for the CENP-C and D) CENP-T pathways determined by RNAi (this figure) and truncation analyses (Figures 1 and 2). For CENP-T, KNL1/Mis12 complex recruitment requires the Ndc80 complex and a second region on CENP-T. E) Representative immunofluorescence images showing anti-CENP-A and anti-Mis12 complex levels in HeLa cells. Quantification of Mis12 is shown in bottom right as fraction of control RNAi +/- standard deviation. N = 10. Student's t-test (for panels A-C) - NS: not significant, *: $p<0.05$, **: $p<0.01$; ***: $p<0.001$. Scale bars, 5 μm.

CDK phosphorylation regulates the recruitment of KMN network components through multiple distinct regions within CENP-T

Although CENP-C and CENP-T are present at centromeres throughout the cell cycle, the KMN network assembles prior to mitotic entry and disassembles at mitotic exit (Gascoigne and Cheeseman, 2013a). Therefore, we next assessed the regulation of outer kinetochore assembly downstream of CENP-C and CENP-T. Our previous work highlighted the importance of cyclin-dependent kinase (CDK) in promoting the binding and recruitment of the Ndc80 complex to CENP-T (Gascoigne and Cheeseman, 2013a; Gascoigne et al., 2011; Nishino et al., 2013). This work identified residues 76-106 in CENP-T as a key Ndc80 complex binding region (Nishino et al., 2013). Based on

sequence homology, there is a similar motif at amino acids 11-25 in CENP-T. Each motif includes a mapped CDK phosphorylation site (residue T11 or T85) (Figure 5A; Gascoigne and Cheeseman, 2013a; Nishino et al., 2013). Disrupting these motifs individually through an N-terminal truncation (CENP-T aa 25-375), or using non-phosphorylatable T11A or T85A single mutants, did not prevent KMN network recruitment to the ectopic locus (Figure 5B, 5C, 6A, 6B). In contrast, a T11A T85A double mutant abrogated recruitment of the KMN network (Figure 5B, 5C, 6A, 6B). This suggests that both Ndc80 complex binding motifs are functional. However, our data do not distinguish whether a single CENP-T simultaneously recruits two Ndc80 complexes (with incomplete occupancy of these sites), or whether these motifs act together to create a robust binding interface for a single Ndc80 molecule.

We next tested the regulation of KNL1 and Mis12 complex localization downstream of CENP-T. Our truncation analysis identified amino acids 200-230 in CENP-T as critical for KNL1 and Mis12 complex recruitment (Figure 1D, 2B). Therefore, we generated a phospho-inhibitory mutation in the neighboring CDK phosphorylation site, T195 (Figure 5A). Although Ndc80 complex localization to CENP-T T195A mutant foci was largely unaffected (Figure 5C), the levels of KNL1/Mis12 were strongly reduced (Figure 5B, 5C, 6A, 6B). Despite the importance in vivo of phosphorylation of T11, T85, and T195, phospho-mimetic mutations cannot reconstitute robust interactions between CENP-T and the complete KMN network in vitro (Figure 3B).

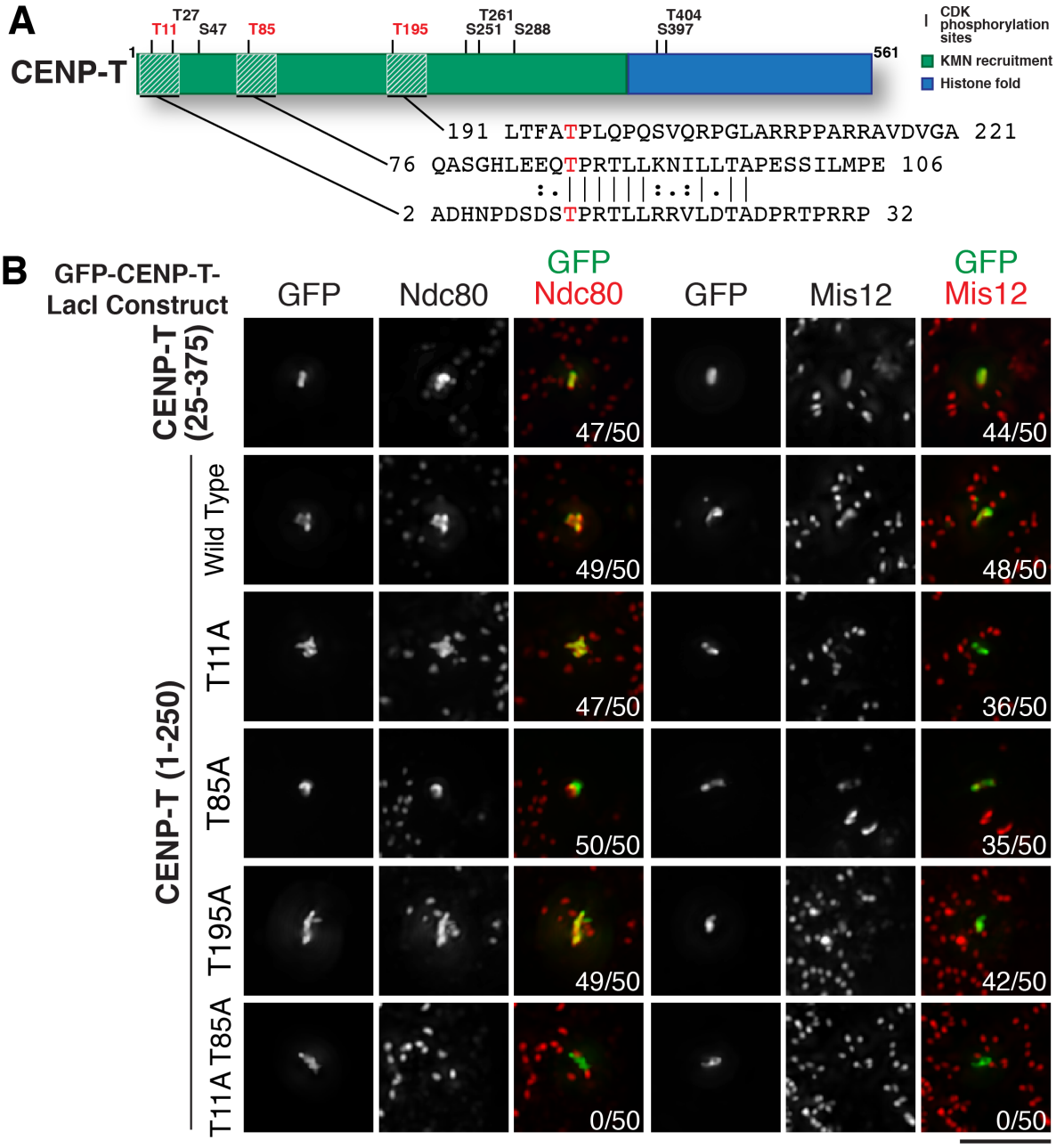
A
CENP-T
T11
T27
S47
T85
T195
T261
S251
S288
T404
S397
1
561
CDK phosphorylation sites
KMN recruitment
Histone fold
191 LTFATPLQPQSVQRPGLARRPPARRAVDVGA 221
76 QASGHLEEQTPRTLLKNILLTAPESSILMPE 106
2 ADHNPDSDSTPRTLLRRVLDTADPRTPRRP 32
B
GFP-CENP-T-LacI Construct
GFP
Ndc80
GFP Ndc80
GFP
Mis12
GFP Mis12
CENP-T (25-375)
CENP-T (1-250)
Wild Type
T11A
T85A
T195A
T11A T85A
47/50
44/50
49/50
48/50
47/50
36/50
50/50
35/50
49/50
42/50
0/50
0/50
C
Normalized Ndc80/GFP Fluorescence
Normalized Mis12/GFP Fluorescence
1.5
1.0
0.5
0.0
***
NS
*
NS
**
WT
T11A
T85A
T195A
T11A T85A
GFP-CENP-T (1-250)-LacI

D

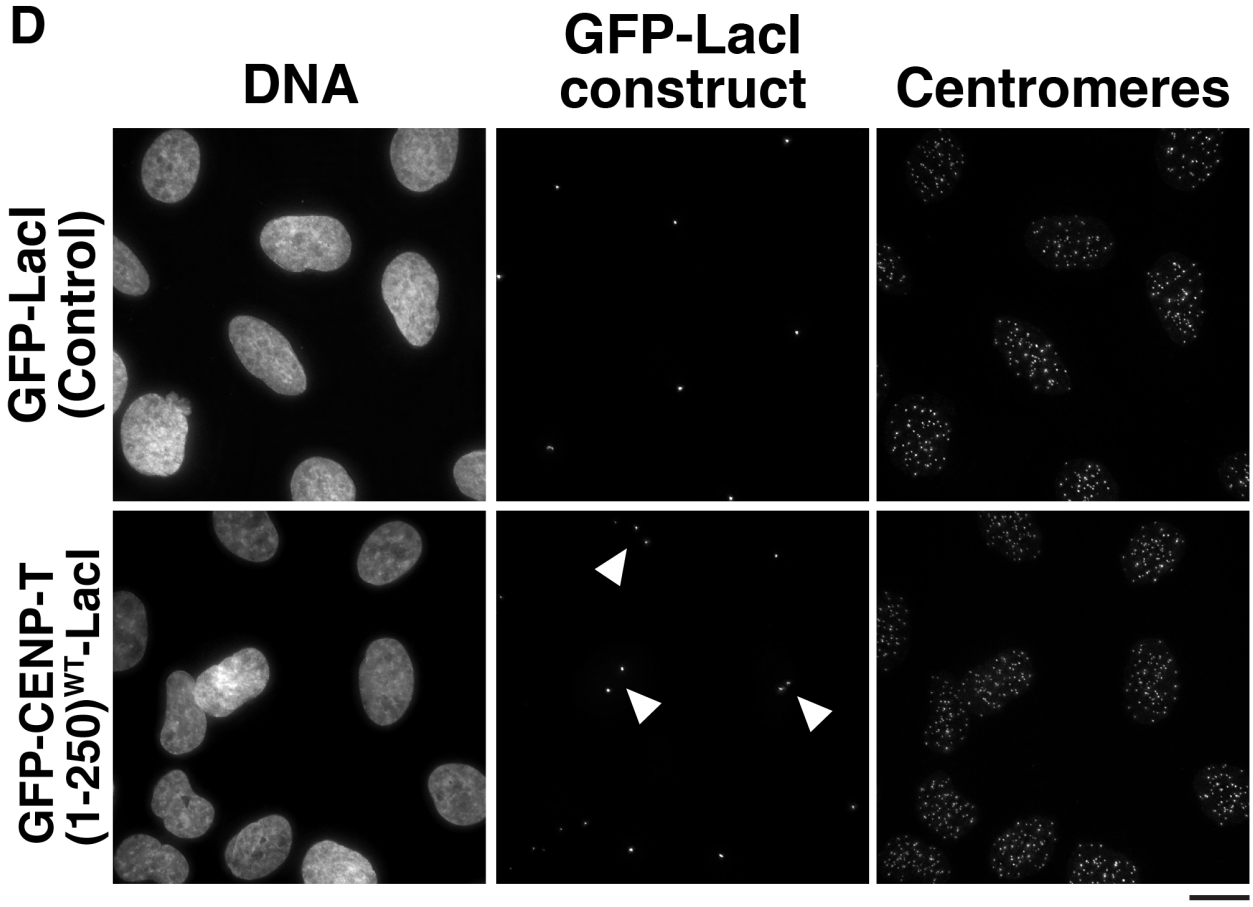

E

GFP-CENP-T (1-250) -LacI Fusion	% Cells with >1 LacI Focus
GFP-LacI (control)	**0%**
WT	**52%**
T11A	**12%**
T85A	**29%**
T195A	**49%**
T11A T85A	**8%**

Figure 5: Recruitment of KMN network to CENP-T is dependent on CDK phosphorylation. A) CENP-T schematic indicating its KMN network recruitment (Gascoigne et al., 2011) and histone fold (Nishino et al., 2012) domains. Indicated residues correspond to CDK phosphorylation sites (Gascoigne and Cheeseman, 2013a; Nishino et al., 2013) with those analyzed in this study in red. Sequences corresponding to hatched regions are shown below. Alignment was performed using EMBOSS Water (McWilliam et al., 2013). B) Representative immunofluorescence images showing GFP-CENP-T-LacI foci co-stained for Ndc80 or Mis12 complexes in nocodazole-treated cells. Images were scaled independently to show the full range of data. Numbers in lower right indicate the number of mitotic cells with co-localization between GFP and the indicated KMN component. Wild type CENP-T (1-250) images are duplicated from Figure 2. Scale bar, 5 μm. C) Quantification of antibody/GFP fluorescence ratio (+/- SEM) at the indicated foci normalized to wild type CENP-T. N = 10 cells/condition. Student's t-test, NS: not significant, *: $p<0.05$, **: $p<0.01$; ***: $p<0.001$. D) Immunofluorescence images of cells following 72 hr IPTG washout. Cells with >1 GFP focus are marked with arrowheads. Centromeres stained with anti-centromere antibodies (ACA). Scale bar, 15 μm. E) Table showing the frequency of cells with multiple GFP foci following 72 hr IPTG washout. N = 100 cells/condition.

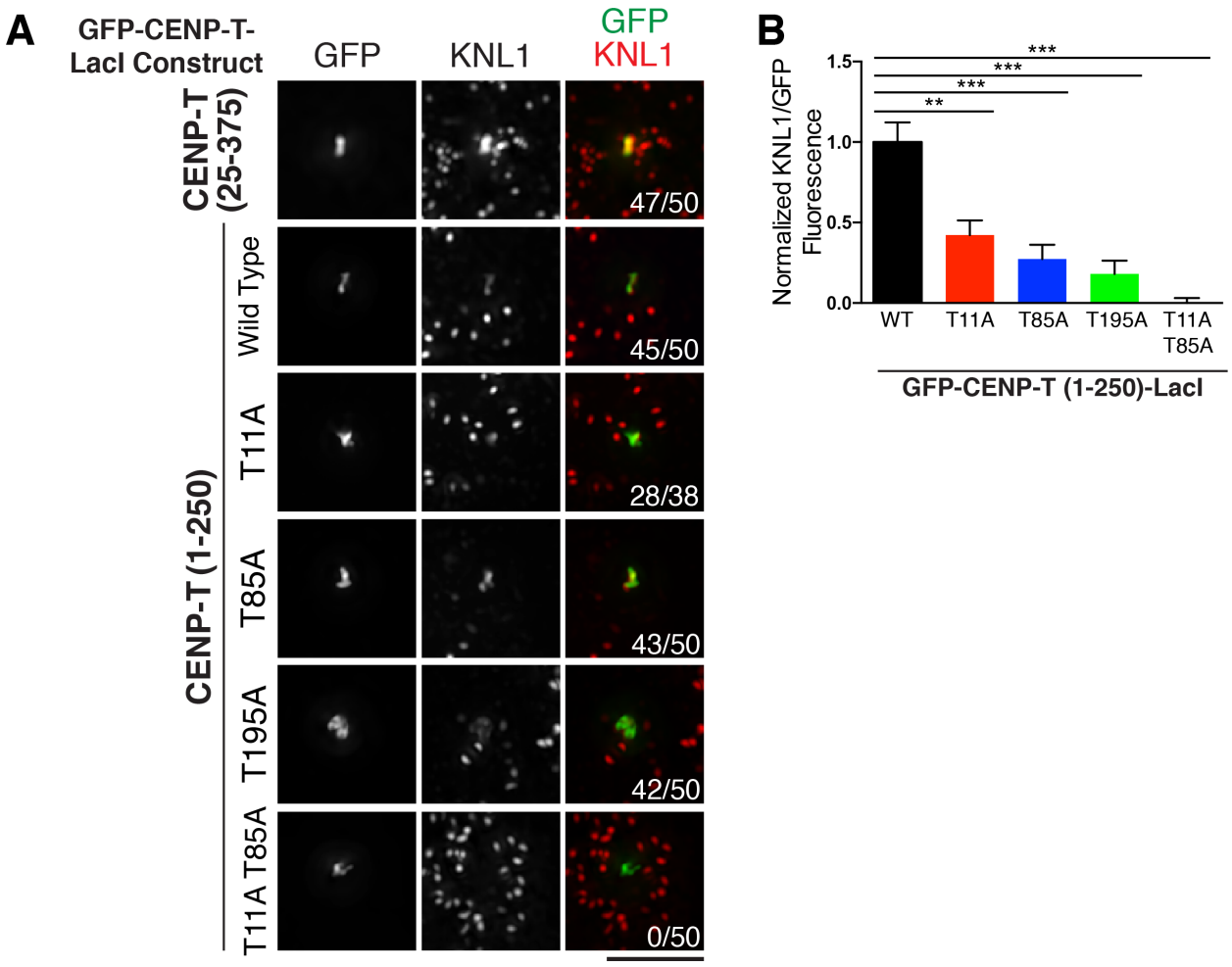

Figure 6: Analysis of KNL1 localization to CENP-T phospho-mutant foci. A) Representative immunofluorescence images showing GFP-CENP-T-LacI foci co-stained for KNL1 in nocodazole-treated cells. All images were scaled independently to show the full range of the data. Numbers in lower right corner indicate the number of mitotic cells that showed co-localization between the GFP focus and KNL1. The images for the wild type CENP-T 1-250 construct are duplicated from Figure 2. Scale bar, 5 μm. B) Graph showing the average ratio KNL1/GFP fluorescence (+/- SEM) for the indicated GFP-CENP-T-LacI foci (N = 10 cells/condition). Student's t-test - **: p<0.01; ***: p<0.001.

Finally, we tested the effect of altering KMN network recruitment downstream of CENP-T on chromosome segregation. Due to the integration of *lacO* in the arm of chromosome 1 in these cell lines, ectopic targeting of the CENP-T-LacI fusion creates a dicentric-like chromosome that strongly perturbs chromosome segregation (Gascoigne et al., 2011; Gascoigne and Cheeseman, 2013b). This behavior results in the accumulation of GFP foci (Gascoigne and Cheeseman, 2013b), but is suppressed by

the addition of IPTG to disrupt the *lacO*/LacI interaction. Cells expressing GFP-LacI as a control displayed a single focus in each cell, consistent with proper chromosome segregation (Figure 5D, E). In contrast, after removal of IPTG from the growth media for 72 hours, ~50% of cells expressing the wild type or T195A GFP-CENP-T-LacI construct had >1 focus, indicating chromosome missegregation (Figure 5D, 5E). However, CENP-T T11A, T85A, and T11A T85A mutants showed attenuated defects (Figure 5E), consistent with their reduced ability to recruit the KMN network (Figure 5C, 6B). Together, these data indicate that CDK regulates the interaction of CENP-T with the KMN network at multiple distinct sites, with functional consequences for chromosome segregation.

Aurora B kinase activity is required for kinetochore assembly downstream of CENP-C

We next analyzed the regulation of the CENP-C pathway. Aurora B kinase, which plays a key role in controlling kinetochore-microtubule attachments (Lampson and Cheeseman, 2011), has been implicated in kinetochore assembly in *Xenopus laevis* (Emanuele et al., 2008) and budding yeast (Akiyoshi et al., 2013). Although we previously observed that Aurora B inhibition in HeLa cells resulted in only a modest defect in kinetochore assembly (Welburn et al., 2010), we considered that this defect might be magnified when the CENP-C and CENP-T-based assembly pathways were analyzed separately. Indeed, treatment with the Aurora B inhibitor ZM447439 significantly reduced localization of all KMN network components to CENP-C-LacI foci (Figure 7A). In contrast, Ndc80 complex recruitment to the CENP-T-LacI focus was unaffected by ZM447439 treatment (Figure 7B). However, we observed significant loss of KNL1 and Mis12 complex localization to the CENP-T-LacI focus, suggesting that

Aurora B phosphorylation may play a role in stabilizing the Mis12/KNL1 interaction, or contribute to KNL1 and Mis12 complex recruitment downstream of CENP-T.

We next tested the role of Aurora B in regulating endogenous kinetochore assembly. We reasoned that if Aurora B promotes kinetochore assembly downstream of CENP-C, the effect of Aurora B inhibition would be magnified in the absence of the CENP-T-based assembly pathway. Indeed, combining CENP-T RNAi and ZM447439 treatment led to an enhanced reduction in Mis12 complex localization relative to the individual treatments (Figure 7C). In contrast, combining CENP-C RNAi and ZM447439 treatment did not lead to a further reduction in Mis12 complex localization relative to CENP-C depletion alone (Figure 7C).

Aurora B kinase directly phosphorylates KNL1, Ndc80, and the Mis12 complex subunit Dsn1 (Welburn et al., 2010). However, phosphorylation of KNL1 regulates its interactions with PP1 (Liu et al., 2012) and microtubules (Welburn et al., 2010), and Ndc80 phosphorylation regulates its interactions with microtubules (Cheeseman et al., 2006; DeLuca et al., 2006). Therefore, we evaluated the contribution of Aurora B phosphorylation of Dsn1 for promoting Mis12 complex localization. To test this, we analyzed a GFP-Dsn1 mutant in which the mapped Aurora B phosphorylation sites were mutated to aspartic acid (SD) to mimic constitutive phosphorylation (Welburn et al., 2010). This mutant localized to mitotic kinetochores similarly to wild type Dsn1. However, we found that the GFP-Dsn1 SD mutant displayed enhanced localization to G1 and G2 kinetochores (Figure 7D). This increased G1 localization was not affected by CENP-T depletion, but was strongly compromised following CENP-C depletion (Figure 8). In contrast, we previously reported that the corresponding GFP-Dsn1 phospho-

inhibitory mutant had minimal effects on its mitotic kinetochores localization (Welburn et al., 2010), suggesting that additional interactions promote mitotic Mis12 complex recruitment. In addition, the KMN network is able to interact with CENP-C in vitro regardless of its phosphorylation state (Figure 2A; data not shown; Screpanti et al., 2011). Together, these data suggest Aurora B kinase promotes the recruitment of the KMN network to kinetochores, particularly downstream of CENP-C.

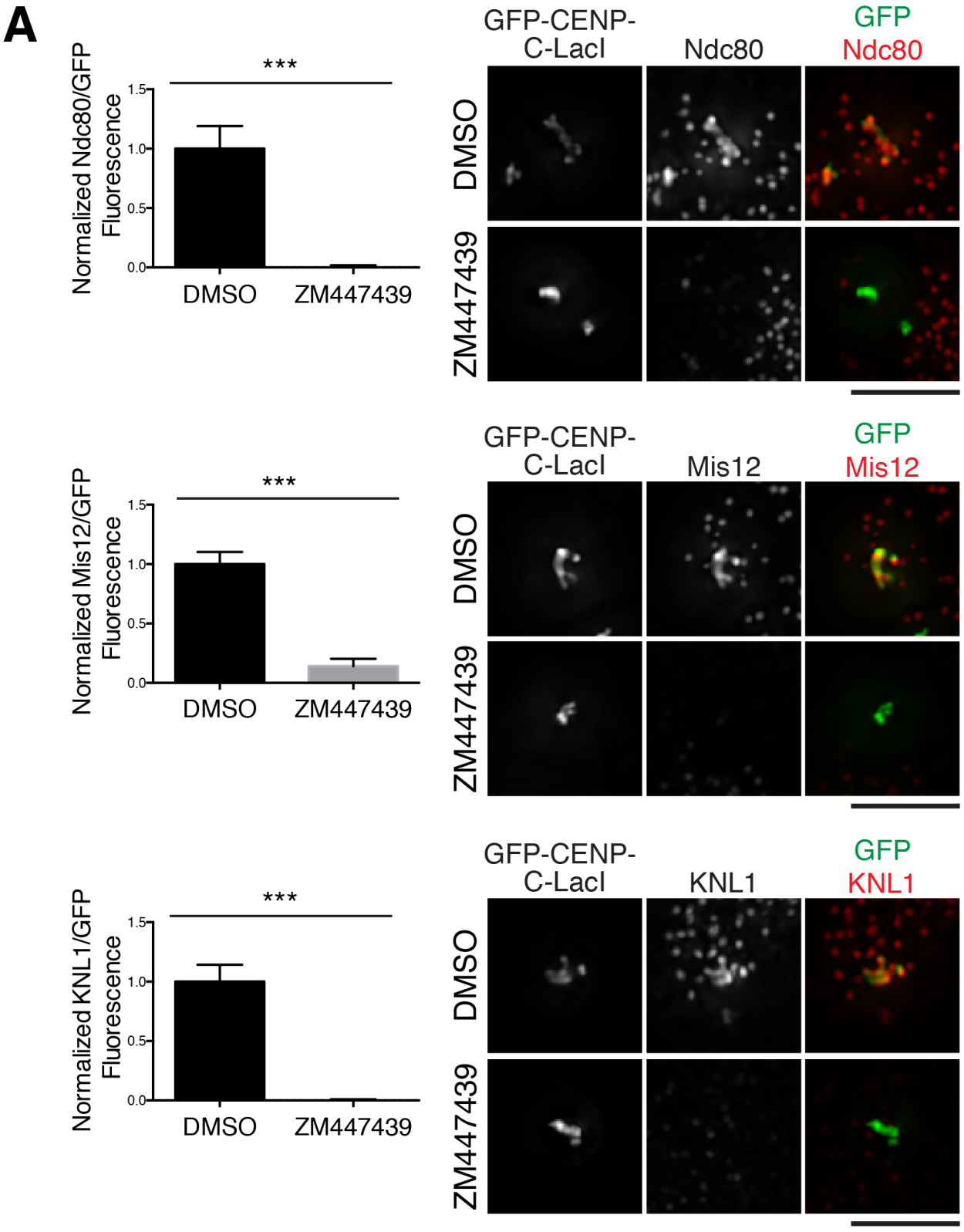
A
Normalized Ndc80/GFP Fluorescence
***
1.5
1.0
0.5
0.0
DMSO
ZM447439
GFP-CENP-C-LacI
Ndc80
GFP Ndc80
DMSO
ZM447439
Normalized Mis12/GFP Fluorescence
***
1.5
1.0
0.5
0.0
DMSO
ZM447439
GFP-CENP-C-LacI
Mis12
GFP Mis12
DMSO
ZM447439
Normalized KNL1/GFP Fluorescence
***
1.5
1.0
0.5
0.0
DMSO
ZM447439
GFP-CENP-C-LacI
KNL1
GFP KNL1
DMSO
ZM447439

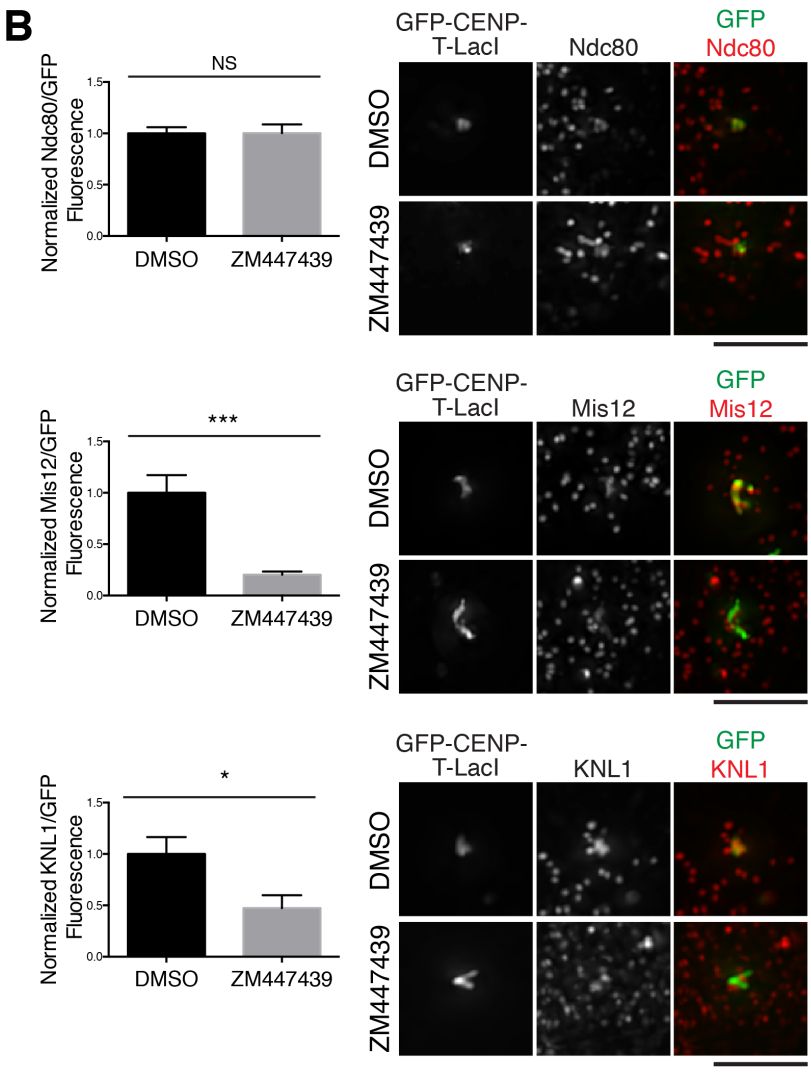
B
NS
Normalized Ndc80/GFP Fluorescence
DMSO
ZM447439
GFP-CENP-T-LacI
Ndc80
GFP Ndc80
DMSO
ZM447439
***
Normalized Mis12/GFP Fluorescence
DMSO
ZM447439
GFP-CENP-T-LacI
Mis12
GFP Mis12
DMSO
ZM447439
*
Normalized KNL1/GFP Fluorescence
DMSO
ZM447439
GFP-CENP-T-LacI
KNL1
GFP KNL1
DMSO
ZM447439

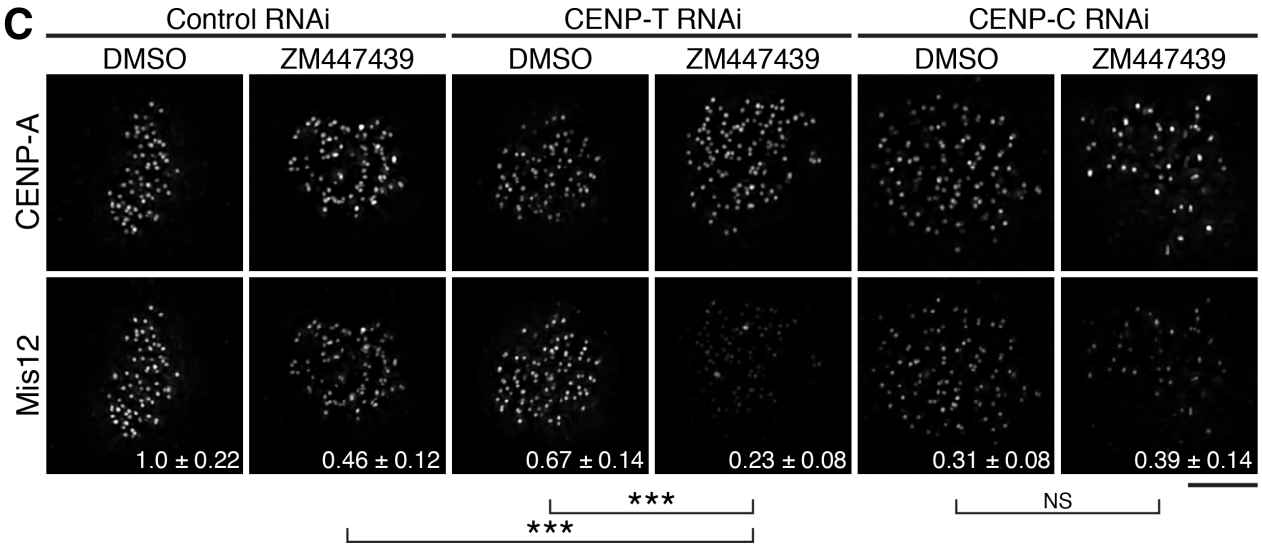
C
Control RNAi
CENP-T RNAi
CENP-C RNAi
DMSO
ZM447439
DMSO
ZM447439
DMSO
ZM447439
CENP-A
Mis12
1.0 ± 0.22
0.46 ± 0.12
0.67 ± 0.14
0.23 ± 0.08
0.31 ± 0.08
0.39 ± 0.14
***
***
NS

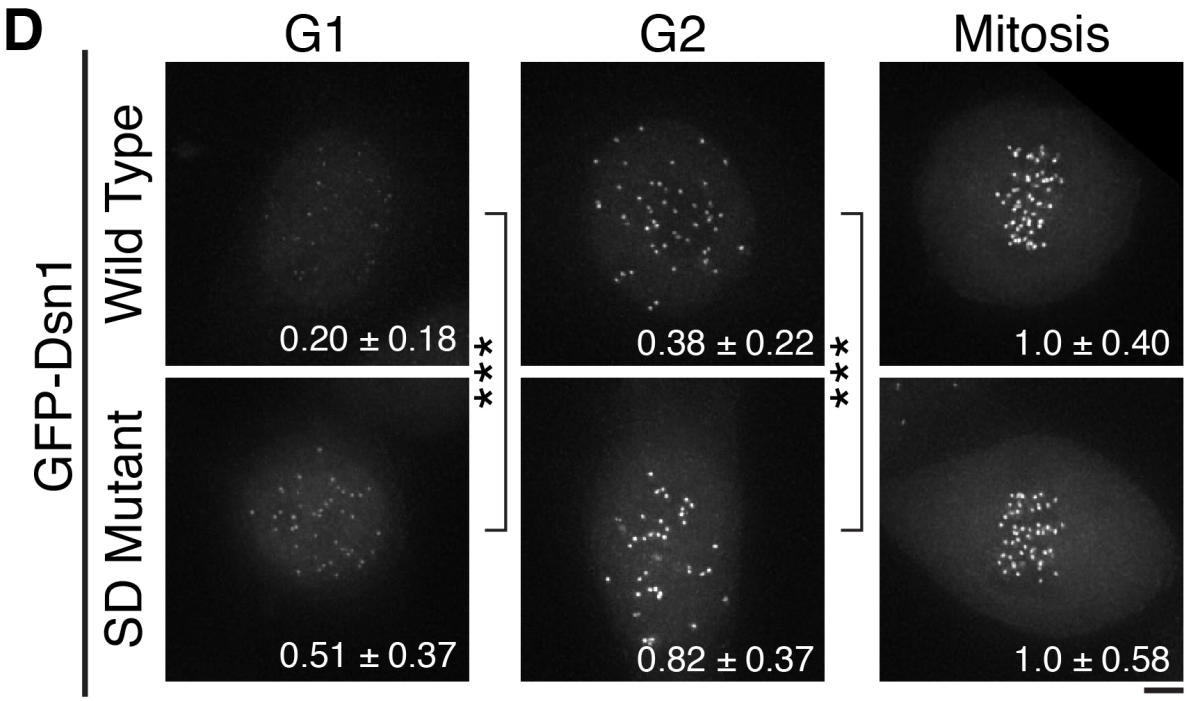

Figure 7: Aurora B kinase regulates KMN network recruitment downstream of CENP-C. A and B) Left: Quantification of antibody/GFP intensity normalized to DMSO treatment for the indicated conditions (+/- SEM). N=20. Right: Representative immunofluorescence images of GFP-CENP-C (1-100)-LacI (A) and GFP-CENP-T (1-250)-LacI (B) foci after treatment. C) Representative immunofluorescence images showing CENP-A and Mis12 levels in HeLa cells. Quantification of Mis12 at mitotic kinetochores is shown in bottom right as a fraction of control RNAi + DMSO +/- standard deviation. N = 10. All images were scaled relative to their DMSO and RNAi control. D) Representative immunofluorescence images of GFP-Dsn1 wild type and Aurora B phospho-mimetic (S28D S78D S100D S109D) mutant expressing HeLa cells after RNAi depletion of endogenous Dsn1. GFP fluorescence is shown in bottom right as a fraction of mitotic kinetochore fluorescence for each construct +/- standard deviation. N = 90-300 kinetochores/condition from multiple cells. Images were scaled equivalently within each cell line. Student's t-test (for panels A-D) - NS: not significant, *: $p < 0.05$, ***: $p < 0.001$. Scale bars, 5 μm.

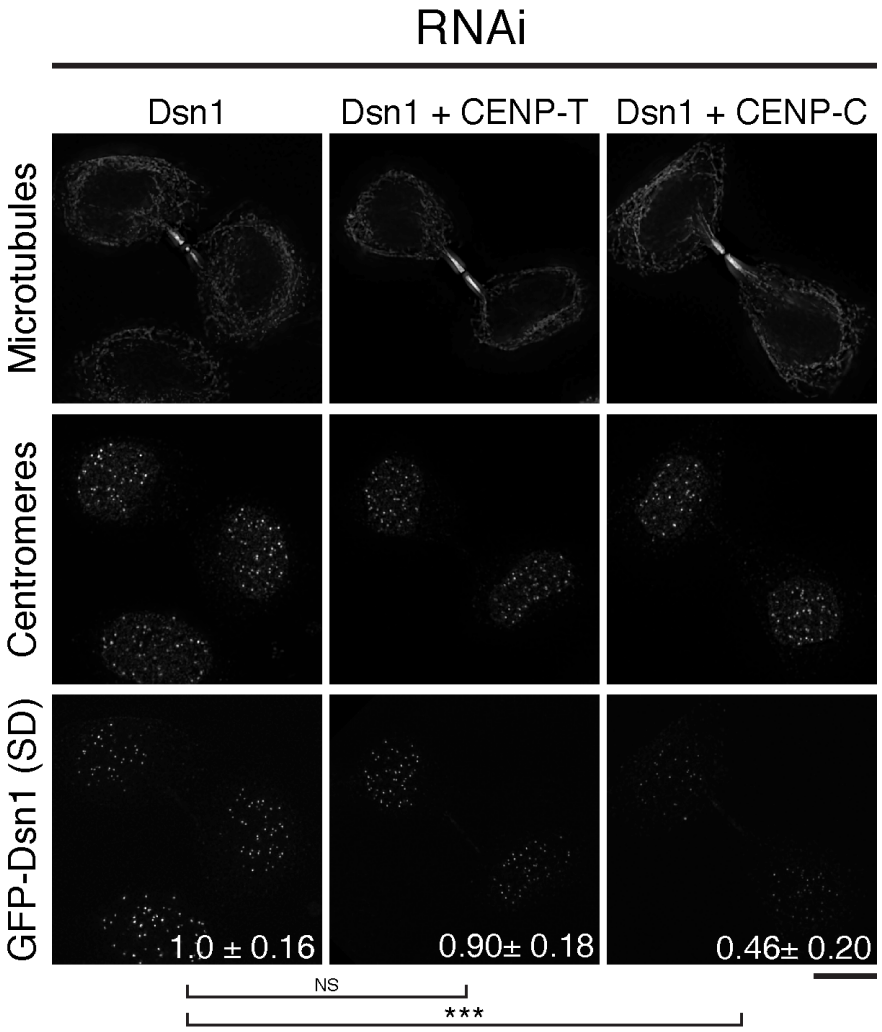

Figure 8: Dsn1 Aurora B mutants require CENP-C for their interphase localization. Representative immunofluorescence images showing the localization of the GFP-Dsn1 Aurora B phosphomimetic (SD; S28D, S78D, S100D, S109D) mutant in G1 cells. Cells were depleted of endogenous Dsn1, and were additionally co-depleted for CENP-C or CENP-T as indicated. Cells were probed with antibodies against centromeres (ACA) and microtubules (DM1alpha). Microtubule staining is scaled in gamma to visualize the range of data. Numbers indicate the fluorescence intensity of the GFP-Dsn1 mutant relative to cells depleted for endogenous Dsn1 alone +/- standard deviation. 20 G1 cells pairs were quantified for each condition. Student's t-test - NS: not significant, ***: $p<0.001$. Scale bar, 10 μM.

Discussion

Despite the identification of more than 100 different components of the human kinetochore, defining the basic kinetochore architecture remains an ongoing challenge. In particular, it was unclear how kinetochore components assemble downstream of the recently defined CENP-C- and CENP-T-based pathways. Here, we demonstrated that these two pathways are not simply duplications, but rather each pathway displays distinct regulation and functional relationships for KMN network recruitment (Figure 9).

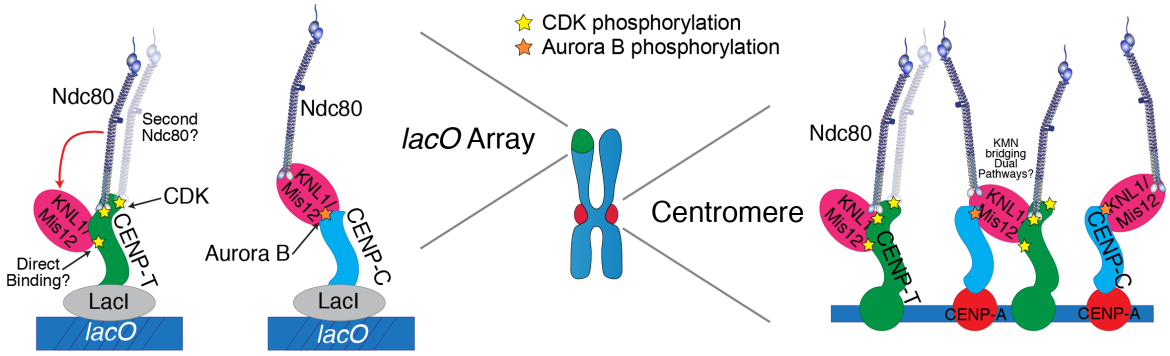

Figure 9: Model for KMN network recruitment at CENP-T or CENP-C foci (left) or endogenous kinetochores (right). It remains unknown whether KNL1/Mis12 interact directly with CENP-T, whether two Ndc80 complexes bind simultaneously to CENP-T, and whether a single KNL1/Mis12 complex can bridge CENP-T and CENP-C at endogenous kinetochores. Stars indicate phosphorylation by the indicated kinase.

Recent work from Kim and Yu also identified similar differences in the behavior and regulation of these pathways (2015). When tested separately at the ectopic focus, CENP-T and CENP-C are capable of independently recruiting the entire KMN network. However, it remains to be determined how the two pathways interact when both are present at endogenous kinetochores. For example, the KMN network components may be recruited independently by CENP-C and CENP-T, or a KMN unit may simultaneously interact with both receptors (Figure 9). We also cannot rule out the possibility that additional kinetochore components contribute to the recruitment of KNL1 and the Mis12

complex downstream of CENP-T at endogenous kinetochores. In summary, our work has uncovered a complex architecture for the core kinetochore components.

Materials and Methods

Cell Culture

U2OS *lacO* (Janicki et al., 2004) and HeLa cell lines were cultured in DMEM supplemented with 10% FBS, penicillin/streptomycin, and 2 mM L-glutamine. U2OS cells were maintained in 10 mM IPTG and 0.25 mg/mL Hygromycin B (Invitrogen). IPTG was washed out 24 (Figure 1, 5B, 5C, 7A, 7B, 2A, 2B, 6), 48 (4A, 4B), or 72 (4D, 4E) hr prior to fixation to allow recruitment of the LacI fusions to the *lacO* array. Where indicated, U2OS cells were incubated in 330 nM nocodazole for 14 hr to enrich for mitotic cells. For Aurora B kinase inhibition assays, cells were incubated in 2 μM ZM447439 (Tocris Bioscience) for 2 – 2.5 hr prior to fixation.

Cell Line Generation and Transfection

Clonal cell lines stably expressing GFP^{LAP} fusions were generated in U2OS *lacO* and HeLa cells as previously described (Cheeseman et al., 2004). RNAi resistant CENP-T and CENP-C used for fusion cloning were described previously (Gascoigne et al., 2011). Phosphomutants were generated using site-directed mutagenesis. All indicated truncations were generated by cloning into a GFP^{LAP}-X-LacI backbone (Gascoigne et al., 2011). Small interfering RNAs (siRNAs) against Nuf2 (5'-AAGCAUGCCGUGAAACGUAUAUU-3') (DeLuca et al., 2002), Dsn1 (5'-GGAAACUGAUGGAACUCUA-3', 5'-GGAGAUGAAUCAAGGCGUU, GAUCAUCAAUUGGAAUCAA-3', 5'-GCGGCGAGCAAGUAUGAAA-3') (Kline et al., 2006), KNL1 (5'-GGAAUCCAAUGCUUUGAGA-3') (Cheeseman et al., 2008), CENP-T (5'-CGGAGAGCCCUGCUUGAAA-3') (Gascoigne et al., 2011), CENP-C (5'-GAACAGAAUCCAUCACAAA-3') (Gascoigne et al., 2011), and a nontargeting control

were obtained from Dharmacon. siRNAs were transfected using Lipofectamine RNAi MAX and serum-free OptiMEM (Invitrogen). DMEM plus 10% FBS was added after 6 hr and cells were fixed 48 hr after transfection.

Immunofluorescence and Microscopy

U2OS cells were pre-extracted for 3 minutes in PBS plus 0.1% Triton X-100 before fixation in 4% formaldehyde in PBS. HeLa cell lines in which mitotic populations were analyzed were pre-extracted for 5 minutes in PBS plus 0.5% Triton X-100 before fixation in 4% formaldehyde in PBS. In cases where G1 populations were being observed, pre-extraction was performed in PHEM (60 mM PIPES, 25 mM HEPES, 10 mM EGTA, 2 mM $MgCl_2$, pH 6.9) plus 0.5% Triton X-100, and subsequently fixed in 4% formaldehyde in PHEM. Ndc80 was detected using either mouse anti-Hec1 (9G3, Abcam; for Figure 4A, 4B) or a polyclonal rabbit anti-$Ndc80^{Bonsai}$ against the entire Ndc80 complex ((Schmidt et al., 2012); for Figure 1A, 1C, 5B, 5C, 7A, 7B, 2A, 2B). KNL1 was detected using polyclonal rabbit anti-$KNL1^{1413\text{-}1624}$ ((Cheeseman et al., 2008); for Figure 1C, 4A, 4B, 7A, 7B, 2A, 2B, 6) or a mouse anti-Blinkin ((Kiyomitsu et al., 2007); for Figure 4A and 4B). Affinity-purified rabbit polyclonal antibodies were generated against the complete Mis12 complex as described previously (Desai et al., 2003). CENP-A was detected using mouse anti-CENP-A (3-19) (Abcam). Human centromeres were detected using anti-centromere antibodies (ACA) (Antibodies, Inc.). Microtubules were detected with mouse DM1alpha (Sigma). Cy2-, Cy3- and Cy5-conjugated secondary antibodies were obtained from Jackson Laboratories. DNA was visualized using 10 µg/mL Hoechst.

Immunofluorescence images were acquired on a Nikon Eclipse Ti-E microscope equipped with an Andor Clara charge-coupled device (CCD) camera using the NIS-Elements AR software (v4.2). Z sections were acquired at 0.2 μm steps over 4 μm (U2OS cell lines) or 2 μm (for HeLa cell lines and U2OS cell lines in Figure 3C and S3B) using a 60x/ 1.4 numerical aperture (NA) Nikon Plan Apochromat λ objective plus 1.5x optovar. Images were deconvolved using the 3D Landweber deconvolution package accompanying NIS Elements when appropriate. Fluorescent images of focus segregation were acquired on a DeltaVision Core deconvolution microscope (Applied Precision) equipped with a CoolSnap HQ2 CCD camera with approximately 10 Z-sections acquired at 0.2 μm steps using a 60×/ 1.42 NA Olympus U-PlanApo objective and deconvolved using DeltaVision software. Images are scaled equivalently when shown for comparison, unless otherwise stated. Quantification of fluorescence intensity was conducted on unprocessed images using Metamorph (Molecular Devices). Due to the irregularity in GFP focus size and brightness, normalization was performed by measuring the intensity of the entire focus area for each channel over background. A ratio of test protein/GFP intensity was then calculated and averaged.

Protein Expression and Purification

Proteins were purified using the previously described bacterial expression constructs for GST-Ndc80^{Bonsai} (Ciferri et al., 2008), His-tagged full-length Mis12 complex (Kline et al., 2006), which was co-expressed with KNL1$^{2106-2316}$ cloned as described previously (Petrovic et al., 2010) and GST-CENP-C$^{1-234}$ (Gascoigne et al., 2011). CENP-T$^{1-250}$ was His-tagged by PCR and then cloned into pET3aTr. Phospho-mimetic mutations were introduced into the appropriate expression constructs (CENP-T T11, T27, S47, T85,

T195 [Figure 3B] ; Dsn1 [Figure 3A] S28, S30, S58, S76, S80, S100, S109, S330) using site-directed mutagenesis. To purify GST-tagged proteins, bacteria were lysed in PBS, 250 mM NaCl, 0.1% Tween-20 and the lysate was bound to glutathione agarose (Sigma) for 1 hr at 4 °C. The resin was washed three times with PBS, 250 mM NaCl, 0.1% Tween-20, and 1 mM DTT. The proteins were then cleaved off the beads by overnight cleavage with PreScission protease at 4 °C. All His-tagged proteins were purified by Ni-NTA affinity purification. Bacteria were lysed in 50 mM sodium phosphate buffer (NaPi), pH 8.0, 300 mM NaCl, 10 mM imidazole, 5 mM beta-mercaptoethanol (βME) and then incubated with Ni-NTA agarose (Qiagen) for 1 hr at 4 °C. The resin was washed three times with 50 mM NaPi, pH 8.0, 500 mM NaCl, 40 mM imidazole, 5 mM βME, followed by elution with 50 mM NaPi, 500 mM NaCl, 250 mM imidazole, 5 mM βME. All proteins were further purified by gel filtration on a Superdex 200 column into 50 mM Tris, pH 7.6, 150 mM NaCl, 1 mM DTT. Peak fractions were pooled and concentrated using Vivaspin 20 concentrators and snap frozen in liquid nitrogen.

Protein Binding Assays

Protein binding was assessed by mixing the appropriate proteins at final concentrations of 3 μM each in a final volume of 250 μl and incubating for 15 min on ice, followed by a 15 min spin at 4 °C at > 20,000 x g to remove any aggregates. The cleared supernatant was applied to a Superose 6 10/300 column in 50 mM Tris, pH 7.6, 150 mM NaCl, 1 mM DTT, and the peak fractions were analyzed on acrylamide gels and visualized using Coomassie R-250.

Chapter IV: Discussion and Future Directions

Models for Kinetochore Force Resistance

The model described in this thesis for the assembly of the core structural components of the kinetochore has important implications for the force-resistance properties of the kinetochore. As described in Chapter I, there are many different ways in which a large macromolecular assembly like the kinetochore can resist disassembly under the pulling forces put on it by depolymerizing microtubules. The data presented here supports both the presence of multiple, weak attachment pathways as well as the potential for cross-linking between pathways. The third model, using elastic components within the kinetochore, has also been supported by recent research (Suzuki et al., 2014).

Here, I showed that the CCAN components CENP-T and CENP-C form independent recruitment sites for assembly of the outer kinetochore KMN network, particularly the Ndc80 complex. A strategy for force dissipation is to dissipate force over multiple attachments, thereby preventing excessive force being put on a single contact point, which can result in rupture of the protein-protein interaction. It had previously been shown that multiple Ndc80 complexes assemble per microtubule (Lawrimore et al., 2011; Joglekar et al., 2006). However, with the previous models for kinetochore assembly, it remained unclear how these multiple Ndc80 complex units could be recruited. With both CENP-C and CENP-T having the potential to recruit individual Ndc80 complexes, and additionally the two potential binding sites for the Ndc80 complex on a single CENP-T molecule, this provides a novel model for force dissipation at the kinetochore (Figure 1A). Additionally, the data in this thesis provides a pathway for recruitment of multiple KNL1 molecules. KNL1 has also been previously shown to have weak microtubule-binding activity (Cheeseman et al., 2006). Together, these data

provide the potential for up to five microtubule-binding events per CENP-C and CENP-T pair.

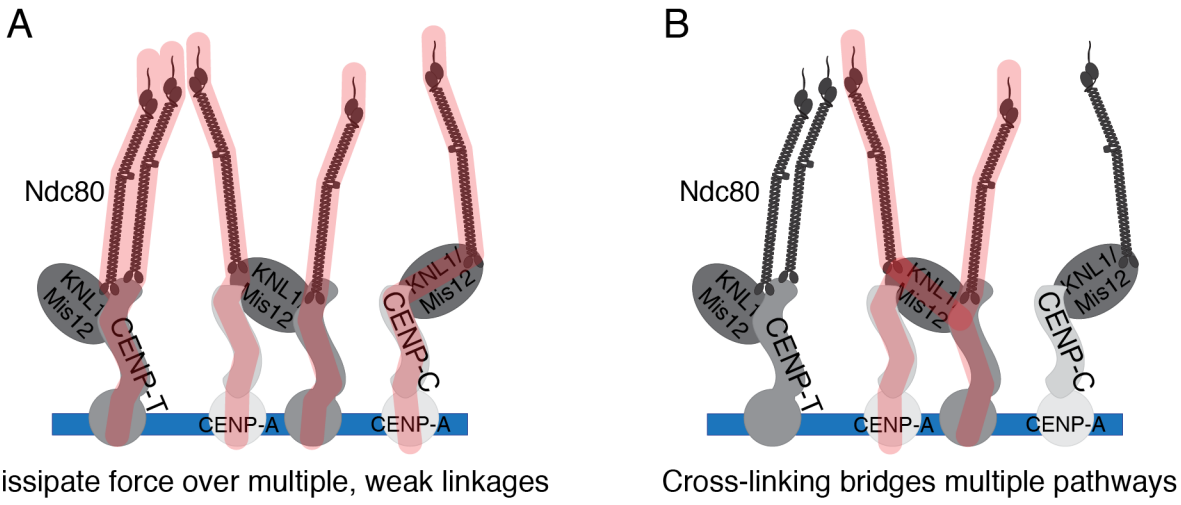

Figure 1: Models for force dissipation supported by the new model of kinetochore organization. Model for kinetochore organization modified from Chapter III, Figure 9. A) The paths for force dissipation over the multiple linkages formed by Ndc80 molecules bound to the CENP-C and CENP-T based receptors are shown in red. B) The possibility of force dissipation over CENP-C and CENP-T pathways cross-linked by KNL1/Mis12complex is highlighted in red.

Another way in which macromolecular assemblies can resist rupture is by dissipating force over crosslinks between different attachment pathways. The data from the ectopic targeting assays discussed in Chapter III demonstrated alternative organization for the KMN network components on CENP-T and CENP-C. Additionally, the biochemical data showed that the interaction of the Ndc80 complex and CENP-T is mutually exclusive of the interaction of the Ndc80 complex and KNL1 and Mis12 complex in the canonically defined KMN network organization via interaction with the Ndc80 complex subunit Spc25. Together this suggests that the interaction of KNL1/Mis12 complex with CENP-T may not occur via the same interface as the KNL1/Mis12 complex interaction with CENP-C, since the KNL1/Mis12 complex interface with the Ndc80 complex is necessarily different for each pathway. Perhaps there is a

novel interaction interface on KNL1/Mis12 complex, presenting the possibility of a three-way interaction for a single KNL1/Mis12 complex unit between CENP-C and CENP-T. In this assembly, KNL1/Mis12 complex would interact with CENP-C and a single Ndc80 complex unit in the previously described manner. Then, a third interface on KNL1/Mis12 complex would bridge and interact with the CENP-T/Ndc80 complex-based binding site. This would allow a cross-link between the two pathways and could serve as a point of force dissipation when force was applied to the CENP-C and CENP-T pathway via Ndc80 complex microtubule attachment (Figure 1B).

Finally, recent work by Suzuki et al has shown that the CENP-C and CENP-T branches are both under tension and loss of either pathway or a third component, the CENP-H/I complex, leads to hyper-extension of CENP-C and CENP-T, implying that the two work together to resist over-stretching of the kinetochore and premature stabilization of kinetochore-microtubule interactions (2014). This supports a model in which the disordered N-termini of CENP-C and CENP-T function as entropic springs to absorb the force applied by the mitotic spindle. Interestingly, the extension of CENP-T remains the same over a 2-fold change in centromere stretch, suggesting that the CENP-T pathway remains intact over a range of tensile forces. Additionally, they demonstrated that CENP-T-W-S-X and the CENP-H/I impart structural rigidity to the centromere, preventing over-stretching of the centromeric chromatin as well. This further emphasizes the importance of chromatin structure within the model of force resistance at the chromosome-microtubule interface.

Together these data provide support for a very complex model of the kinetochore under tension. By utilizing multiple attachment points, possible cross-linking activities,

and elastic components, the kinetochore is able to resist rupture events and maintain chromosome-spindle attachment. This is particularly important during metaphase, the stage of highest applied tension, which is concurrent with the period during which the Aurora B tension sensor and spindle assembly checkpoint proteins are working together to ensure both complete microtubule attachment and bi-orientation of the chromosomes. During the metaphase oscillations, any loss of chromosome-microtubule attachment would lead to checkpoint arrest and delay anaphase onset. Excessive delay in the metaphase to anaphase transition leads to eventual cohesion fatigue and subsequent problems in correctly separating sister chromatids (Stevens et al., 2011; Daum et al., 2011). Therefore, it is important that once a correct microtubule attachment is made, it is maintained until the checkpoint is bypassed so that mitosis can be completed in a timely manner.

Biological significance of building two *distinct* pathways

One surprising result of the work described here is the different regulation of each pathway that was observed. While assembly of the CENP-C based pathway was primarily regulated by Aurora B kinase activity, CENP-T based assembly was only partially affected by Aurora B kinase inhibition, and primarily regulated by CDK phosphorylation-dependent recruitment of the Ndc80 complex. Disruption of the mapped CDK phosphorylation site at residue serine 73 in CENP-C by mutation to alanine did not affect the ability of a LacI fusion to recruit the components of the KMN network (unpublished results). While multiple layers of regulation for kinetochore assembly have been previously described, the distinct effects of each on the two

pathways suggests unique layers of regulation for each. Since the discovery of the two individual pathways, a key question has concerned the biological relevance of the two distinct pathways. In yeast, although a CENP-T homologue is present and functional, the protein is not essential for viability (Schleiffer et al., 2012). In *C. elegans* and *D. melanogaster*, only the CENP-C pathway exists (Schleiffer et al., 2012). This implies a possible difference in function for the two pathways. If the human kinetochore simply required additional points of attachment, then an expansion of the CENP-C pathway would have been sufficient and a more evolutionarily conservative solution. As described above, it is possible that the CENP-T pathway provides novel, structural integrity to the kinetochore. Additionally, it is possible that the human kinetochore is under unique stresses that require multiple, orthologous attachment pathways to ensure proper chromosome segregation, and the distinct regulation of each serves as a mechanism to ensure that under certain perturbations, the integrity of both pathways is not affected.

Does CENP-T bind multiple Ndc80 molecules?

The identification of two Ndc80 binding domains in CENP-T suggested the possibility of multiple Ndc80 binding events per CENP-T molecule, expanding the number of potential microtubule attachment events per kinetochore. In the parallel model of force dissipation additional linkages between the inner kinetochore and microtubule allow the force produced by microtubule depolymerization to be divided over these attachments, reducing the risk of protein-protein interaction rupture. Although by sequence conservation alone it is possible that the two sites in CENP-T are Ndc80-binding

competent, the CDK mutations in CENP-T characterized in Chapter III did not result in large decreases in Ndc80 recruitment levels to the ectopic foci. This suggests that the sites are in some sort of equilibrium, binding only a single Ndc80 molecule per CENP-T. Alternatively, the individual mutations may only weaken Ndc80 complex binding, not abolish it, resulting in only partial loss of Ndc80 complex recruitment. Surprisingly, despite having only a minor effect on Ndc80 complex recruitment, these mutations lead to drastic loss of KNL1 and Mis12 complex at the foci.

This suggests a more complicated model of kinetochore assembly than previously described. The loss of a single Ndc80 binding site must affect the binding mode of the Ndc80 complex in a way that changes its ability to recruit KNL1 and the Mis12 complex or some other stabilizing/recruitment molecule. Or perhaps the loss of phosphorylation on CENP-T changes the conformation of CENP-T such that it can no longer recruit KNL1 and the Mis12 complex. Similar logic may explain the results observed for mutation of T195 in CENP-T, which also resulted in a large decrease of KNL1 and Mis12 complex recruitment, but very little effect on Ndc80 recruitment to the ectopic foci. Furthermore, the mutants, although nearly identical in their KMN network recruitment competency, showed drastically different outcomes in the chromosome segregation assay. Again, this may be due to a favoring of different conformations of CENP-T influenced by the various CDK phosphorylation events. These different conformation biases may have different functional outcomes, with the combination of mutation at both T11 and T85 resulting in a CENP-T molecule that is unable to adapt a conformation capable of recruiting any of the KMN network components. Evidence thus far suggests that in vitro binding experiments do not fully capture the binding activities of

CENP-T, so it will be important to further characterize CENP-T in cells to determine whether it is truly binding one or two Ndc80 molecules and the phenotypic consequences of altering binding at either site.

Future Directions

Although the work presented here makes considerable strides in defining the molecular architecture of the kinetochore, it remains to be shown how KNL1 and the Mis12 complex are being recruited to the CENP-T pathway. As described above, the data from the ectopic kinetochore assemblies result in multiple possible models for assembly at the endogenous kinetochore. It still needs to be determined whether the KMN network is interacting with both CENP-C and CENP-T at once, or if the pathways are mutually exclusive. Previous research has provided potential interaction interfaces on the Mis12 complex for both KNL1 and the Ndc80 complex. EM structures and biochemical analyses by the Musacchio lab have indicated where some of these sites may lie on the Nsl1 subunit of the Mis12 complex (Petrovic et al., 2014; 2010). Additionally, the Westermann group has described a site for Ndc80 binding in the yeast Dsn1 homologue (Malvezzi et al., 2013). Together these studies suggest potential targets for genetic manipulations of the Mis12 complex to perturb recruitment to either pathway. Preliminary characterizations have shown that none of these sites affect recruitment to either CENP-T or CENP-C ectopic foci (unpublished results), but more careful characterization may reveal differences in outer kinetochore assembly. With targeted sites on the Mis12 complex that affect KMN assembly on either the CENP-C or CENP-T focus, one could study the effects of disrupting either pathway at endogenous

kinetochores by replacement assays and test the importance of these pathways in the context of the entire kinetochore assembly. In addition, it would be possible to disrupt only the CENP-T pathway without affecting the integrity of the rest of the kinetochore by creating endogenous replacement constructs of CENP-T with the appropriate CDK mutations to specifically target the ability to recruit the KMN network without causing a structural collapse from losing a key component of the CCAN.

This thesis presents a novel model for CENP-T pathway assembly, but the molecular basis for KNL1 and Mis12 complex recruitment to CENP-T remains elusive. The data presented here indicate that robust recruitment of KNL1/Mis12 complex requires a region of the CENP-T protein in the region surrounding amino acids 200-230, a CDK phosphorylation event at residue 195, and recruitment of the Ndc80 complex. However, these are not the only requirements as reconstitution of all of these components with either a phosphomimetic version of CENP-T or with pre-incubation with CDK kinase (data not shown) are not sufficient to result in assembly of the entire KMN network with CENP-T. There are a few possible explanations for this. The first is due to the differences between the proteins used in the in vitro binding assays versus those found in cells. Because of the difficulty of reconstituting the full-length Ndc80 complex, the studies presented here used a truncated version of the complex, $Ndc80^{Bonsai}$, and it is possible that this shortened molecule is not competent for full reconstitution of the KMN network bound to CENP-T. There is no published data indicating that the full-length complex and truncated construct behave differently, but it is possible that the longer protein complex is necessary to reconstitute the full interactions of the KMN network with CENP-T. Another possibility, is that another

kinetochore component not present in our biochemical reconstitutions is providing an interaction interface between Ndc80 and KNL1/Mis12 complex, CENP-T and KNL1/Mis12 complex, or both. The most likely candidates are components of the CCAN, which have been previously shown to interact with CENP-T. Alternatively, another, uncharacterized post-translational modification, such as phosphorylation by another kinase, may be required for full assembly. Lastly, it is possible that due to the intrinsically unstructured nature of the CENP-T N-terminus, the biochemically reconstituted protein does not sample the correct conformations that can bind KNL1 and Mis12 complex robustly in vitro.

Concluding Remarks

The kinetochore provides the structural foundation for chromosome-microtubule attachment, ensuring the fidelity of chromosome segregation. This structure is under constant physical stress during mitosis as it comes under the tension and compression forces imposed by dynamic microtubules. The architecture of the kinetochore plays a critical role in withstanding these forces. Here, we show a new model for kinetochore assembly. First, two separate, inner kinetochore receptors, CENP-C and CENP-T, form separate platforms for assembly of the outer kinetochore KMN network. This provides exciting new detail for how the kinetochore is modeled. Additionally, the distinct regulation of each pathway by CDK and Aurora B kinase also suggests that perhaps the two pathways are not functionally equivalent microtubule attachment sites. Looking forward, it will be important to determine the molecular details that separate these two pathways and the functional roles of each.

References

Adams, P.D., P.V. Afonine, G. Bunkóczi, V.B. Chen, I.W. Davis, N. Echols, J.J. Headd, L.-W. Hung, G.J. Kapral, R.W. Grosse-Kunstleve, A.J. McCoy, N.W. Moriarty, R. Oeffner, R.J. Read, D.C. Richardson, J.S. Richardson, T.C. Terwilliger, and P.H. Zwart. 2010. PHENIX: a comprehensive Python-based system for macromolecular structure solution. *Acta Crystallogr. D Biol. Crystallogr.* 66:213–221. doi:10.1107/S0907444909052925.

Akiyoshi, B., C.R. Nelson, and S. Biggins. 2013. The aurora B kinase promotes inner and outer kinetochore interactions in budding yeast. *Genetics*. 194:785–789. doi:10.1534/genetics.113.150839.

Akiyoshi, B., C.R. Nelson, J.A. Ranish, and S. Biggins. 2009. Quantitative proteomic analysis of purified yeast kinetochores identifies a PP1 regulatory subunit. *Genes Dev*. 23:2887–2899. doi:10.1101/gad.1865909.

Akiyoshi, B., K.K. Sarangapani, A.F. Powers, C.R. Nelson, S.L. Reichow, H. Arellano-Santoyo, T. Gonen, J.A. Ranish, C.L. Asbury, and S. Biggins. 2010. Tension directly stabilizes reconstituted kinetochore-microtubule attachments. *Nature*. 468:576–579. doi:10.1038/nature09594.

Al-Bassam, J., and F. Chang. 2011. Regulation of microtubule dynamics by TOG-domain proteins XMAP215/Dis1 and CLASP. *Trends Cell Biol.* 21:604–614. doi:10.1016/j.tcb.2011.06.007.

Allshire, R.C., and G.H. Karpen. 2008. Epigenetic regulation of centromeric chromatin: old dogs, new tricks? *Nat Rev Genet*. 9:923–937. doi:10.1038/nrg2466.

Alushin, G.M., V.H. Ramey, S. Pasqualato, D.A. Ball, N. Grigorieff, A. Musacchio, and E. Nogales. 2010. The Ndc80 kinetochore complex forms oligomeric arrays along microtubules. *Nature*. 467:805–810. doi:10.1038/nature09423.

Amano, M., A. Suzuki, T. Hori, C. Backer, K. Okawa, I.M. Cheeseman, and T. Fukagawa. 2009. The CENP-S complex is essential for the stable assembly of outer kinetochore structure. *The Journal of Cell Biology*. 186:173–182. doi:10.1083/jcb.200903100.

Bader, J.R., and K.T. Vaughan. 2010. Dynein at the kinetochore: Timing, Interactions and Functions. *Semin. Cell Dev. Biol.* 21:269–275. doi:10.1016/j.semcdb.2009.12.015.

Barnhart, M.C., P.H.J.L. Kuich, M.E. Stellfox, J.A. Ward, E.A. Bassett, B.E. Black, and D.R. Foltz. 2011. HJURP is a CENP-A chromatin assembly factor sufficient to form a functional de novo kinetochore. *The Journal of Cell Biology*. 194:229–243. doi:10.1083/jcb.201012017.

Bayless, B.A., T.H. Giddings, M. Winey, and C.G. Pearson. 2012. Bld10/Cep135

stabilizes basal bodies to resist cilia-generated forces. *Mol. Biol. Cell*. 23:4820–4832. doi:10.1091/mbc.E12-08-0577.

Bennink, M.L., S.H. Leuba, G.H. Leno, J. Zlatanova, B.G. de Grooth, and J. Greve. 2001. Unfolding individual nucleosomes by stretching single chromatin fibers with optical tweezers. *Nat Struct Biol*. 8:606–610. doi:10.1038/89646.

Bloom, K.S. 2008. Beyond the code: the mechanical properties of DNA as they relate to mitosis. *Chromosoma*. 117:103–110. doi:10.1007/s00412-007-0138-0.

Bock, L.J., C. Pagliuca, N. Kobayashi, R.A. Grove, Y. Oku, K. Shrestha, C. Alfieri, C. Golfieri, A. Oldani, M. Dal Maschio, R. Bermejo, T.R. Hazbun, T.U. Tanaka, and P. De Wulf. 2012. Cnn1 inhibits the interactions between the KMN complexes of the yeast kinetochore. *Nat. Cell Biol.* 14:614–624. doi:10.1038/ncb2495.

Bouck, D.C., and K. Bloom. 2007. Pericentric chromatin is an elastic component of the mitotic spindle. *Curr. Biol.* 17:741–748. doi:10.1016/j.cub.2007.03.033.

Brower-Toland, B.D., C.L. Smith, R.C. Yeh, J.T. Lis, C.L. Peterson, and M.D. Wang. 2002. Mechanical disruption of individual nucleosomes reveals a reversible multistage release of DNA. *Proc Natl Acad Sci USA*. 99:1960–1965. doi:10.1073/pnas.022638399.

Cane, S., A.A. Ye, S.J. Luks-Morgan, and T.J. Maresca. 2013. Elevated polar ejection forces stabilize kinetochore-microtubule attachments. *The Journal of Cell Biology*. 200:203–218. doi:10.1083/jcb.201211119.

Carroll, C.W., K.J. Milks, and A.F. Straight. 2010. Dual recognition of CENP-A nucleosomes is required for centromere assembly. *J. Cell Biol.* 189:1143–1155. doi:10.1083/jcb.201001013.

Cheeseman, I.M. 2014. The Kinetochore. *Cold Spring Harb Perspect Biol*. 6:a015826–a015826. doi:10.1101/cshperspect.a015826.

Cheeseman, I.M., and A. Desai. 2008. Molecular architecture of the kinetochore-microtubule interface. *Nat Rev Mol Cell Biol*. 9:33–46. doi:10.1038/nrm2310.

Cheeseman, I.M., J.S. Chappie, E.M. Wilson-Kubalek, and A. Desai. 2006. The conserved KMN network constitutes the core microtubule-binding site of the kinetochore. *Cell*. 127:983–997. doi:10.1016/j.cell.2006.09.039.

Cheeseman, I.M., S. Niessen, S. Anderson, F. Hyndman, J.R. Yates, K. Oegema, and A. Desai. 2004. A conserved protein network controls assembly of the outer kinetochore and its ability to sustain tension. *Genes Dev*. 18:2255–2268. doi:10.1101/gad.1234104.

Cheeseman, I.M., T. Hori, T. Fukagawa, and A. Desai. 2008. KNL1 and the CENP-H/I/K complex coordinately direct kinetochore assembly in vertebrates. *Mol. Biol. Cell*.

19:587–594. doi:10.1091/mbc.E07-10-1051.

Chen, W., and D. Zhang. 2004. Kinetochore fibre dynamics outside the context of the spindle during anaphase. *Nat. Cell Biol.* 6:227–231. doi:10.1038/ncb1104.

Ciferri, C., J. De Luca, S. Monzani, K.J. Ferrari, D. Ristic, C. Wyman, H. Stark, J. Kilmartin, E.D. Salmon, and A. Musacchio. 2005. Architecture of the human ndc80-hec1 complex, a critical constituent of the outer kinetochore. *J Biol Chem*. 280:29088–29095. doi:10.1074/jbc.M504070200.

Ciferri, C., S. Pasqualato, E. Screpanti, G. Varetti, S. Santaguida, G. Dos Reis, A. Maiolica, J. Polka, J.G. De Luca, P. De Wulf, M. Salek, J. Rappsilber, C.A. Moores, E.D. Salmon, and A. Musacchio. 2008. Implications for kinetochore-microtubule attachment from the structure of an engineered Ndc80 complex. *Cell*. 133:427–439. doi:10.1016/j.cell.2008.03.020.

Corbett, K.D., C.K. Yip, L.-S. Ee, T. Walz, A. Amon, and S.C. Harrison. 2010. The monopolin complex crosslinks kinetochore components to regulate chromosome-microtubule attachments. *Cell*. 142:556–567. doi:10.1016/j.cell.2010.07.017.

Cottingham, F.R., L. Gheber, D.L. Miller, and M.A. Hoyt. 1999. Novel roles for saccharomyces cerevisiae mitotic spindle motors. *J. Cell Biol.* 147:335–350. doi:10.1083/jcb.147.2.335.

Coue, M., V.A. Lombillo, and J.R. McIntosh. 1991. Microtubule depolymerization promotes particle and chromosome movement in vitro. *J. Cell Biol.* 112:1165–1175. doi:10.1083/jcb.112.6.1165.

Cui, Y., and C. Bustamante. 2000. Pulling a single chromatin fiber reveals the forces that maintain its higher-order structure. *Proc Natl Acad Sci USA*. 97:127–132. doi:10.1073/pnas.97.1.127.

Daum, J.R., T.A. Potapova, S. Sivakumar, J.J. Daniel, J.N. Flynn, S. Rankin, and G.J. Gorbsky. 2011. Cohesion Fatigue Induces Chromatid Separation in Cells Delayed at Metaphase. *Curr. Biol.* 21:1018–1024. doi:10.1016/j.cub.2011.05.032.

DeLuca, J.G., and A. Musacchio. 2012. Structural organization of the kinetochore-microtubule interface. *Curr. Opin. Cell Biol.* 24:48–56. doi:10.1016/j.ceb.2011.11.003.

DeLuca, J.G., B. Moree, J.M. Hickey, J.V. Kilmartin, and E.D. Salmon. 2002. hNuf2 inhibition blocks stable kinetochore-microtubule attachment and induces mitotic cell death in HeLa cells. *J. Cell Biol.* 159:549–555. doi:10.1083/jcb.200208159.

DeLuca, J.G., W.E. Gall, C. Ciferri, D. Cimini, A. Musacchio, and E.D. Salmon. 2006. Kinetochore Microtubule Dynamics and Attachment Stability Are Regulated by Hec1. *Cell*. 127:969–982. doi:10.1016/j.cell.2006.09.047.

Desai, A., and T.J. Mitchison. 1997. Microtubule polymerization dynamics. *Annu. Rev. Cell Dev. Biol.* 13:83–117. doi:10.1146/annurev.cellbio.13.1.83.

Desai, A., S. Rybina, T. Müller-Reichert, A. Shevchenko, A. Shevchenko, A. Hyman, and K. Oegema. 2003. KNL-1 directs assembly of the microtubule-binding interface of the kinetochore in C. elegans. *Genes Dev*. 17:2421–2435. doi:10.1101/gad.1126303.

Dogterom, M., and B. Yurke. 1997. Measurement of the force-velocity relation for growing microtubules. *Science*. 278:856–860.

Dumont, S., E.D. Salmon, and T.J. Mitchison. 2012. Deformations within moving kinetochores reveal different sites of active and passive force generation. *Science*. 337:355–358. doi:10.1126/science.1221886.

Dyson, H.J., and P.E. Wright. 2005. Intrinsically unstructured proteins and their functions. *Nat Rev Mol Cell Biol*. 6:197–208. doi:10.1038/nrm1589.

Elting, M.W., C.L. Hueschen, D.B. Udy, and S. Dumont. 2014. Force on spindle microtubule minus ends moves chromosomes. *The Journal of Cell Biology*. 206:245–256. doi:10.1083/jcb.201401091.

Emanuele, M.J., W. Lan, M. Jwa, S.A. Miller, C.S.M. Chan, and P.T. Stukenberg. 2008. Aurora B kinase and protein phosphatase 1 have opposing roles in modulating kinetochore assembly. *The Journal of Cell Biology*. 181:241–254. doi:10.1083/jcb.200710019.

Evans, E. 2001. Probing the relation between force--lifetime--and chemistry in single molecular bonds. *Annu Rev Biophys Biomol Struct*. 30:105–128. doi:10.1146/annurev.biophys.30.1.105.

Ferraro-Gideon, J., R. Sheykhani, Q. Zhu, M.L. Duquette, M.W. Berns, and A. Forer. 2013. Measurements of forces produced by the mitotic spindle using optical tweezers. *Mol. Biol. Cell*. 24:1375–1386. doi:10.1091/mbc.E12-12-0901.

Finan, K., P.R. Cook, and D. Marenduzzo. 2011. Non-specific (entropic) forces as major determinants of the structure of mammalian chromosomes. *Chromosome Res.* 19:53–61. doi:10.1007/s10577-010-9150-y.

Fisher, J.K., M. Ballenger, E.T. O'Brien, J. Haase, R. Superfine, and K. Bloom. 2009. DNA relaxation dynamics as a probe for the intracellular environment. *Proc Natl Acad Sci USA*. 106:9250–9255. doi:10.1073/pnas.0812723106.

Franck, A.D., A.F. Powers, D.R. Gestaut, T. Gonen, T.N. Davis, and C.L. Asbury. 2007. Tension applied through the Dam1 complex promotes microtubule elongation providing a direct mechanism for length control in mitosis. *Nat. Cell Biol.* 9:832–837. doi:10.1038/ncb1609.

Gascoigne, K.E., and I.M. Cheeseman. 2011. Kinetochore assembly: if you build it, they will come. *Curr. Opin. Cell Biol.* 23:102–108. doi:10.1016/j.ceb.2010.07.007.

Gascoigne, K.E., and I.M. Cheeseman. 2013a. CDK-dependent phosphorylation and nuclear exclusion coordinately control kinetochore assembly state. *The Journal of Cell Biology*. 201:23–32. doi:10.1083/jcb.201301006.

Gascoigne, K.E., and I.M. Cheeseman. 2013b. Induced dicentric chromosome formation promotes genomic rearrangements and tumorigenesis. *Chromosome Res.* 21:407–418. doi:10.1007/s10577-013-9368-6.

Gascoigne, K.E., K. Takeuchi, A. Suzuki, T. Hori, T. Fukagawa, and I.M. Cheeseman. 2011. Induced Ectopic Kinetochore Assembly Bypasses the Requirement for CENP-A Nucleosomes. *Cell*. 145:410–422. doi:10.1016/j.cell.2011.03.031.

Gennerich, A., A.P. Carter, S.L. Reck-Peterson, and R.D. Vale. 2007. Force-induced bidirectional stepping of cytoplasmic dynein. *Cell*. 131:952–965. doi:10.1016/j.cell.2007.10.016.

Gorrec, F. 2009. The MORPHEUS protein crystallization screen. *J Appl Crystallogr*. 42:1035–1042. doi:10.1107/S0021889809042022.

Gregan, J., S. Polakova, L. Zhang, I.M. Tolić-Nørrelykke, and D. Cimini. 2011. Merotelic kinetochore attachment: causes and effects. *Trends Cell Biol.* 21:374–381. doi:10.1016/j.tcb.2011.01.003.

Grishchuk, E.L., and J.R. McIntosh. 2006. Microtubule depolymerization can drive poleward chromosome motion in fission yeast. *EMBO J*. 25:4888–4896. doi:10.1038/sj.emboj.7601353.

Grishchuk, E.L., M.I. Molodtsov, F.I. Ataullakhanov, and J.R. McIntosh. 2005. Force production by disassembling microtubules. *Nature*. 438:384–388. doi:10.1038/nature04132.

Guse, A., C.W. Carroll, B. Moree, C.J. Fuller, and A.F. Straight. 2011. In vitro centromere and kinetochore assembly on defined chromatin templates. *Nature*. 477:354–358. doi:10.1038/nature10379.

Haase, J., A. Stephens, J. Verdaasdonk, E. Yeh, and K. Bloom. 2012. Bub1 kinase and Sgo1 modulate pericentric chromatin in response to altered microtubule dynamics. *Curr. Biol.* 22:471–481. doi:10.1016/j.cub.2012.02.006.

Hill, T.L. 1985. Theoretical problems related to the attachment of microtubules to kinetochores. *Proc Natl Acad Sci USA*. 82:4404–4408.

Hori, T., M. Amano, A. Suzuki, C.B. Backer, J.P. Welburn, Y. Dong, B.F. McEwen, W.-H. Shang, E. Suzuki, K. Okawa, I.M. Cheeseman, and T. Fukagawa. 2008. CCAN makes multiple contacts with centromeric DNA to provide distinct pathways to the

outer kinetochore. *Cell*. 135:1039–1052. doi:10.1016/j.cell.2008.10.019.

Hori, T., T. Haraguchi, Y. Hiraoka, H. Kimura, and T. Fukagawa. 2003. Dynamic behavior of Nuf2-Hec1 complex that localizes to the centrosome and centromere and is essential for mitotic progression in vertebrate cells. *J. Cell. Sci.* 116:3347–3362. doi:10.1242/jcs.00645.

Hunt, A.J., and J.R. McIntosh. 1998. The dynamic behavior of individual microtubules associated with chromosomes in vitro. *Mol. Biol. Cell*. 9:2857–2871.

Inoué, S., and E.D. Salmon. 1995. Force generation by microtubule assembly/disassembly in mitosis and related movements. *Mol. Biol. Cell*. 6:1619–1640.

Janicki, S.M., T. Tsukamoto, S.E. Salghetti, W.P. Tansey, R. Sachidanandam, K.V. Prasanth, T. Ried, Y. Shav-Tal, E. Bertrand, R.H. Singer, and D.L. Spector. 2004. From Silencing to Gene Expression. *Cell*. 116:683–698. doi:10.1016/S0092-8674(04)00171-0.

Joglekar, A.P., D. Bouck, K. Finley, X. Liu, Y. Wan, J. Berman, X. He, E.D. Salmon, and K.S. Bloom. 2008. Molecular architecture of the kinetochore-microtubule attachment site is conserved between point and regional centromeres. *J. Cell Biol.* 181:587–594. doi:10.1083/jcb.200803027.

Joglekar, A.P., D.C. Bouck, J.N. Molk, K.S. Bloom, and E.D. Salmon. 2006. Molecular architecture of a kinetochore-microtubule attachment site. *Nat. Cell Biol.* 8:581–585. doi:10.1038/ncb1414.

Johnston, K., A. Joglekar, T. Hori, A. Suzuki, T. Fukagawa, and E.D. Salmon. 2010. Vertebrate kinetochore protein architecture: protein copy number. *J. Cell Biol.* 189:937–943. doi:10.1083/jcb.200912022.

Jun, S., and A. Wright. 2010. Entropy as the driver of chromosome segregation. *Nat. Rev. Microbiol.* 8:600–607. doi:10.1038/nrmicro2391.

Kapoor, T.M., M.A. Lampson, P. Hergert, L. Cameron, D. Cimini, E.D. Salmon, B.F. McEwen, and A. Khodjakov. 2006. Chromosomes can congress to the metaphase plate before biorientation. *Science*. 311:388–391. doi:10.1126/science.1122142.

Kim, S., and H. Yu. 2015. Multiple assembly mechanisms anchor the KMN spindle checkpoint platform at human mitotic kinetochores. *The Journal of Cell Biology*. 208:181–196. doi:10.1083/jcb.201407074.

Kiyomitsu, T., C. Obuse, and M. Yanagida. 2007. Human Blinkin/AF15q14 Is Required for Chromosome Alignment and the Mitotic Checkpoint through Direct Interaction with Bub1 and BubR1. *Developmental Cell*. 13:663–676. doi:10.1016/j.devcel.2007.09.005.

Kline, S.L., I.M. Cheeseman, T. Hori, T. Fukagawa, and A. Desai. 2006. The human Mis12 complex is required for kinetochore assembly and proper chromosome segregation. *J. Cell Biol.* 173:9–17. doi:10.1083/jcb.200509158.

Koshland, D.E., T.J. Mitchison, and M.W. Kirschner. 1988. Polewards chromosome movement driven by microtubule depolymerization in vitro. *Nature*. 331:499–504. doi:10.1038/331499a0.

Kwon, M.-S., T. Hori, M. Okada, and T. Fukagawa. 2007. CENP-C is involved in chromosome segregation, mitotic checkpoint function, and kinetochore assembly. *Mol. Biol. Cell*. 18:2155–2168. doi:10.1091/mbc.E07-01-0045.

LaFountain, J.R., C.S. Cohan, A.J. Siegel, and D.J. LaFountain. 2004. Direct visualization of microtubule flux during metaphase and anaphase in crane-fly spermatocytes. *Mol. Biol. Cell*. 15:5724–5732. doi:10.1091/mbc.E04-08-0750.

LaFountain, J.R., R. Oldenbourg, R.W. Cole, and C.L. Rieder. 2001. Microtubule flux mediates poleward motion of acentric chromosome fragments during meiosis in insect spermatocytes. *Mol. Biol. Cell*. 12:4054–4065.

Lampert, F., P. Hornung, and S. Westermann. 2010. The Dam1 complex confers microtubule plus end-tracking activity to the Ndc80 kinetochore complex. *J. Cell Biol.* 189:641–649. doi:10.1083/jcb.200912021.

Lampson, M.A., and I.M. Cheeseman. 2011. Sensing centromere tension: Aurora B and the regulation of kinetochore function. *Trends Cell Biol.* 21:133–140. doi:10.1016/j.tcb.2010.10.007.

Lawrimore, J., K.S. Bloom, and E.D. Salmon. 2011. Point centromeres contain more than a single centromere-specific Cse4 (CENP-A) nucleosome. *J. Cell Biol.* 195:573–582. doi:10.1083/jcb.201106036.

Leckband, D. 2000. Measuring the forces that control protein interactions. *Annu Rev Biophys Biomol Struct*. 29:1–26. doi:10.1146/annurev.biophys.29.1.1.

Li, X., and R.B. Nicklas. 1995. Mitotic forces control a cell-cycle checkpoint. *Nature*. 373:630–632. doi:10.1038/373630a0.

Lin, S., J. Chen, and L. Huang. 2005. Measurements of the forces in protein interactions with atomic force microscopy. *Current Proteomics*. doi:10.1016/j.micron.2006.06.014.

Liu, D., G. Vader, M.J.M. Vromans, M.A. Lampson, and S.M.A. Lens. 2009. Sensing chromosome bi-orientation by spatial separation of aurora B kinase from kinetochore substrates. *Science*. 323:1350–1353. doi:10.1126/science.1167000.

Liu, D., O. Davydenko, and M.A. Lampson. 2012. Polo-like kinase-1 regulates kinetochore-microtubule dynamics and spindle checkpoint silencing. *The Journal of*

Cell Biology. 198:491–499. doi:10.1083/jcb.201205090.

Liu, S.-T., J.B. Rattner, S.A. Jablonski, and T.J. Yen. 2006. Mapping the assembly pathways that specify formation of the trilaminar kinetochore plates in human cells. *J. Cell Biol.* 175:41–53. doi:10.1083/jcb.200606020.

London, N., and S. Biggins. 2014. Signalling dynamics in the spindle checkpoint response. *Nat Rev Mol Cell Biol*. 15:736–748. doi:10.1038/nrm3888.

Maddox, P., A. Straight, P. Coughlin, T.J. Mitchison, and E.D. Salmon. 2003. Direct observation of microtubule dynamics at kinetochores in Xenopus extract spindles: implications for spindle mechanics. *J. Cell Biol.* 162:377–382. doi:10.1083/jcb.200301088.

Malvezzi, F., G. Litos, A. Schleiffer, A. Heuck, K. Mechtler, T. Clausen, and S. Westermann. 2013. A structural basis for kinetochore recruitment of the Ndc80 complex via two distinct centromere receptors. *EMBO J*. 32:409–423. doi:10.1038/emboj.2012.356.

Maresca, T.J., and E.D. Salmon. 2009. Intrakinetochore stretch is associated with changes in kinetochore phosphorylation and spindle assembly checkpoint activity. *J. Cell Biol.* 184:373–381. doi:10.1083/jcb.200808130.

Martin-Lluesma, S., V.M. Stucke, and E.A. Nigg. 2002. Role of Hec1 in spindle checkpoint signaling and kinetochore recruitment of Mad1/Mad2. *Science*. 297:2267–2270. doi:10.1126/science.1075596.

Maskell, D.P., X.-W. Hu, and M.R. Singleton. 2010. Molecular architecture and assembly of the yeast kinetochore MIND complex. *The Journal of Cell Biology*. 190:823–834. doi:10.1083/jcb.201002059.

Matos, I., and H. Maiato. 2011. Prevention and correction mechanisms behind anaphase synchrony: implications for the genesis of aneuploidy. *Cytogenet. Genome Res.* 133:243–253. doi:10.1159/000323803.

Mazumdar, M., and T. Misteli. 2005. Chromokinesins: multitalented players in mitosis. *Trends Cell Biol.* 15:349–355. doi:10.1016/j.tcb.2005.05.006.

McCleland, M.L., R.D. Gardner, M.J. Kallio, J.R. Daum, G.J. Gorbsky, D.J. Burke, and P.T. Stukenberg. 2003. The highly conserved Ndc80 complex is required for kinetochore assembly, chromosome congression, and spindle checkpoint activity. *Genes Dev*. 17:101–114. doi:10.1101/gad.1040903.

McIntosh, J.R., E.L. Grishchuk, M.K. Morphew, A.K. Efremov, K. Zhudenkov, V.A. Volkov, I.M. Cheeseman, A. Desai, D.N. Mastronarde, and F.I. Ataullakhanov. 2008. Fibrils connect microtubule tips with kinetochores: a mechanism to couple tubulin dynamics to chromosome motion. *Cell*. 135:322–333. doi:10.1016/j.cell.2008.08.038.

McWilliam, H., W. Li, M. Uludag, S. Squizzato, Y.M. Park, N. Buso, A.P. Cowley, and R. Lopez. 2013. Analysis Tool Web Services from the EMBL-EBI. *Nucleic Acids Res*. 41:W597–600. doi:10.1093/nar/gkt376.

Meinhart, A., and P. Cramer. 2004. Recognition of RNA polymerase II carboxy-terminal domain by 3|[prime]|-RNA-processing factors. *Nature*. 430:223–226. doi:10.1038/nature02679.

Merkel, R., P. Nassoy, A. Leung, K. Ritchie, and E. Evans. 1999. Energy landscapes of receptor-ligand bonds explored with dynamic force spectroscopy. *Nature*. 397:50–53. doi:10.1038/16219.

Milks, K.J., B. Moree, and A.F. Straight. 2009. Dissection of CENP-C-directed centromere and kinetochore assembly. *Mol. Biol. Cell*. 20:4246–4255. doi:10.1091/mbc.E09-05-0378.

Mitchison, T.J., and E.D. Salmon. 1992. Poleward kinetochore fiber movement occurs during both metaphase and anaphase-A in newt lung cell mitosis. *J. Cell Biol.* 119:569–582. doi:10.1083/jcb.119.3.569.

Molodtsov, M.I., E.A. Ermakova, E.E. Shnol, E.L. Grishchuk, J.R. McIntosh, and F.I. Ataullakhanov. 2005. A molecular-mechanical model of the microtubule. *Biophys. J.* 88:3167–3179. doi:10.1529/biophysj.104.051789.

Moses, A.M., J.-K. Hériché, and R. Durbin. 2007. Clustering of phosphorylation site recognition motifs can be exploited to predict the targets of cyclin-dependent kinase. *Genome Biol.* 8:R23. doi:10.1186/gb-2007-8-2-r23.

Newman, J., D. Egan, T.S. Walter, R. Meged, I. Berry, M. Ben Jelloul, J.L. Sussman, D.I. Stuart, and A. Perrakis. 2005. Towards rationalization of crystallization screening for small- to medium-sized academic laboratories: the PACT/JCSG+ strategy. *Acta Crystallogr. D Biol. Crystallogr.* 61:1426–1431. doi:10.1107/S0907444905024984.

Nicklas, R.B. 1965. Chromosome velocity during mitosis as a function of chromosome size and position. *J. Cell Biol.* 25:SUPPL:119–35. doi:10.1083/jcb.25.1.119.

Nicklas, R.B. 1983. Measurements of the force produced by the mitotic spindle in anaphase. *J. Cell Biol.* 97:542–548. doi:10.1083/jcb.97.2.542.

Nicklas, R.B. 1988. The forces that move chromosomes in mitosis. *Annu Rev Biophys Biophys Chem*. 17:431–449. doi:10.1146/annurev.bb.17.060188.002243.

Nicklas, R.B., S.C. Ward, and G.J. Gorbsky. 1995. Kinetochore chemistry is sensitive to tension and may link mitotic forces to a cell cycle checkpoint. *J. Cell Biol.* 130:929–939. doi:10.1083/jcb.130.4.929.

Nishimura, K., T. Fukagawa, H. Takisawa, T. Kakimoto, and M. Kanemaki. 2009. An

auxin-based degron system for the rapid depletion of proteins in nonplant cells. *Nat Meth*. 6:917–922. doi:10.1038/nmeth.1401.

Nishino, T., F. Rago, T. Hori, K. Tomii, I.M. Cheeseman, and T. Fukagawa. 2013. CENP-T provides a structural platform for outer kinetochore assembly. *EMBO J*. 32:424–436. doi:10.1038/emboj.2012.348.

Nishino, T., K. Takeuchi, K.E. Gascoigne, A. Suzuki, T. Hori, T. Oyama, K. Morikawa, I.M. Cheeseman, and T. Fukagawa. 2012. CENP-T-W-S-X Forms a Unique Centromeric Chromatin Structure with a Histone-like Fold. *Cell*. 148:487–501. doi:10.1016/j.cell.2011.11.061.

Nogales, E. 2000. Structural insights into microtubule function. *Annu Rev Biochem*. 69:277–302. doi:10.1146/annurev.biochem.69.1.277.

Nogales, E., and H.-W. Wang. 2006. Structural mechanisms underlying nucleotide-dependent self-assembly of tubulin and its relatives. *Current Opinion in Structural Biology*. 16:221–229. doi:10.1016/j.sbi.2006.03.005.

Obuse, C., O. Iwasaki, T. Kiyomitsu, G. Goshima, Y. Toyoda, and M. Yanagida. 2004. A conserved Mis12 centromere complex is linked to heterochromatic HP1 and outer kinetochore protein Zwint-1. *Nat. Cell Biol.* 6:1135–1141. doi:10.1038/ncb1187.

Okada, M., I.M. Cheeseman, T. Hori, K. Okawa, I.X. McLeod, J.R. Yates, A. Desai, and T. Fukagawa. 2006. The CENP-H-I complex is required for the efficient incorporation of newly synthesized CENP-A into centromeres. *Nat. Cell Biol.* 8:446–457. doi:10.1038/ncb1396.

Pearlman, S.M., Z. Serber, and J.E. Ferrell. 2011. A mechanism for the evolution of phosphorylation sites. *Cell*. 147:934–946. doi:10.1016/j.cell.2011.08.052.

Pearson, C.G., P.S. Maddox, E.D. Salmon, and K. Bloom. 2001. Budding yeast chromosome structure and dynamics during mitosis. *J. Cell Biol.* 152:1255–1266. doi:10.1083/jcb.152.6.1255.

Perpelescu, M., and T. Fukagawa. 2011. The ABCs of CENPs. *Chromosoma*. 120:425–446. doi:10.1007/s00412-011-0330-0.

Petrovic, A., S. Mosalaganti, J. Keller, M. Mattiuzzo, K. Overlack, V. Krenn, A. De Antoni, S. Wohlgemuth, V. Cecatiello, S. Pasqualato, S. Raunser, and A. Musacchio. 2014. Modular assembly of RWD domains on the Mis12 complex underlies outer kinetochore organization. *Mol Cell*. 53:591–605. doi:10.1016/j.molcel.2014.01.019.

Petrovic, A., S. Pasqualato, P. Dube, V. Krenn, S. Santaguida, D. Cittaro, S. Monzani, L. Massimiliano, J. Keller, A. Tarricone, A. Maiolica, H. Stark, and A. Musacchio. 2010. The MIS12 complex is a protein interaction hub for outer kinetochore assembly. *The Journal of Cell Biology*. 190:835–852. doi:10.1083/jcb.201002070.

Powers, A.F., A.D. Franck, D.R. Gestaut, J. Cooper, B. Gracyzk, R.R. Wei, L. Wordeman, T.N. Davis, and C.L. Asbury. 2009. The Ndc80 kinetochore complex forms load-bearing attachments to dynamic microtubule tips via biased diffusion. *Cell*. 136:865–875. doi:10.1016/j.cell.2008.12.045.

Przewloka, M.R., Z. Venkei, V.M. Bolanos-Garcia, J. Debski, M. Dadlez, and D.M. Glover. 2011. CENP-C is a structural platform for kinetochore assembly. *Curr. Biol.* 21:399–405. doi:10.1016/j.cub.2011.02.005.

Rago, F., and I.M. Cheeseman. 2013. Review series: The functions and consequences of force at kinetochores. *The Journal of Cell Biology*. 200:557–565. doi:10.1083/jcb.201211113.

Roca-Cusachs, P., T. Iskratsch, and M.P. Sheetz. 2012. Finding the weakest link - exploring integrin-mediated mechanical molecular pathways. *J. Cell. Sci.* 125:3025–3038. doi:10.1242/jcs.095794.

Sandall, S., F. Severin, I.X. McLeod, J.R. Yates, K. Oegema, A. Hyman, and A. Desai. 2006. A Bir1-Sli15 complex connects centromeres to microtubules and is required to sense kinetochore tension. *Cell*. 127:1179–1191. doi:10.1016/j.cell.2006.09.049.

Santaguida, S., and A. Musacchio. 2009. The life and miracles of kinetochores. *EMBO J*. 28:2511–2531. doi:10.1038/emboj.2009.173.

Schleiffer, A., M. Maier, G. Litos, F. Lampert, P. Hornung, K. Mechtler, and S. Westermann. 2012. CENP-T proteins are conserved centromere receptors of the Ndc80 complex. *Nat. Cell Biol.* 14:604–613. doi:10.1038/ncb2493.

Schmidt, J.C., H. Arthanari, A. Boeszoermenyi, N.M. Dashkevich, E.M. Wilson-Kubalek, N. Monnier, M. Markus, M. Oberer, R.A. Milligan, M. Bathe, G. Wagner, E.L. Grishchuk, and I.M. Cheeseman. 2012. The kinetochore-bound Ska1 complex tracks depolymerizing microtubules and binds to curved protofilaments. *Developmental Cell*. 23:968–980. doi:10.1016/j.devcel.2012.09.012.

Schmitzberger, F., and S.C. Harrison. 2012. RWD domain: a recurring module in kinetochore architecture shown by a Ctf19-Mcm21 complex structure. *EMBO Rep.* 13:216–222. doi:10.1038/embor.2012.1.

Screpanti, E., A. De Antoni, G.M. Alushin, A. Petrovic, T. Melis, E. Nogales, and A. Musacchio. 2011. Direct binding of Cenp-C to the Mis12 complex joins the inner and outer kinetochore. *Curr. Biol.* 21:391–398. doi:10.1016/j.cub.2010.12.039.

Sekulic, N., E.A. Bassett, D.J. Rogers, and B.E. Black. 2010. The structure of (CENP-A-H4)(2) reveals physical features that mark centromeres. *Nature*. 467:347–351. doi:10.1038/nature09323.

Sharp, D.J., G.C. Rogers, and J.M. Scholey. 2000. Cytoplasmic dynein is required for poleward chromosome movement during mitosis in Drosophila embryos. *Nat. Cell*

Biol. 2:922–930. doi:10.1038/35046574.

Stephens, A.D., C.W. Quammen, B. Chang, J. Haase, R.M. Taylor, and K. Bloom. 2013. The spatial segregation of pericentric cohesin and condensin in the mitotic spindle. *Mol. Biol. Cell*. 24:3909–3919. doi:10.1091/mbc.E13-06-0325.

Stephens, A.D., J. Haase, L. Vicci, R.M. Taylor, and K. Bloom. 2011. Cohesin, condensin, and the intramolecular centromere loop together generate the mitotic chromatin spring. *The Journal of Cell Biology*. 193:1167–1180. doi:10.1083/jcb.201103138.

Stevens, D., R. Gassmann, K. Oegema, and A. Desai. 2011. Uncoordinated Loss of Chromatid Cohesion Is a Common Outcome of Extended Metaphase Arrest. *PLoS ONE*. 6:e22969. doi:10.1371/journal.pone.0022969.

Suzuki, A., B.L. Badger, X. Wan, J.G. DeLuca, and E.D. Salmon. 2014. The architecture of CCAN proteins creates a structural integrity to resist spindle forces and achieve proper Intrakinetochore stretch. *Developmental Cell*. 30:717–730. doi:10.1016/j.devcel.2014.08.003.

Suzuki, A., T. Hori, T. Nishino, J. Usukura, A. Miyagi, K. Morikawa, and T. Fukagawa. 2011. Spindle microtubules generate tension-dependent changes in the distribution of inner kinetochore proteins. *J. Cell Biol.* 193:125–140. doi:10.1083/jcb.201012050.

Sułkowska, J.I., and M. Cieplak. 2008. Stretching to understand proteins - a survey of the protein data bank. *Biophys. J.* 94:6–13. doi:10.1529/biophysj.107.105973.

Tanaka, T.U. 2002. Bi-orienting chromosomes on the mitotic spindle. *Curr. Opin. Cell Biol.* 14:365–371. doi:10.1016/S0955-0674(02)00328-9.

Taylor, E.W. 1965. Brownian and saltatory movements of cytoplasmic granules and the movement of anaphase chromosomes. *Proceedings of the Fourth International Congress on Rheology*. Part 4:175–191.

Tien, J.F., N.T. Umbreit, D.R. Gestaut, A.D. Franck, J. Cooper, L. Wordeman, T. Gonen, C.L. Asbury, and T.N. Davis. 2010. Cooperation of the Dam1 and Ndc80 kinetochore complexes enhances microtubule coupling and is regulated by aurora B. *J. Cell Biol.* 189:713–723. doi:10.1083/jcb.200910142.

Trazzi, S., G. Perini, R. Bernardoni, M. Zoli, J.C. Reese, A. Musacchio, and G. Della Valle. 2009. The C-terminal domain of CENP-C displays multiple and critical functions for mammalian centromere formation. *PLoS ONE*. 4:e5832. doi:10.1371/journal.pone.0005832.

Uchida, K.S.K., K. Takagaki, K. Kumada, Y. Hirayama, T. Noda, and T. Hirota. 2009. Kinetochore stretching inactivates the spindle assembly checkpoint. *J. Cell Biol.* 184:383–390. doi:10.1083/jcb.200811028.

Umbreit, N.T., D.R. Gestaut, J.F. Tien, B.S. Vollmar, T. Gonen, C.L. Asbury, and T.N. Davis. 2012. The Ndc80 kinetochore complex directly modulates microtubule dynamics. *Proc Natl Acad Sci USA*. 109:16113–16118. doi:10.1073/pnas.1209615109.

Verdaasdonk, J.S., R. Gardner, A.D. Stephens, E. Yeh, and K. Bloom. 2012. Tension-dependent nucleosome remodeling at the pericentromere in yeast. *Mol. Biol. Cell*. 23:2560–2570. doi:10.1091/mbc.E11-07-0651.

Visscher, K., M.J. Schnitzer, and S.M. Block. 1999. Single kinesin molecules studied with a molecular force clamp. *Nature*. 400:184–189. doi:10.1038/22146.

Volkov, V.A., A.V. Zaytsev, N. Gudimchuk, P.M. Grissom, A.L. Gintsburg, F.I. Ataullakhanov, J.R. McIntosh, and E.L. Grishchuk. 2013. Long tethers provide high-force coupling of the Dam1 ring to shortening microtubules. *Proc Natl Acad Sci USA*. 110:7708–7713. doi:10.1073/pnas.1305821110.

Wan, X., D. Cimini, L.A. Cameron, and E.D. Salmon. 2012. The coupling between sister kinetochore directional instability and oscillations in centromere stretch in metaphase PtK1 cells. *Mol. Biol. Cell*. 23:1035–1046. doi:10.1091/mbc.E11-09-0767.

Wan, X., R.P. O'Quinn, H.L. Pierce, A.P. Joglekar, W.E. Gall, J.G. DeLuca, C.W. Carroll, S.-T. Liu, T.J. Yen, B.F. McEwen, P.T. Stukenberg, A. Desai, and E.D. Salmon. 2009. Protein architecture of the human kinetochore microtubule attachment site. *Cell*. 137:672–684. doi:10.1016/j.cell.2009.03.035.

Wang, H.-W., S. Long, C. Ciferri, S. Westermann, D. Drubin, G. Barnes, and E. Nogales. 2008. Architecture and flexibility of the yeast Ndc80 kinetochore complex. *J Mol Biol*. 383:894–903. doi:10.1016/j.jmb.2008.08.077.

Wei, R.R., J. Al-Bassam, and S.C. Harrison. 2007. The Ndc80/HEC1 complex is a contact point for kinetochore-microtubule attachment. *Nat Struct Mol Biol*. 14:54–59. doi:10.1038/nsmb1186.

Wei, R.R., J.R. Schnell, N.A. Larsen, P.K. Sorger, J.J. Chou, and S.C. Harrison. 2006. Structure of a central component of the yeast kinetochore: the Spc24p/Spc25p globular domain. *Structure*. 14:1003–1009. doi:10.1016/j.str.2006.04.007.

Wei, R.R., P.K. Sorger, and S.C. Harrison. 2005. Molecular organization of the Ndc80 complex, an essential kinetochore component. *Proc Natl Acad Sci USA*. 102:5363–5367. doi:10.1073/pnas.0501168102.

Weisel, J.W., H. Shuman, and R.I. Litvinov. 2003. Protein-protein unbinding induced by force: single-molecule studies. *Current Opinion in Structural Biology*. 13:227–235. doi:10.1016/S0959-440X(03)00039-3.

Welburn, J.P.I., E.L. Grishchuk, C.B. Backer, E.M. Wilson-Kubalek, J.R. Yates, and I.M.

Cheeseman. 2009. The human kinetochore Ska1 complex facilitates microtubule depolymerization-coupled motility. *Developmental Cell*. 16:374–385. doi:10.1016/j.devcel.2009.01.011.

Welburn, J.P.I., M. Vleugel, D. Liu, J.R. Yates III, M.A. Lampson, T. Fukagawa, and I.M. Cheeseman. 2010. Aurora B phosphorylates spatially distinct targets to differentially regulate the kinetochore-microtubule interface. *Mol Cell*. 38:383–392. doi:10.1016/j.molcel.2010.02.034.

Wilson-Kubalek, E.M., I.M. Cheeseman, C. Yoshioka, A. Desai, and R.A. Milligan. 2008. Orientation and structure of the Ndc80 complex on the microtubule lattice. *The Journal of Cell Biology*. 182:1055–1061. doi:10.1083/jcb.200804170.

Yaffe, M.B., and A.E.H. Elia. 2001. Phosphoserine/threonine-binding domains. *Curr. Opin. Cell Biol.* 13:131–138. doi:10.1016/S0955-0674(00)00189-7.

Yaffe, M.B., and S.J. Smerdon. 2001. PhosphoSerine/Threonine Binding Domains**:** You Can't pSERious?. *Structure*. 9:R33–R38. doi:10.1016/S0969-2126(01)00580-9.

Yan, J., T.J. Maresca, D. Skoko, C.D. Adams, B. Xiao, M.O. Christensen, R. Heald, and J.F. Marko. 2007. Micromanipulation studies of chromatin fibers in Xenopus egg extracts reveal ATP-dependent chromatin assembly dynamics. *Mol. Biol. Cell*. 18:464–474. doi:10.1091/mbc.E06-09-0800.

Yang, Z., U.S. Tulu, P. Wadsworth, and C.L. Rieder. 2007. Kinetochore Dynein Is Required for Chromosome Motion and Congression Independent of the Spindle Checkpoint. *Current Biology*. 17:973–980. doi:10.1016/j.cub.2007.04.056.

Appendix: Building a minimal kinetochore in vitro

This work was performed in collaboration with Shelley Wickham of the Shih lab at DFCI and Wyss Institute at Harvard Medical School, with helpful technical input from Nathan Derr. Shelley generously designed and made all the O-brick scaffolds.

Introduction

A long-standing goal in the kinetochore field has been in vitro reconstitution of the kinetochore structure. From the limited recapitulations of more complex protein assemblies, it has become readily apparent that many new properties emerge in the context of a large, multiplexed assembly. At its most basic, research has shown that simply putting many microtubule binding components, such as Ndc80 (Powers et al., 2009) and Dam1 (Volkov et al., 2013), on a bead can lead to novel load-bearing and tip-tracking activity on a depolymerizing microtubule that is not observed for the proteins when studied as single molecules. Additionally, studies of the microtubule-binding activities of KMN network components alone and in complex with each other or the Ska1 complex have shown that the various protein synergize, resulting in more robust microtubule binding (Cheeseman et al., 2006; Schmidt et al., 2012). Recently, more complex assemblies have been pulled-down from yeast, and these multi-protein kinetochore particles have only strengthened the notion that the kinetochore proteins behave very differently in complex than individually by imparting novel, “catch-slip” properties to the assembly (Akiyoshi et al., 2010), underscoring the importance of studying higher order assemblies. To date, what has been missing from these studies is the capability to form higher order complexes of known composition, allowing careful analysis and manipulation of the various kinetochore components in the context of a large, macromolecular structure.

Recently, work from the Reck-Peterson and Shih labs has utilized the ability to build DNA scaffolds with pre-determined oligomer attachment sites to build complex kinesin and dynein assemblies, allowing them to study the effects of having these two

motors on a single scaffold (Derr et al., 2012). Here I propose using a similar approach to build ordered kinetochore assemblies for in vitro characterization and show preliminary data toward this goal. Many of the methods presented herein were adapted from protocols from the Reck-Peterson lab for use with the described protein constructs (original protocols available at https://reck-peterson.med.harvard.edu/protocols).

Methods

DNA Scaffold

To build a kinetochore assembly for in vitro characterization, we decided to use an "O-brick" structure made by annealing DNA oligomers to lambda phage DNA. The O-bricks, designed and constructed by the Shih lab, are a cylindrical shape 30 nm in diameter designed with six handles for subsequent protein attachment on one end of the barrel structure (Figure 1). In addition, other modified versions of this structure were also designed by Shelley Wickham for specific uses, including one with biotinylated oligomers on the opposite face of the barrel from the protein attachment sites to allow localization to the surface of a coverslip. Structures were also modified with fluorescently labeled oligomers along the long axis of the barrel, when needed, for localization.

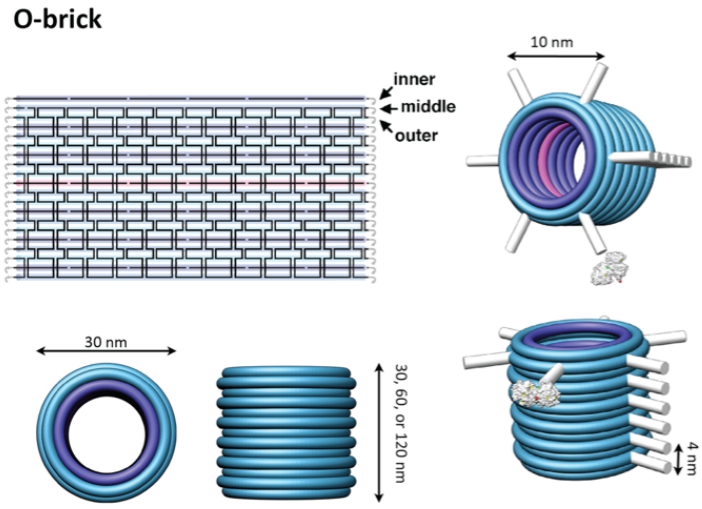

Figure 1: Diagram of DNA O-brick structure showing barrel shape and placement of handles. Diagram provided by Shelley Wickham, Shih lab.

Protein Constructs

The proteins used for attachment to the O-brick were all designed as fusions to the SNAP-tag® protein (NEB). The SNAP-tag protein is a ~20 kDa mutant form of the human O^6-alkylguanine-DNA-alkyltransferase (hAGT), a DNA repair protein. It catalyzes a reaction with a benzylguanine (BG) modified substrate to form a covalent link to the substrate. In addition, some proteins were also designed as GFP fusions, to allow visualization of the scaffolds modified with the SNAP-tag fusion proteins. Three proteins were chosen for eventual attachment to the O-brick scaffold. A modified version of the Ndc80 complex, $Ndc80^{brocolli}$, which contains only the Nuf2 and Ndc80 globular domains and a portion of their coiled-coil domains was modified with GFP (on the Nuf2 subunit) and the SNAP-tag (on the Ndc80 subunit) on their respective C-termini to allow attachment to the scaffold via the complex's coiled-coil domain. Additionally, constructs were made with the CENP-T and CENP-C N-termini fused to the SNAP-tag protein at their C-termini to allow for outer kinetochore assembly on the scaffolds. Finally, a protein expression construct of just the SNAP-tag for use as a control for subsequent experiments was made. All of these constructs were made in vectors appropriate for bacterial expression and also His-tagged to allow for purification.

Modification of DNA oligomers with SNAP substrate

The oligomer sequence used for modification was 5'--3' with a 5' Amino Modifier C6 from Integrated DNA Technologies (IDT). The oligomer was further modified with BG-NHS purchased from New England Biolabs (NEB) following the protocol from the Reck-Peterson lab. Briefly, using non-aqueous DMSO, the SNAP-tag ligand BG-GLA-NHS ester is resuspended to a final concentration of 20 mM. BG-GLA-NHS was mixed with 2

mM oligomer resuspended in water in 15-30x molar excess in HEPES (final concentration 65 mM), pH 8.5 and incubated at room temperature for 30 min. The reacted oligomer was run on a 20% TBE acrylamide gel (Invitrogen) for 65 min at 200 V with a pre-reaction oligomer sample and subsequently stained for 30 min with SYBR gold (Invitrogen). A one base pair shift indicated successful linkage of the substrate to the oligomer (Figure 2).

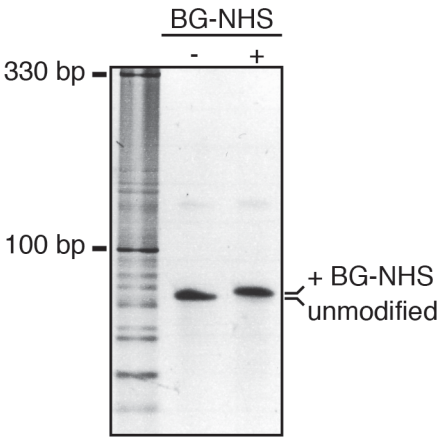

Figure 2: Benzylguanine modified DNA oligomer. A small (~1 bp) shift is observed by gel electrophoresis after DNA oligomer is modified with BG-NHS ester.

Once successful linkage was verified, the modified oligomer was purified from unreacted BG-GLA-NHS using a series of 4 Micro Bio-Spin 6 columns (Bio-Rad) in 10 mM Tris, pH8, 150 mM KCl, and 10% glycerol. The concentration of the purified oligomer was determined by absorbance at 260 nm and it was stored at -20 °C.

Modification of SNAP-tag fusion protein with modified DNA oligomer and purification

To attach the BG-oligomer to the SNAP-tag fusion proteins, the BG-oligomer was mixed with the SNAP-tag fusion in 20-25 fold molar excess (oligomer: protein) in 10 mM Tris, pH8, 150 mM KCl, 10% glycerol, and incubated at room temperature for 30 min. Longer incubation did not affect labeling efficiency when quantified by SDS-PAGE and western blot (Figure 3). To check for activity of the SNAP-tag protein, the red substrate SNAP-Cell® TMR-Star (NEB) can be substituted for the BG-oligomer. In this case when visualized by SDS-PAGE, a red band appears on the gel due to the covalent attachment of the red dye to the protein fusion (data not shown).

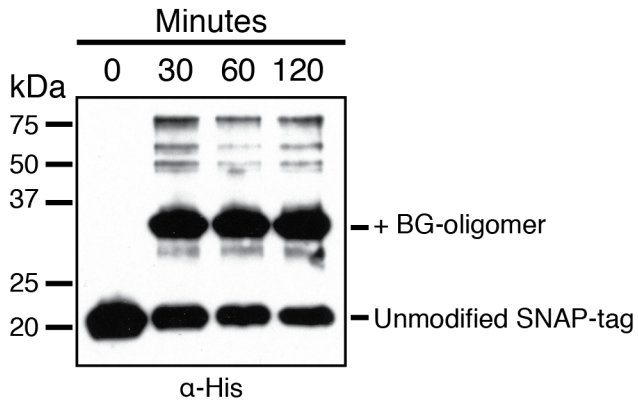

Figure 3: SNAP-tag modification timecourse. SNAP-tag protein was incubated with BG-oligomer for 0, 30, 60, or 120 minutes and then run on 15% SDS-PAGE. The protein was detected using α-His (Invitrogen). The modification with the BG-oligomer resulted in ~13 kDa increase in size of the protein (unmodified, ~ 20 kDa).

The modified protein was subsequently separated from unreacted oligomer by size exclusion chromatography using a Superdex 200 10/300 column (GE Healthcare) in 50 mM Tris, pH 8 , 150 mM KCl, 10 mM $MgCl_2$, 1 mM DTT (Figure 4A). The fractions containing protein-oligomer complex were detected by running fractions on both 20% TBE acrylamide gels (Invitrogen) (15 µl sample + 5 µl Novex Hi-Density TBE sample buffer (Invitrogen)) and detecting DNA using SYBR gold (Figure 4B), and 15% SDS-PAGE and detecting the protein using α-His antibodies (Invitrogen) (Figure 4C). The fractions containing both oligomer and protein (both increased in size) were pooled and snap frozen in liquid nitrogen and stored at -80 °C (Figure 4D).

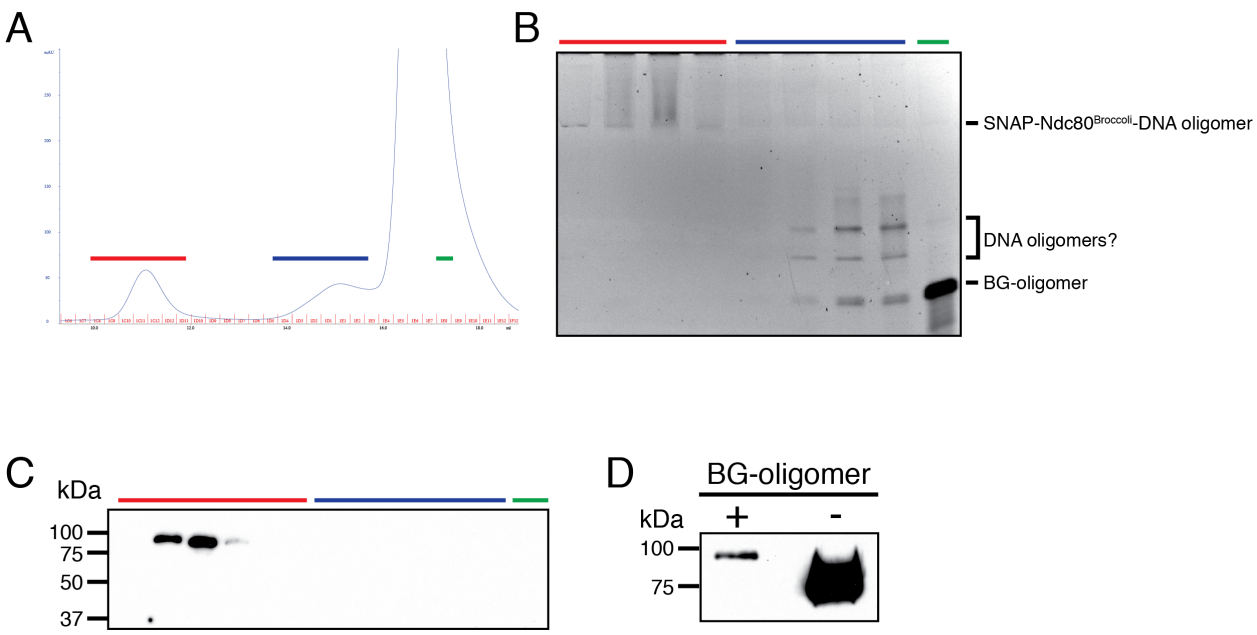

Figure 4: Purification of BG-oligomer-modified SNAP-tag fusion. A) After 30 min incubation at room temperature, BG-oligomer/SNAP-Ndc80^{Broccoli} reaction mixture was applied to an S200 10/300 size exclusion chromatography column (GE Healthcare) and monitored at 280 nm. Three distinct peaks were observed and are indicated in red, blue, and green. B) Fractions from each peak were run on a 20% acrylamide TBE gel and the DNA was visualized with SYBR gold. Distinct species were observed in the each peak. C) Fractions from each peak were run by 15% SDS-PAGE and transferred to a nitrocellulose membrane which was probed using α-His antibody. D) Fractions containing both a large DNA species and protein were pooled (red peak) and run on 10% SDS-PAGE together with unmodified protein. A species approximately 13 kDa larger than the unmodified protein was detected in the pooled fractions using α-His antibody.

Attachment to O-brick scaffold

The oligomer-modified SNAP-tag fusions were annealed to O-bricks by mixing in 45 fold molar excess protein: O-brick in a 1:1 volumetric ratio in 50 mM Tris, pH 8.0, 150 mM KCl, 10 mM $MgCl_2$ and incubated at room temperature for at least 30 min. A sample of the O-brick before and after reaction with the oligomer-modified protein was then run on a 2% agarose TBE gel supplemented with 11 mM $MgCl_2$ and 0.1% LDS for 4 hr at 70 V in 1x TBE + 11 mM $MgCl_2$ + 0.1 % LDS with one buffer change after 2 hr. To maintain running buffer temperature and prevent smearing, gel chambers were placed in a water

bath. O-brick was visualized by staining with SYBR gold in TBE + 11 mM $MgCL_2$ for 1 hr while covered in foil, and then washing in TBE + 11 mM $MgCl_2$ (Figure 5).

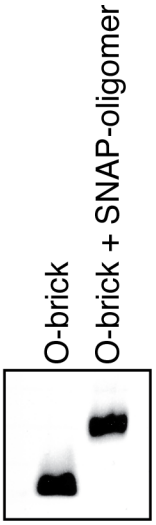

Figure 5: O-brick with annealed SNAP-oligomer

To separate the O-brick with annealed protein from free protein-oligomer, the reaction mixture was applied to 500 µl Sephacryl S-500 HR resin (GE Healthcare) in a micro chromatography spin column equilibrated in PBS + 0.1% Tween-20 (PBST), 10 mM $MgCl_2$ (+ 5 mg/ml BSA if using for TIRF) at 1000g for 10 s. Final concentrations were determined from absorbance at UV 260. The purified O-brick/protein was subsequently used for either visualization by electron microscopy (EM) or total internal reflection fluorescence (TIRF) microscopy.

TIRF Chambers

TIRF chambers were prepared using coverslips cleaned as described previously (Schmidt et al., 2012). They were assembled as described in Figure 6 to make 3 closed chambers set up for continuous fluid exchange.

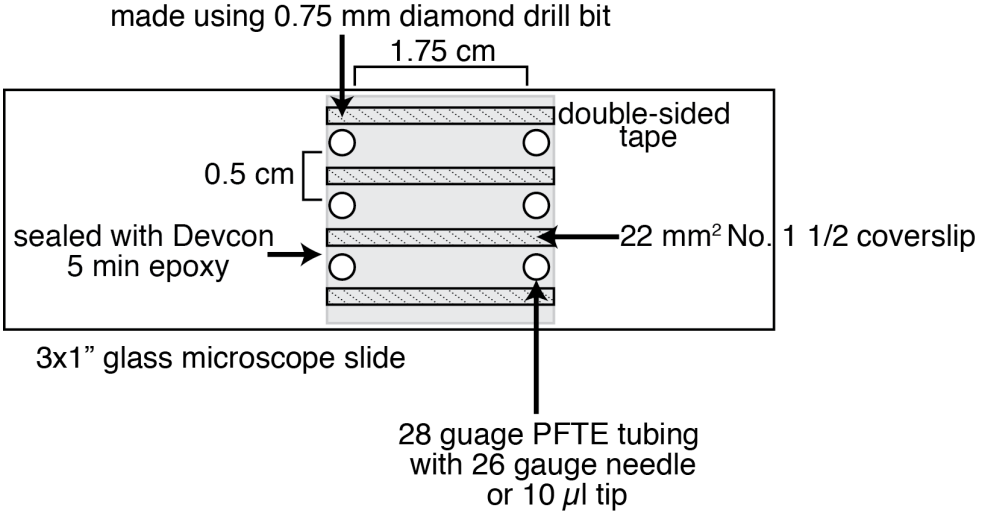

Figure 6: Diagram of TIRF flow chambers.

For use with biotinylated O-bricks, chambers were prepared by flowing in filtered PBST + 0.25 mg/ml biotinylated BSA and incubating at room temperature for 15 min. Chambers were then washed with 100 µl PBST before adding PBST + 0.05 mg/ml streptavidin and incubating for 15 min. The chambers were subsequently washed with 100 µl PBST + 5 mg/ml BSA and incubated for 1 hr. The O-brick in 5 mg/ml BSA was then added and allowed to sit for ~5 min (can modify by watching for particle adherence to slide surface on TIRF microscope) before washing unbound protein with PBST + 5 mg/ml BSA.

Future Directions

With successful attachment of the protein constructs to the O-brick scaffold, it is now important to quantify the number of protein molecules attached to each scaffold. Preliminary attempts to count the number of attached molecules by EM have been unsuccessful due to poor imaging of the protein under ideal DNA imaging conditions (unpublished results). Alternatively, I have designed protein constructs with added GFP fusions, and intend to use these for counting via photo-bleaching assays. For normalization, Shelley Wickham has designed O-bricks with both 3 and 6 handles for protein attachment, as well as fluorescent dyes to allow for easy localization of the scaffolds by TIRF microscopy. Once the average number of protein molecules on each scaffold has been ascertained, these molecules can be used for characterization on microtubules. For this, comparison of the $Ndc80^{broccoli}$ on the scaffolds to more complex mixtures of proteins built on CENP-C or CENP-T platforms will allow insight into how the proteins of the kinetochore interact to build a functional kinetochore. Future experiments will also include various post-translational modifications to study the effects of these.

References

Akiyoshi, B., K.K. Sarangapani, A.F. Powers, C.R. Nelson, S.L. Reichow, H. Arellano-Santoyo, T. Gonen, J.A. Ranish, C.L. Asbury, and S. Biggins. 2010. Tension directly stabilizes reconstituted kinetochore-microtubule attachments. *Nature*. 468:576–579. doi:10.1038/nature09594.

Cheeseman, I.M., J.S. Chappie, E.M. Wilson-Kubalek, and A. Desai. 2006. The conserved KMN network constitutes the core microtubule-binding site of the kinetochore. *Cell*. 127:983–997. doi:10.1016/j.cell.2006.09.039.

Derr, N.D., B.S. Goodman, R. Jungmann, A.E. Leschziner, W.M. Shih, and S.L. Reck-Peterson. 2012. Tug-of-war in motor protein ensembles revealed with a programmable DNA origami scaffold. *Science*. 338:662–665. doi:10.1126/science.1226734.

Powers, A.F., A.D. Franck, D.R. Gestaut, J. Cooper, B. Gracyzk, R.R. Wei, L. Wordeman, T.N. Davis, and C.L. Asbury. 2009. The Ndc80 kinetochore complex forms load-bearing attachments to dynamic microtubule tips via biased diffusion. *Cell*. 136:865–875. doi:10.1016/j.cell.2008.12.045.

Schmidt, J.C., H. Arthanari, A. Boeszoermenyi, N.M. Dashkevich, E.M. Wilson-Kubalek, N. Monnier, M. Markus, M. Oberer, R.A. Milligan, M. Bathe, G. Wagner, E.L. Grishchuk, and I.M. Cheeseman. 2012. The kinetochore-bound Ska1 complex tracks depolymerizing microtubules and binds to curved protofilaments. *Developmental Cell*. 23:968–980. doi:10.1016/j.devcel.2012.09.012.

Volkov, V.A., A.V. Zaytsev, N. Gudimchuk, P.M. Grissom, A.L. Gintsburg, F.I. Ataullakhanov, J.R. McIntosh, and E.L. Grishchuk. 2013. Long tethers provide high-force coupling of the Dam1 ring to shortening microtubules. *Proc Natl Acad Sci USA*. 110:7708–7713. doi:10.1073/pnas.1305821110.